Physics of Life
PHYS-468

AFM
Atomic Force Microscopy

Henning Stahlberg,
LBEM, IPHYS, SB, EPFL

The Nobel Prize in Physics 1986

"for his fundamental work in electron optics, and for the design of the first electron microscope"

"for their design of the scanning tunneling microscope"

Ernst Ruska

◐ 1/2 of the prize

Federal Republic of Germany

Fritz-Haber-Institut der Max-Planck-Gesellschaft Berlin, Federal Republic of Germany

b. 1906
d. 1988

Gerd Binnig

◔ 1/4 of the prize

Federal Republic of Germany

IBM Zurich Research Laboratory Rüschlikon, Switzerland

b. 1947

Heinrich Rohrer

◔ 1/4 of the prize

Switzerland

IBM Zurich Research Laboratory Rüschlikon, Switzerland

b. 1933

The Scanning Tunneling Microscope (STM)

Nobel Laureates Heinrich Rohrer and Gerd Binnig

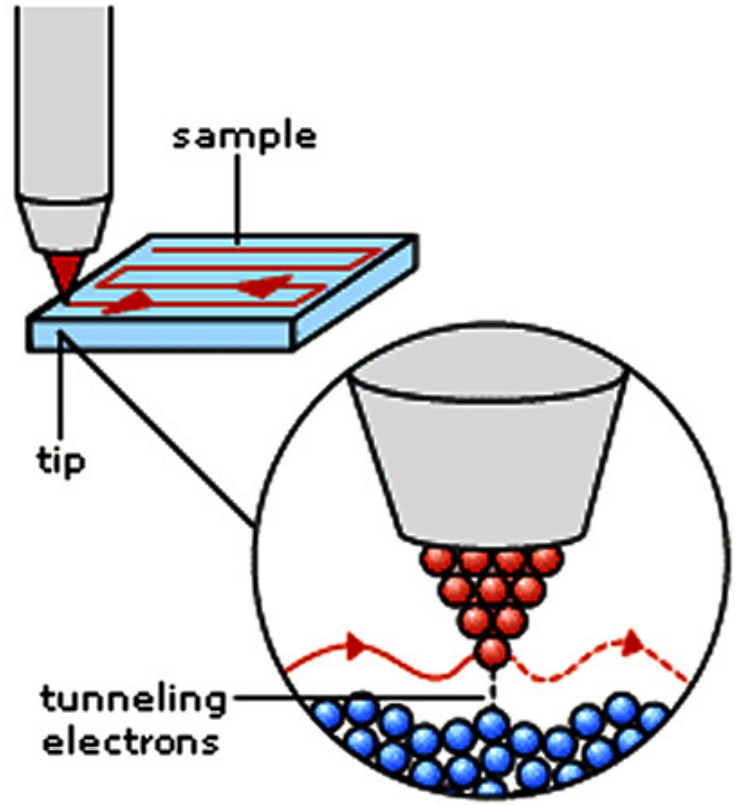

In the STM, the structure of a surface is studied using a stylus that scans the surface at a fixed distance from it.

Currents Control the Surface

An extremely fine conducting probe is held close to the sample. Electrons tunnel between the surface and the stylus, producing an electrical signal. The stylus is extremely sharp, the tip being formed by one single atom. It slowly scans across the surface at a distance of only an atom's diameter. The stylus is raised and lowered in order to keep the signal constant and maintain the distance. This enables it to follow even the smallest details of the surface it is scanning. Recording the vertical movement of the stylus makes it possible to study the structure of the surface atom by atom. A profile of the surface is created, and from that a computer-generated contour map of the surface is produced.

Important in Many Sciences

The study of surfaces is an important part of physics, with particular applications in semiconductor physics and microelectronics. In chemistry, surface reactions also play an important part, for example in catalysis. The STM works best with conducting materials, but it is also possible to fix organic molecules on a surface and study their structures. For example, this technique has been used in the study of DNA molecules.

Invention of Atomic force microscope

2016 KAVLI PRIZE NANOSCIENCE

Recognized "for the invention and realization of atomic force microscopy, a breakthrough in measurement technology and nanosculpting that continues to have a transformative impact on nanoscience and technology."

Gerd Binnig
Former member of IBM Zurich Research Laboratory, Switzerland

Christoph Gerber
University of Basel, Switzerland

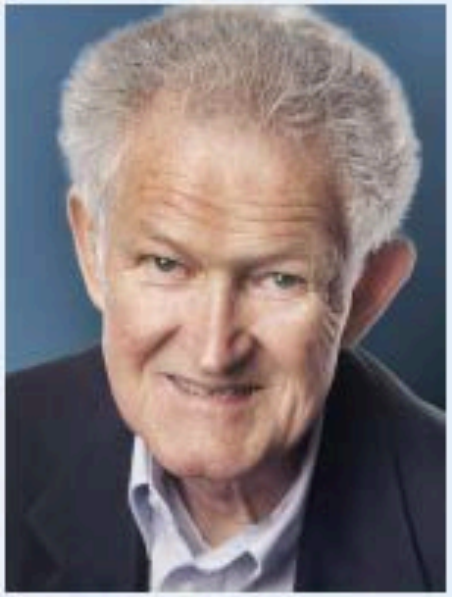

Calvin Quate
Stanford University, USA

Atomic Force Microscope (AFM)

(The AFM is the younger brother of the STM)

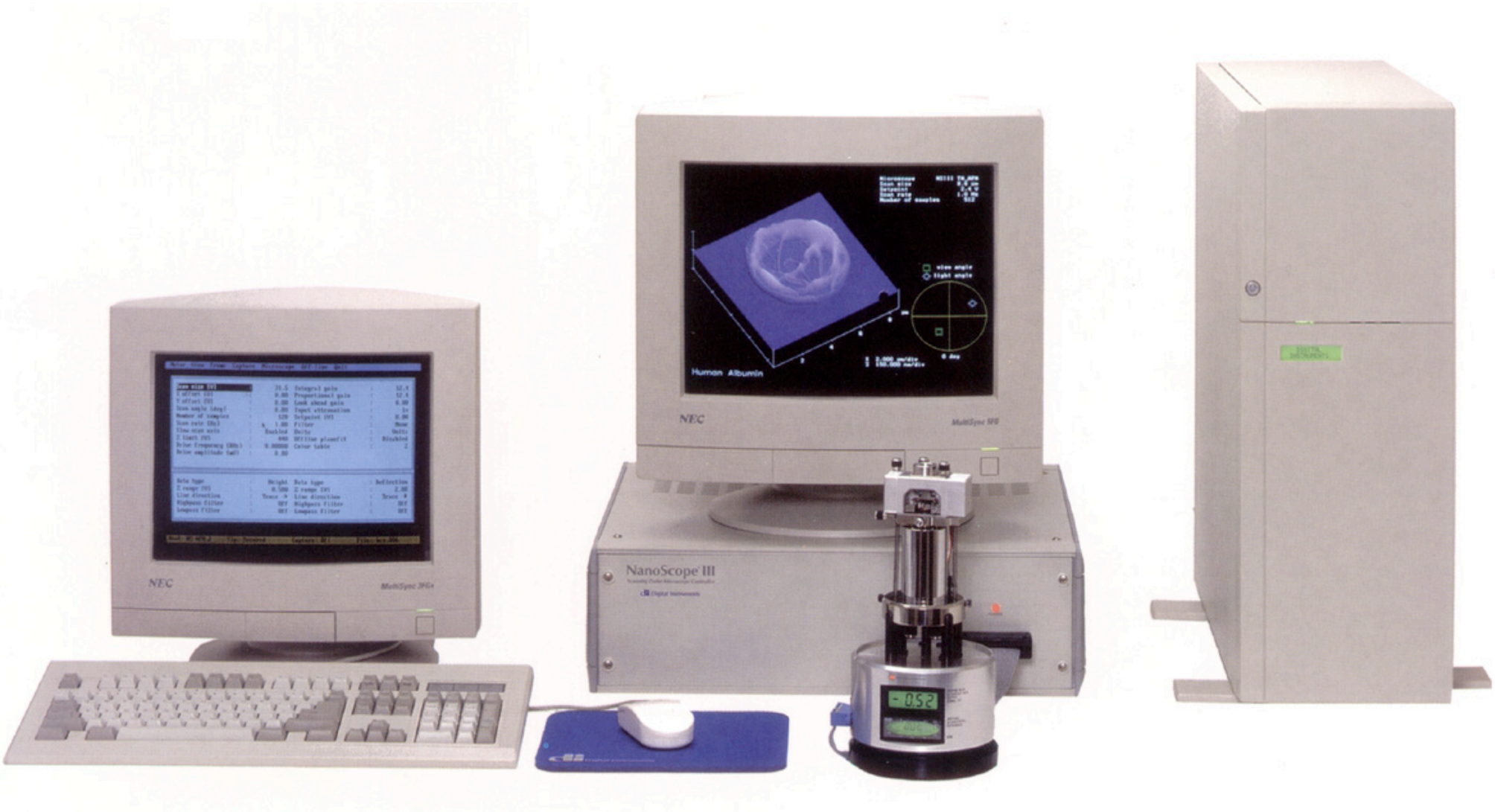

Atomic force microscopy (AFM)

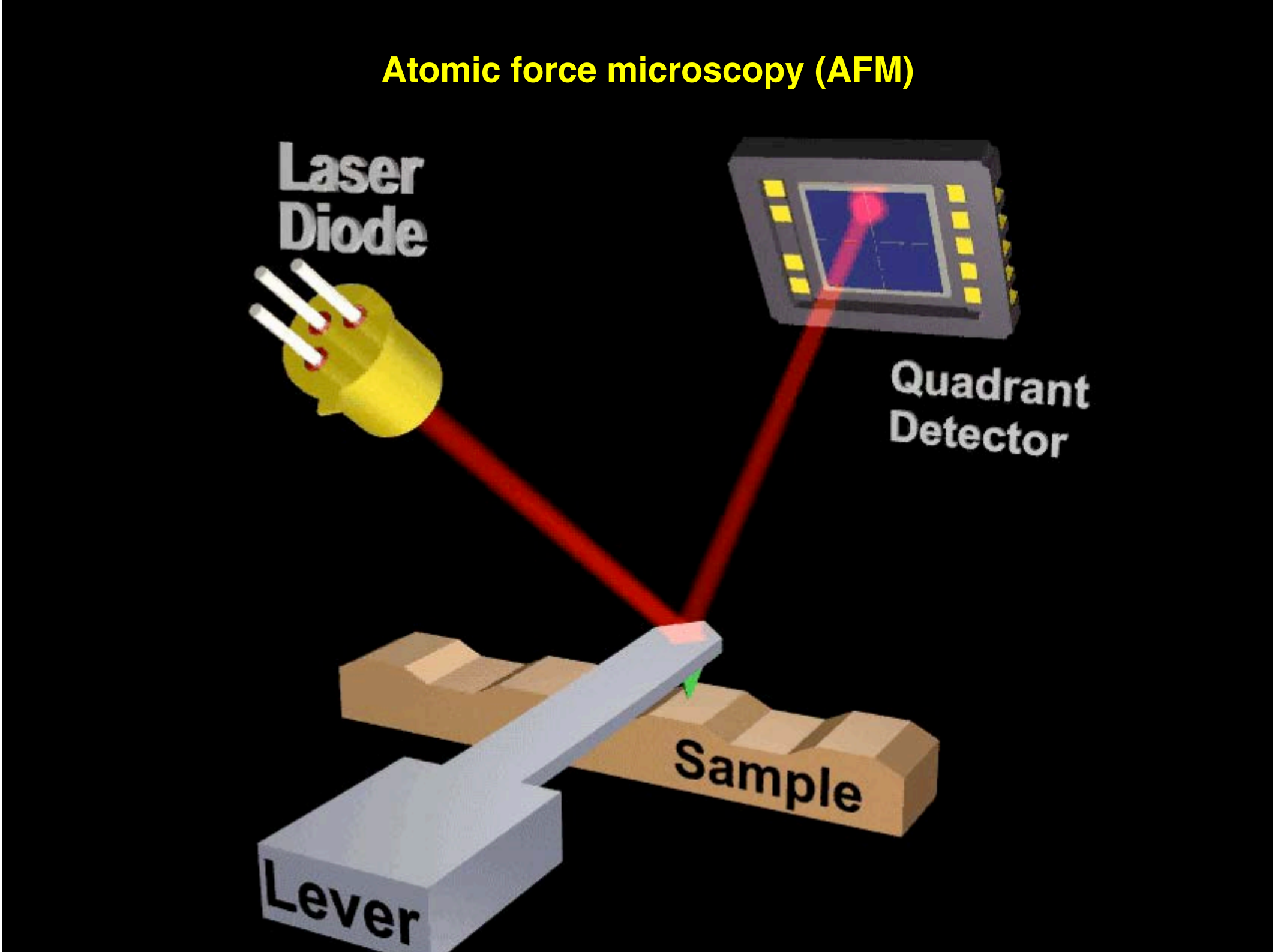

Atomic force microscopy (AFM)

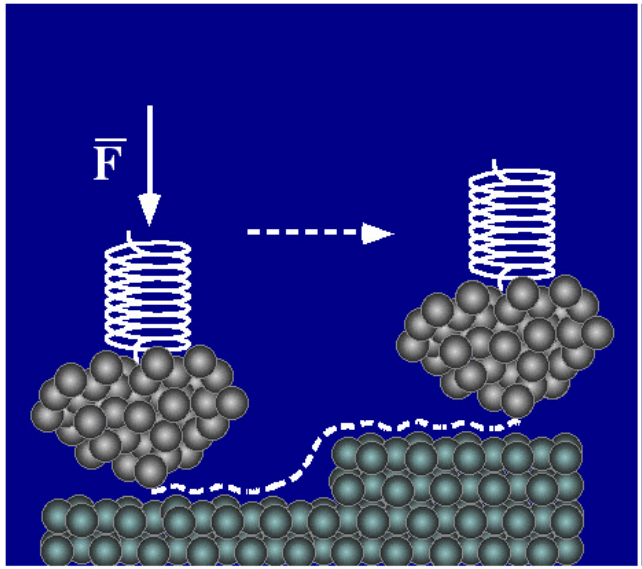

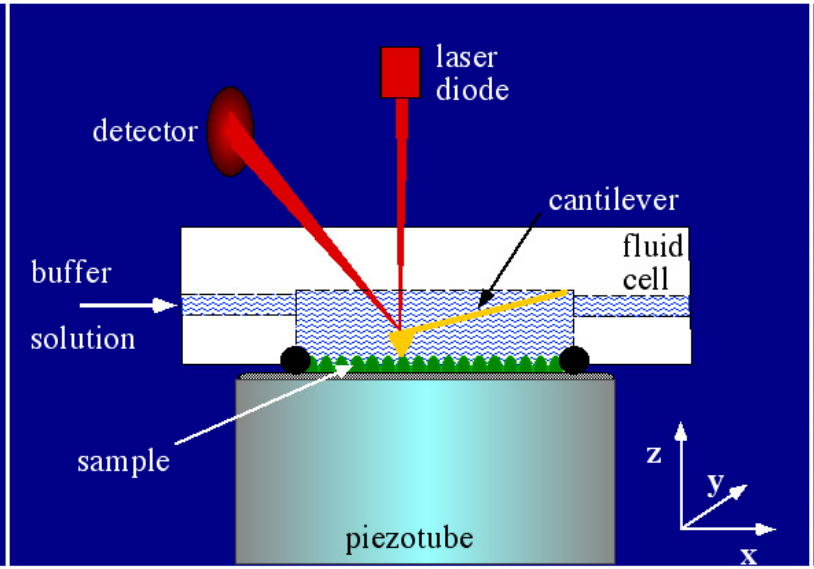

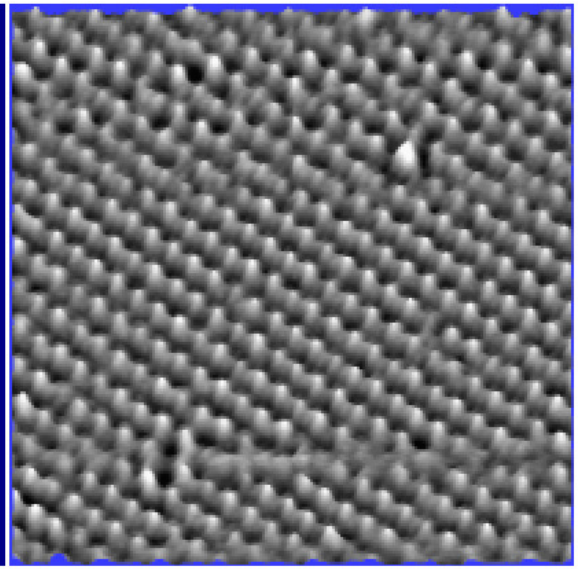

Resolution:

STM on Metals: 1 Å (X,Y,Z)

AFM on Proteins: 5 Å (X,Y), 1Å (Z)

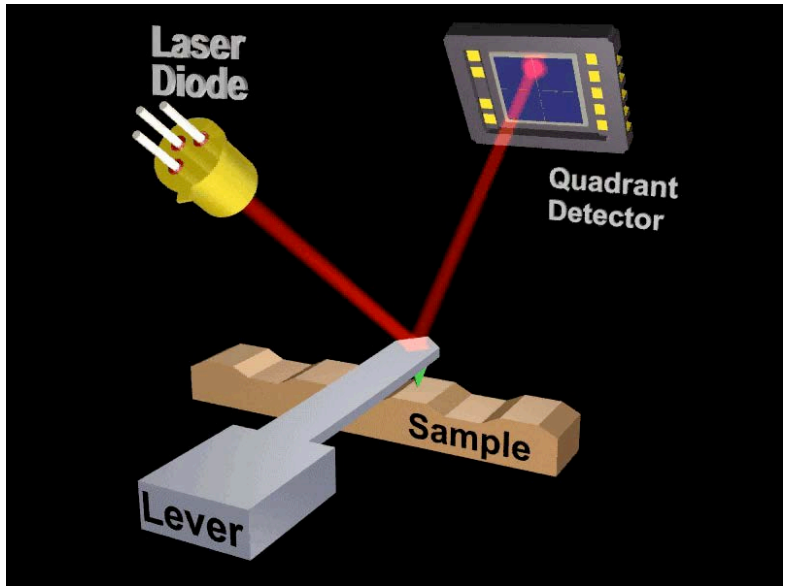

Signal Source:

STM: Electric current between tip and sample.

AFM: Physical bending of the cantilever.

Atomic force microscopy (AFM)

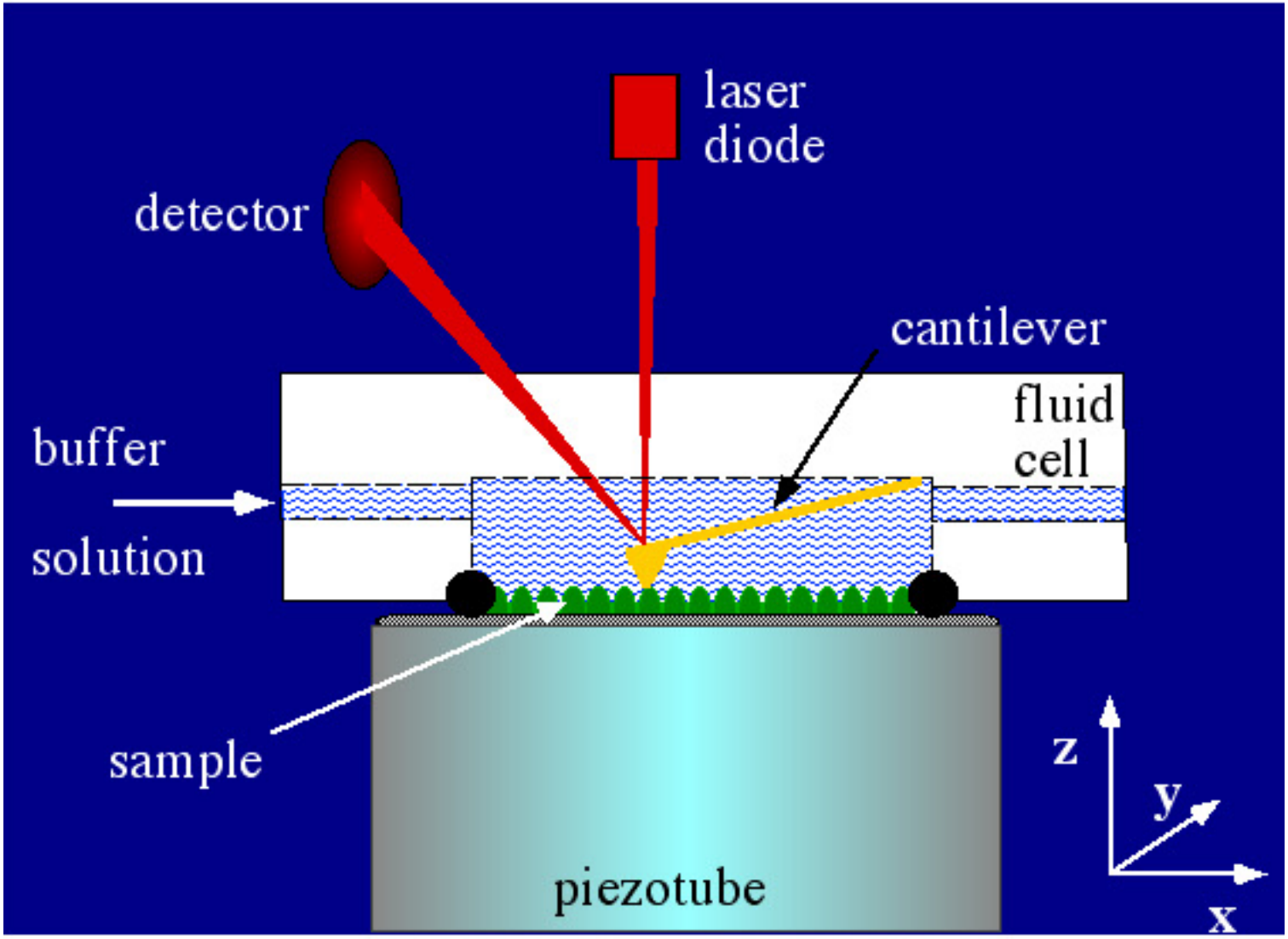

Atomic Force Microscopy

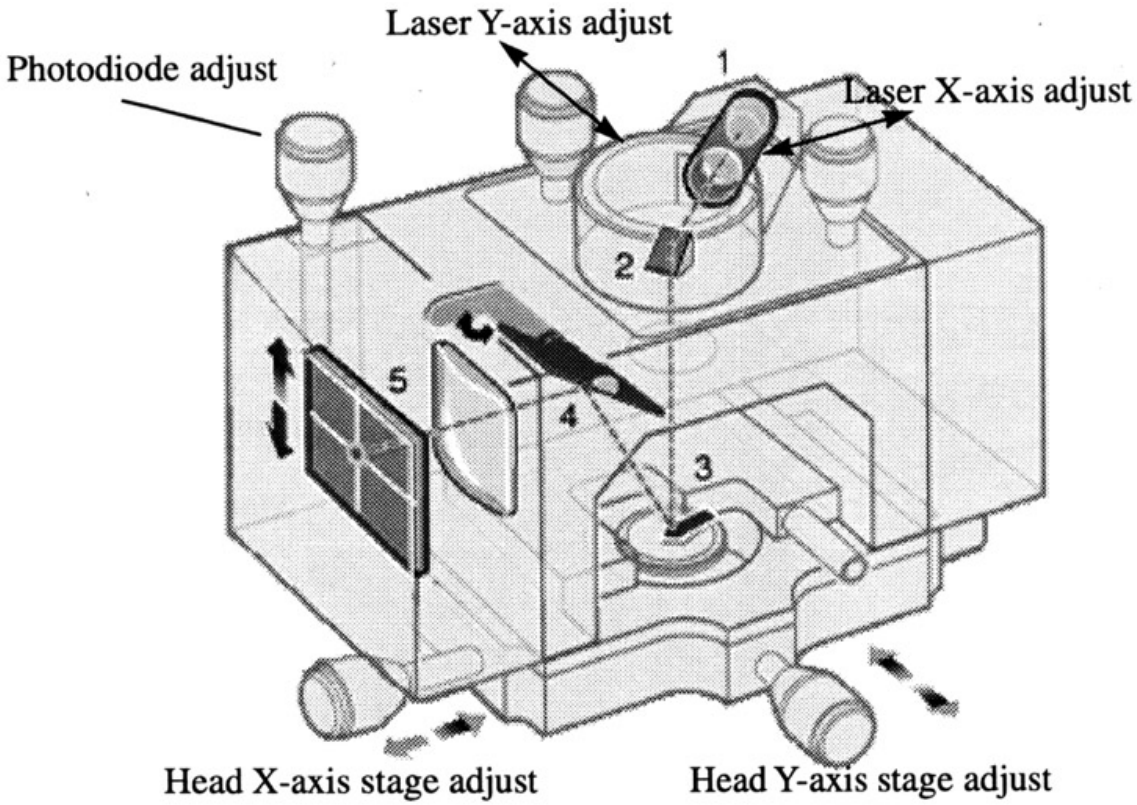

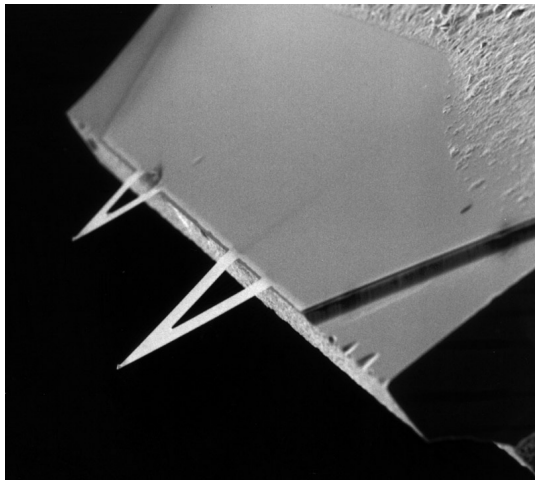

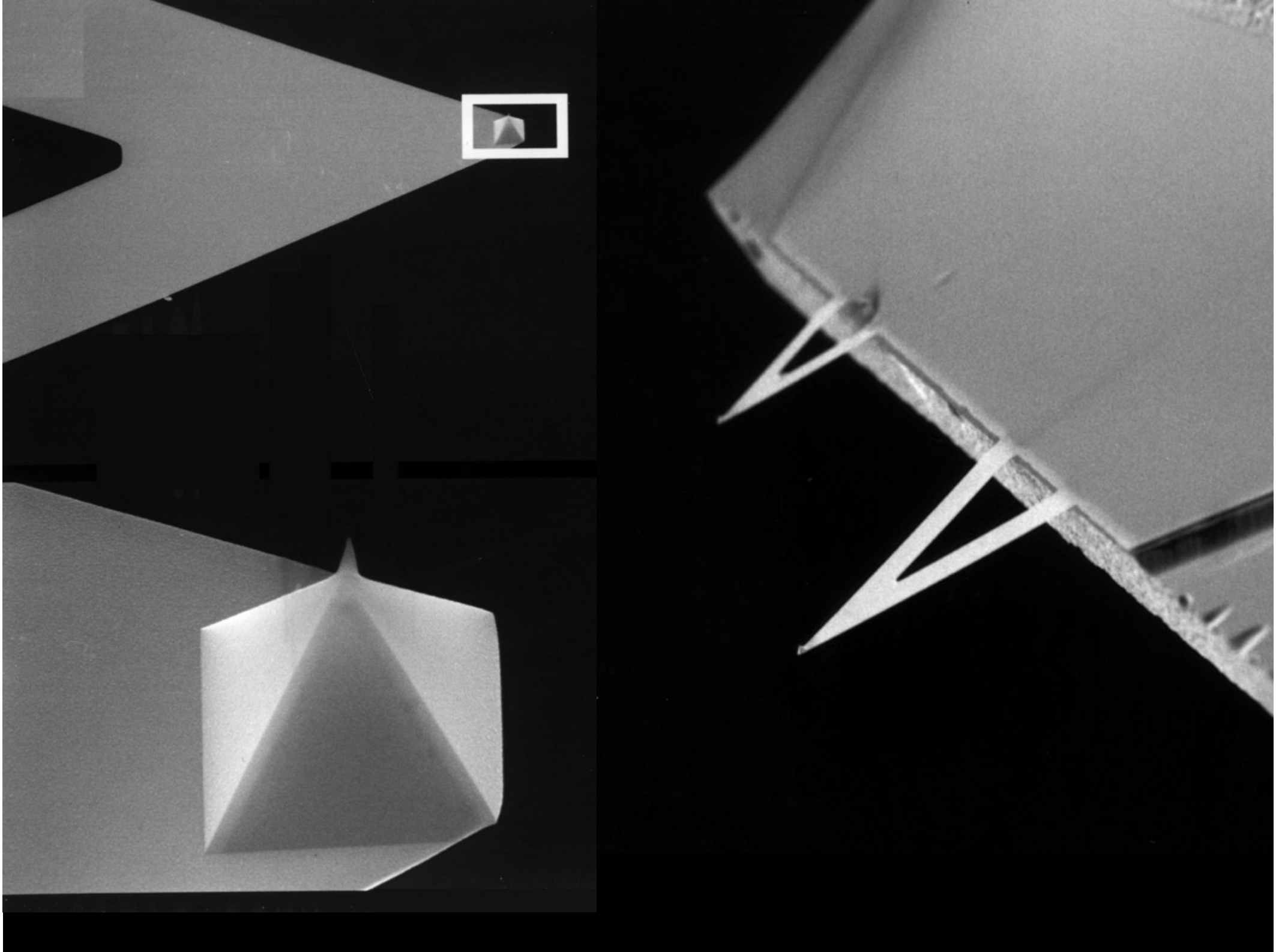

Atomic force microscopy (AFM)

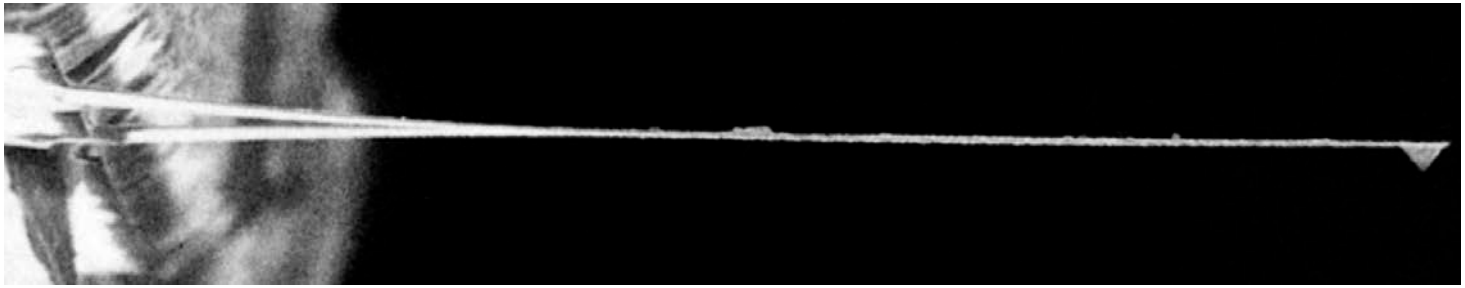

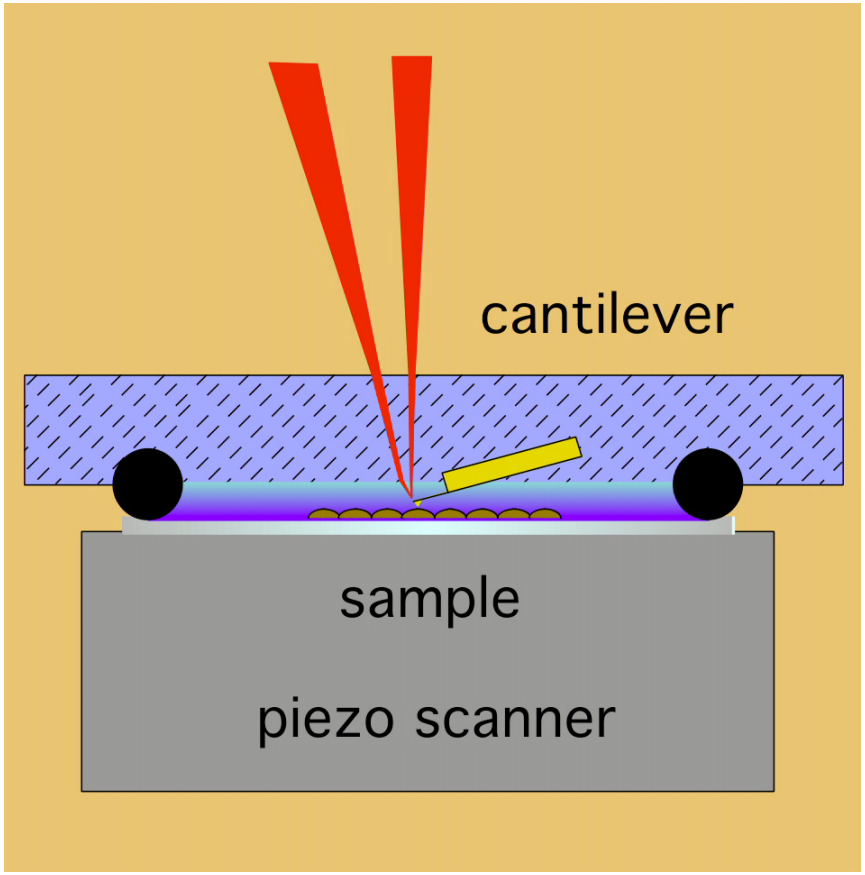

World of Cantilevers

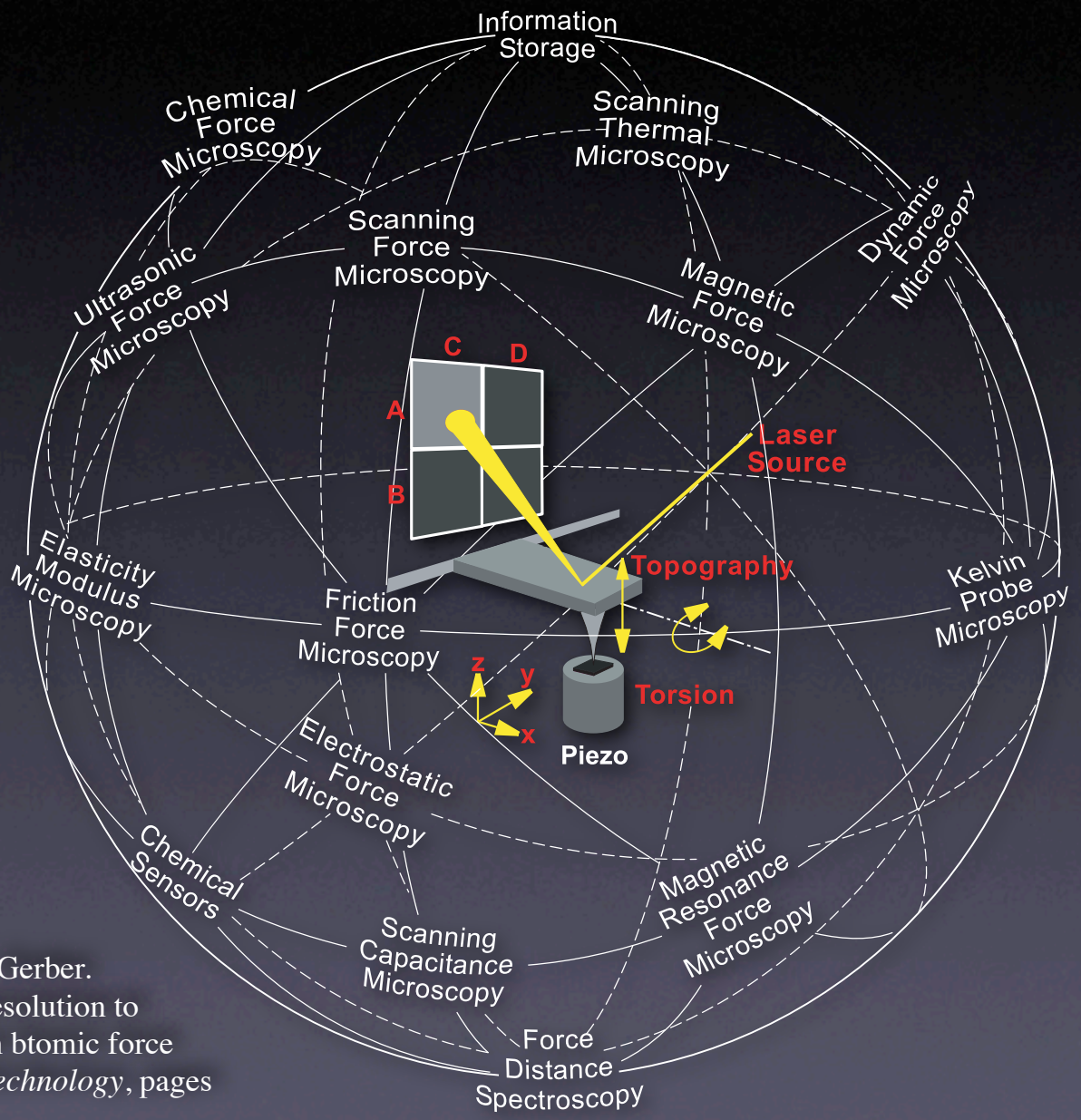

H. P. Lang, M. Hegner, and C. Gerber. Nanomechanics from atomic resolution to molecular recognition based on btomic force microscopy technology. *Nanotechnology*, pages R29–R36, 2002.

Atomic force microscopy (AFM)

Sharp Tip

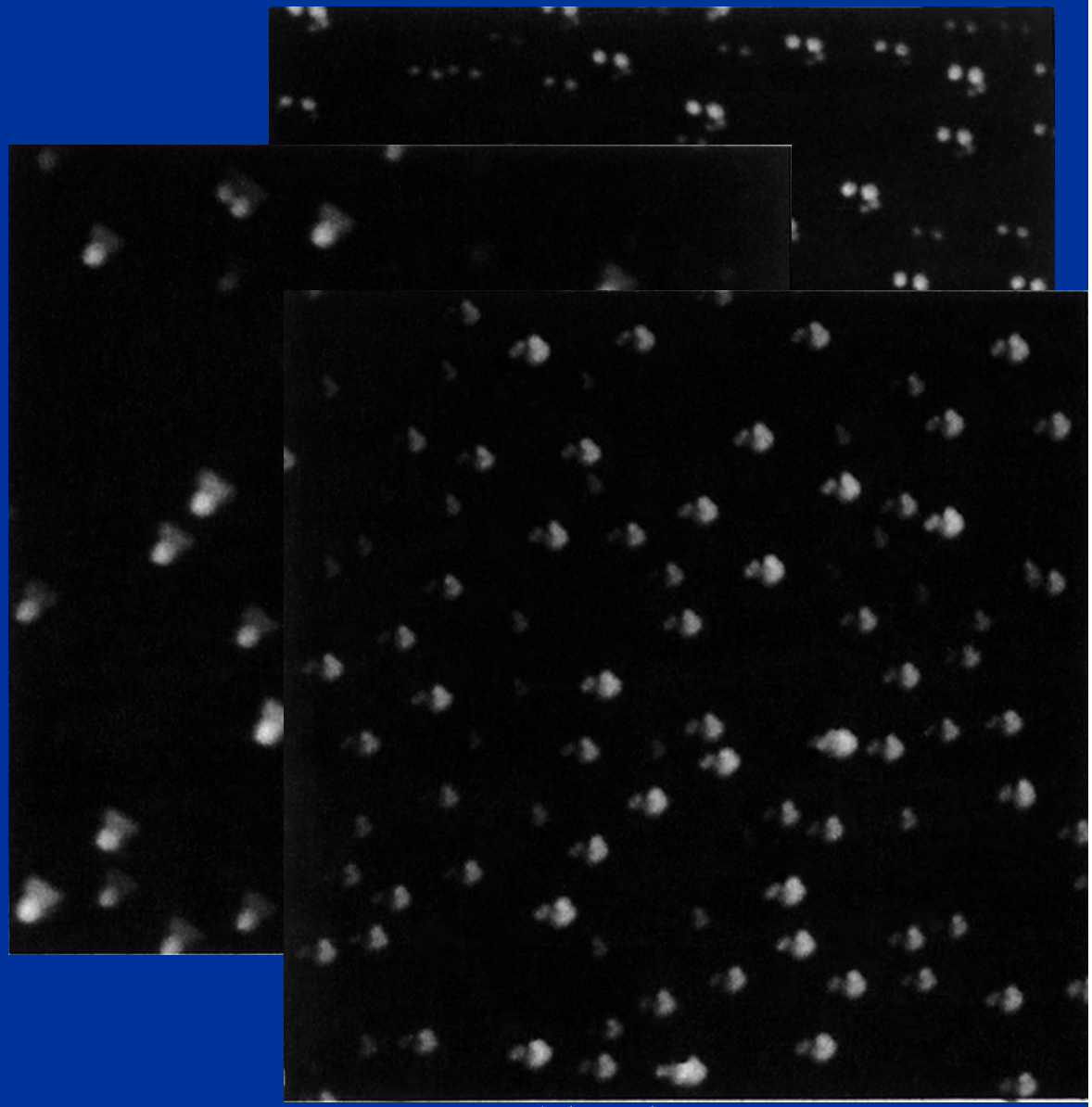

Double Tip

AFM Modes

- Constant Height Mode
- Constant Force Mode
- Friction mode
- Tapping Mode, vibrating mode

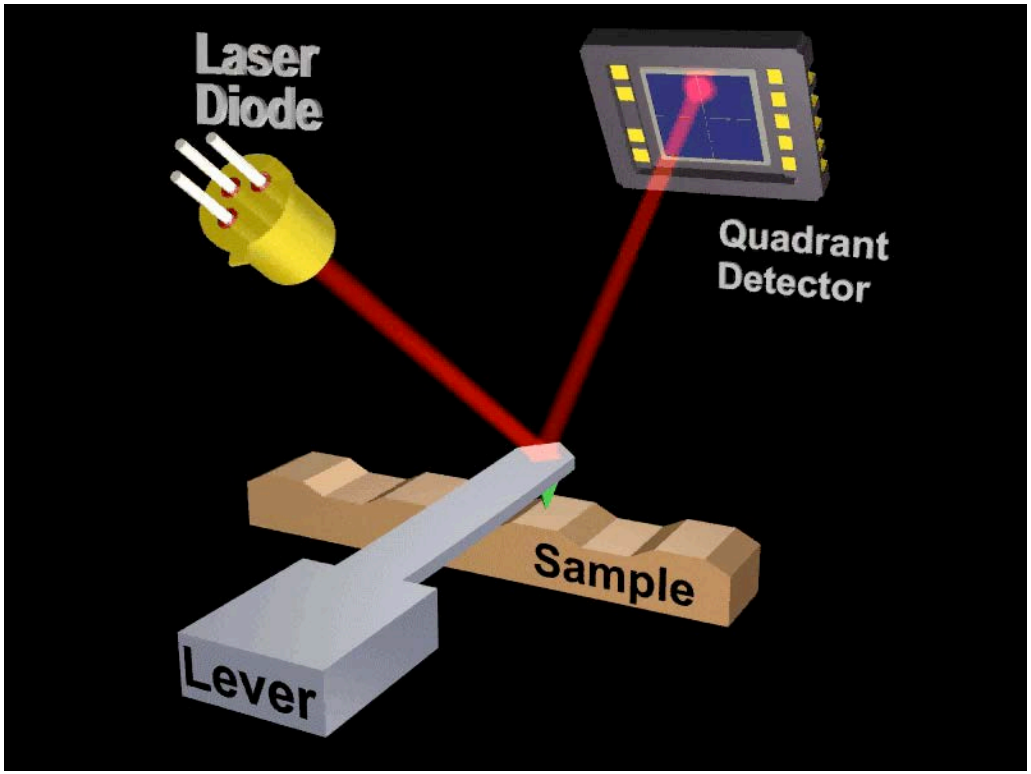

Tip-Sample Interaction in Air

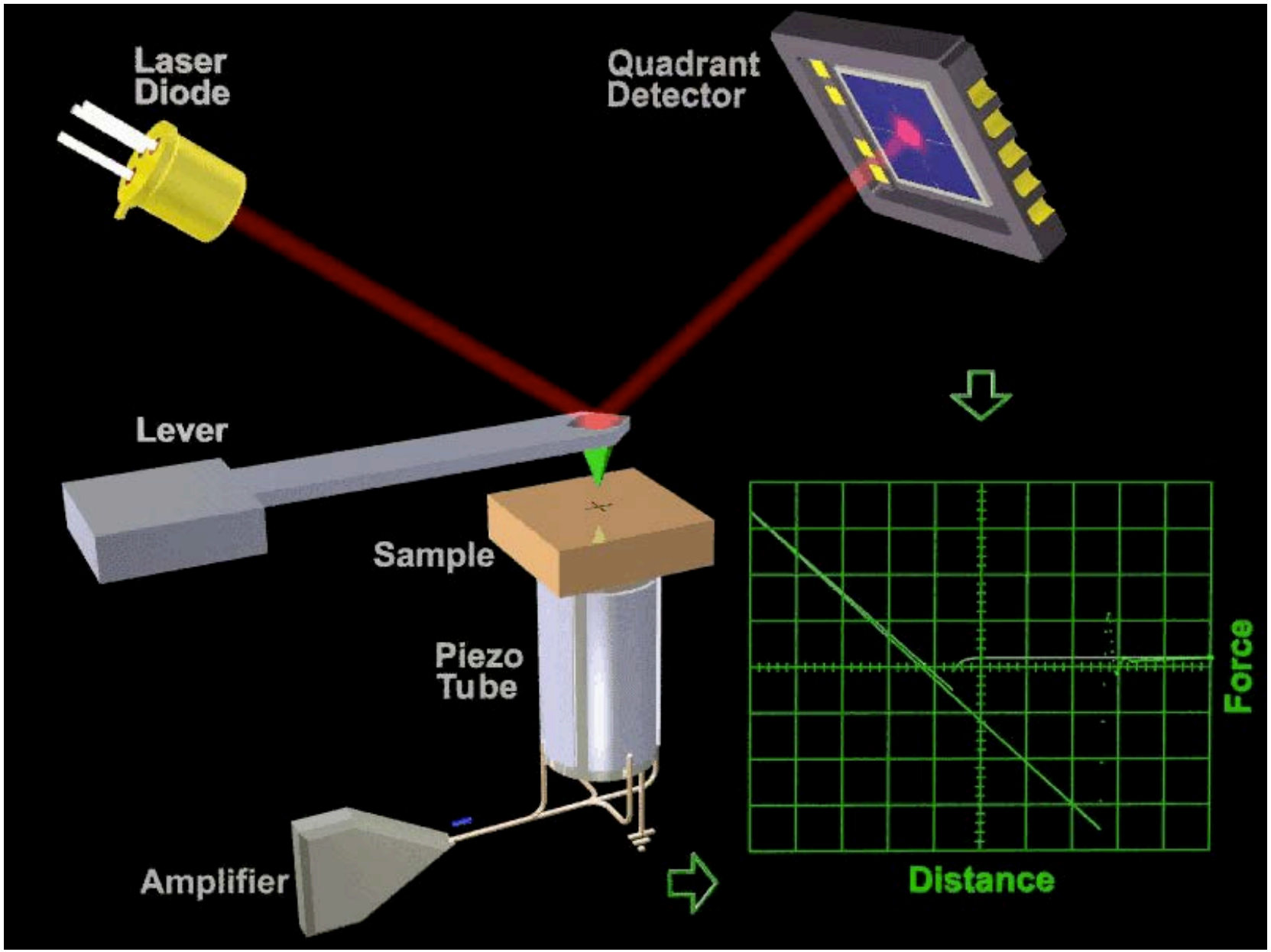

Tip-Sample Interaction in Water

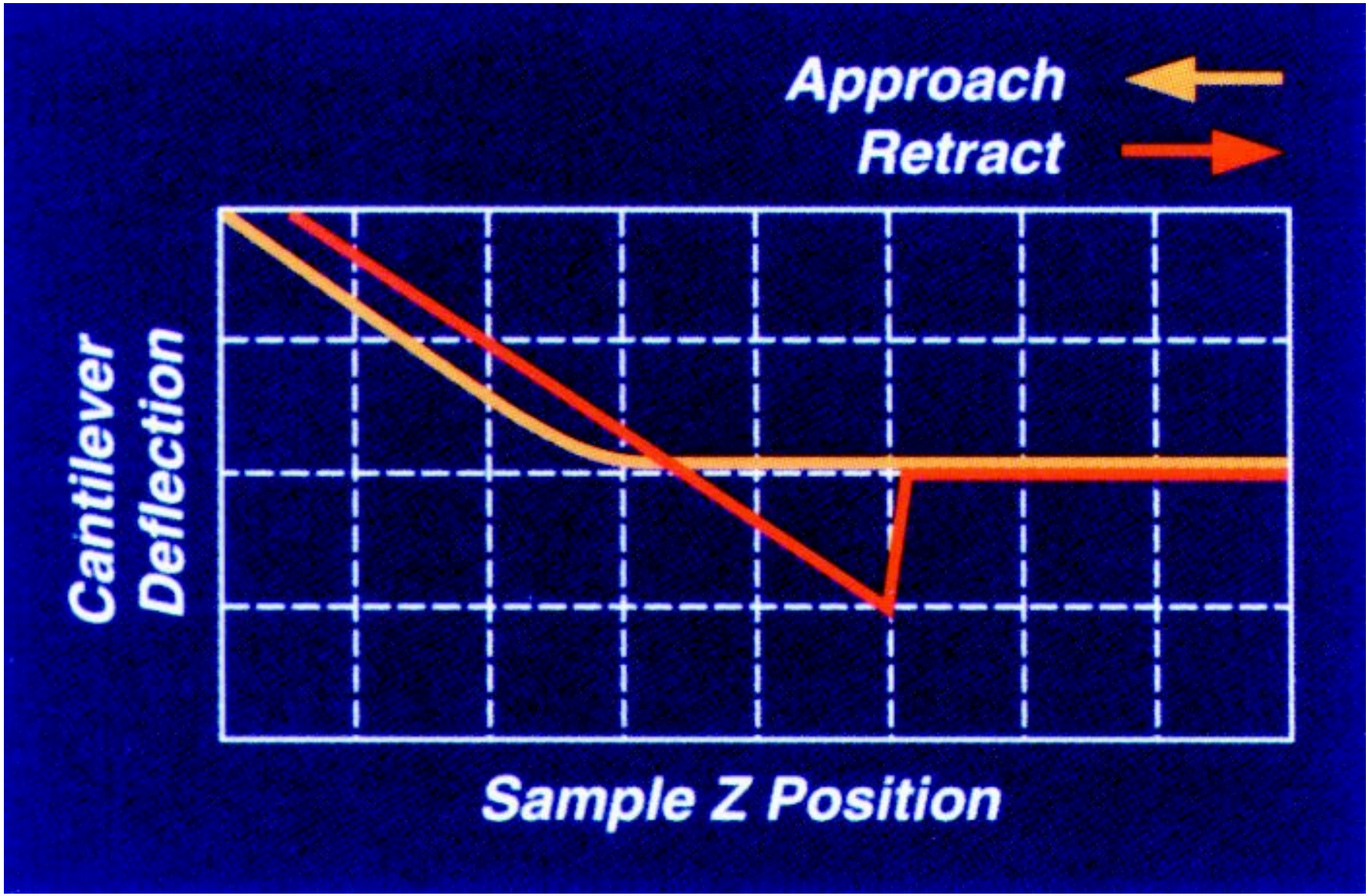

Charting and unzipping the S-layer of *Corynebacterium glutamicum*

The S-layer forms the protective cell wall of bacteria

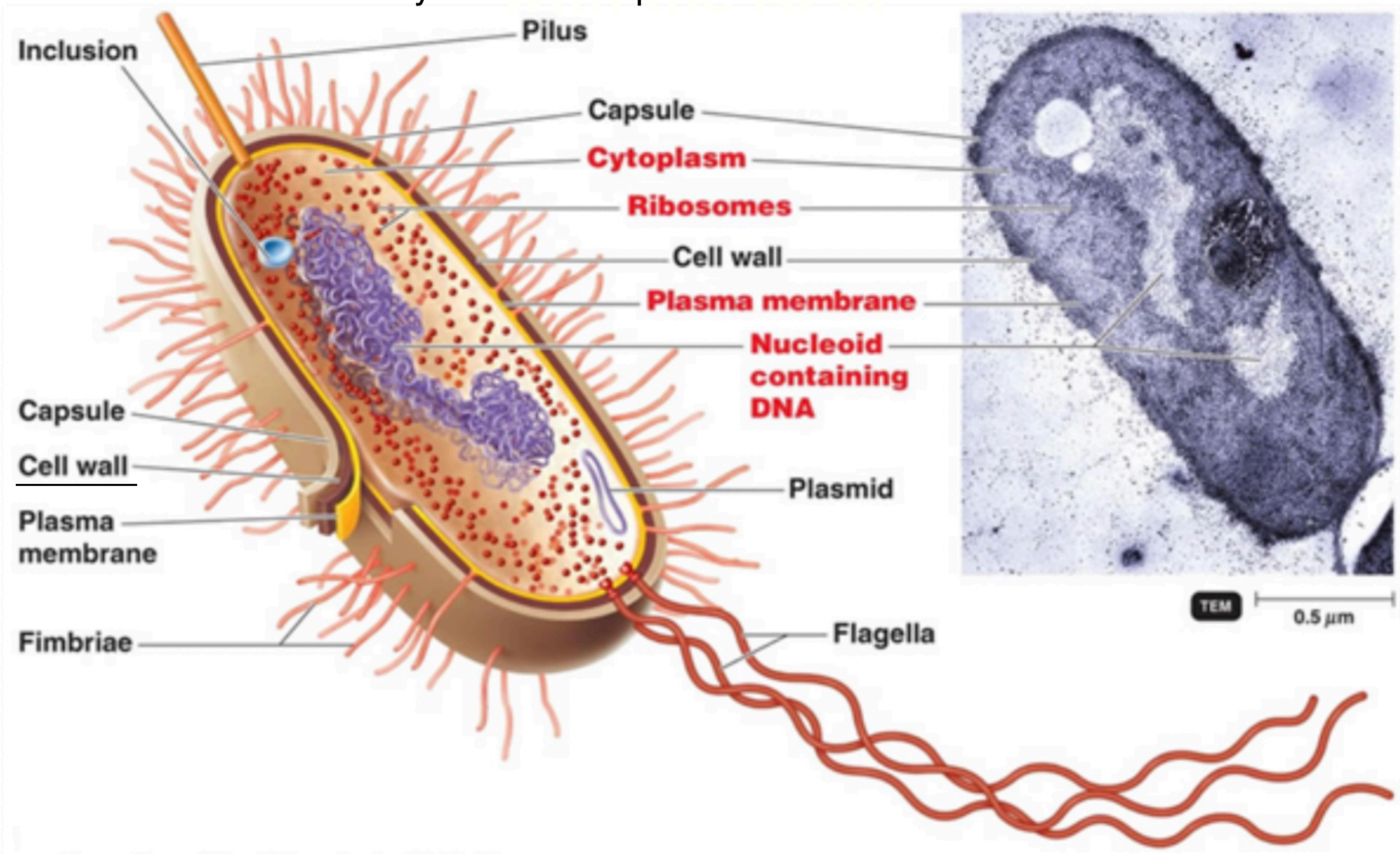

Charting and unzipping the S-layer of *Corynebacterium glutamicum* with the AFM

The S-layer is the protective “armor” of bacterial

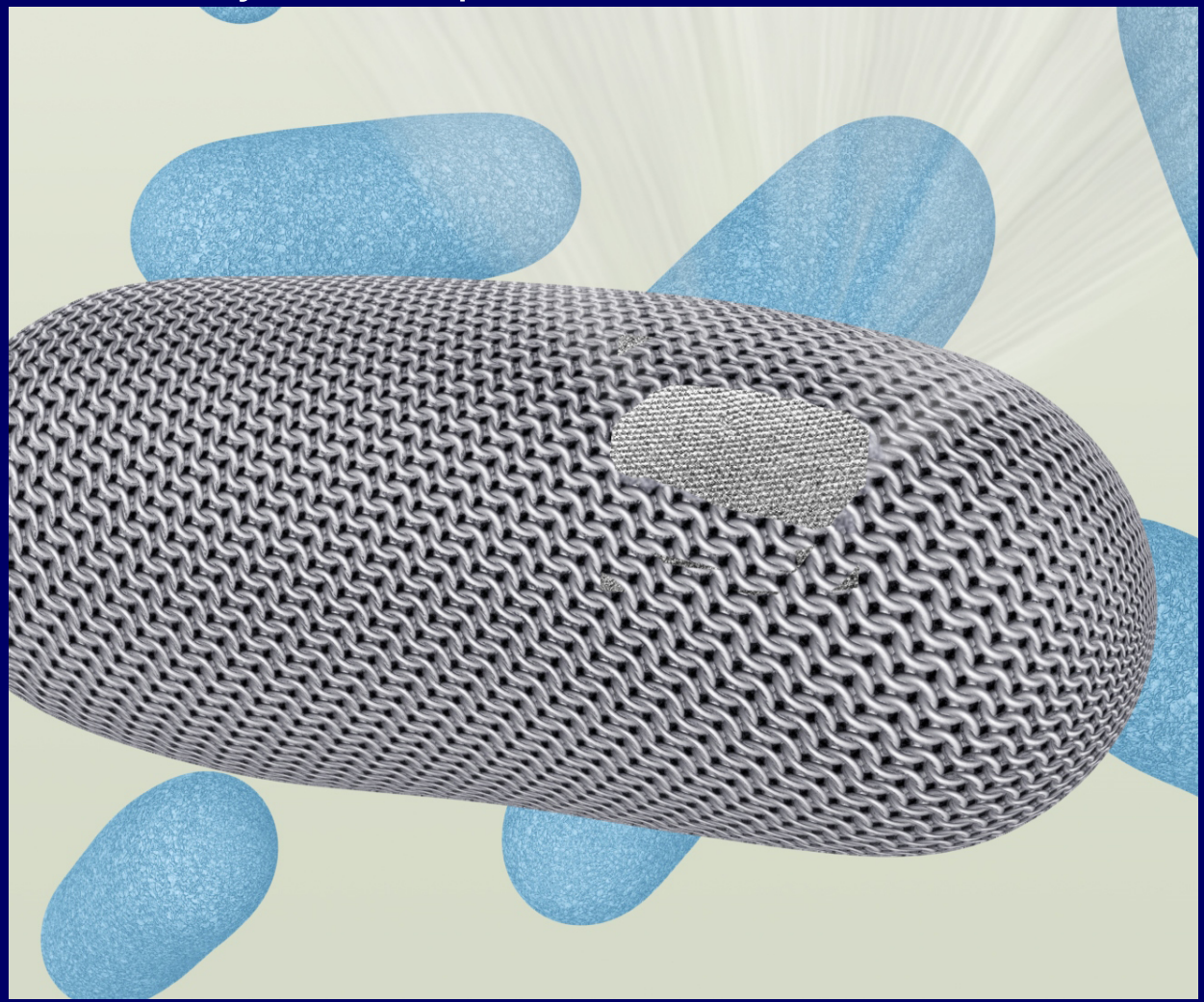

Native S-layer adsorbs double layered
And can be dissected with the AFM tip

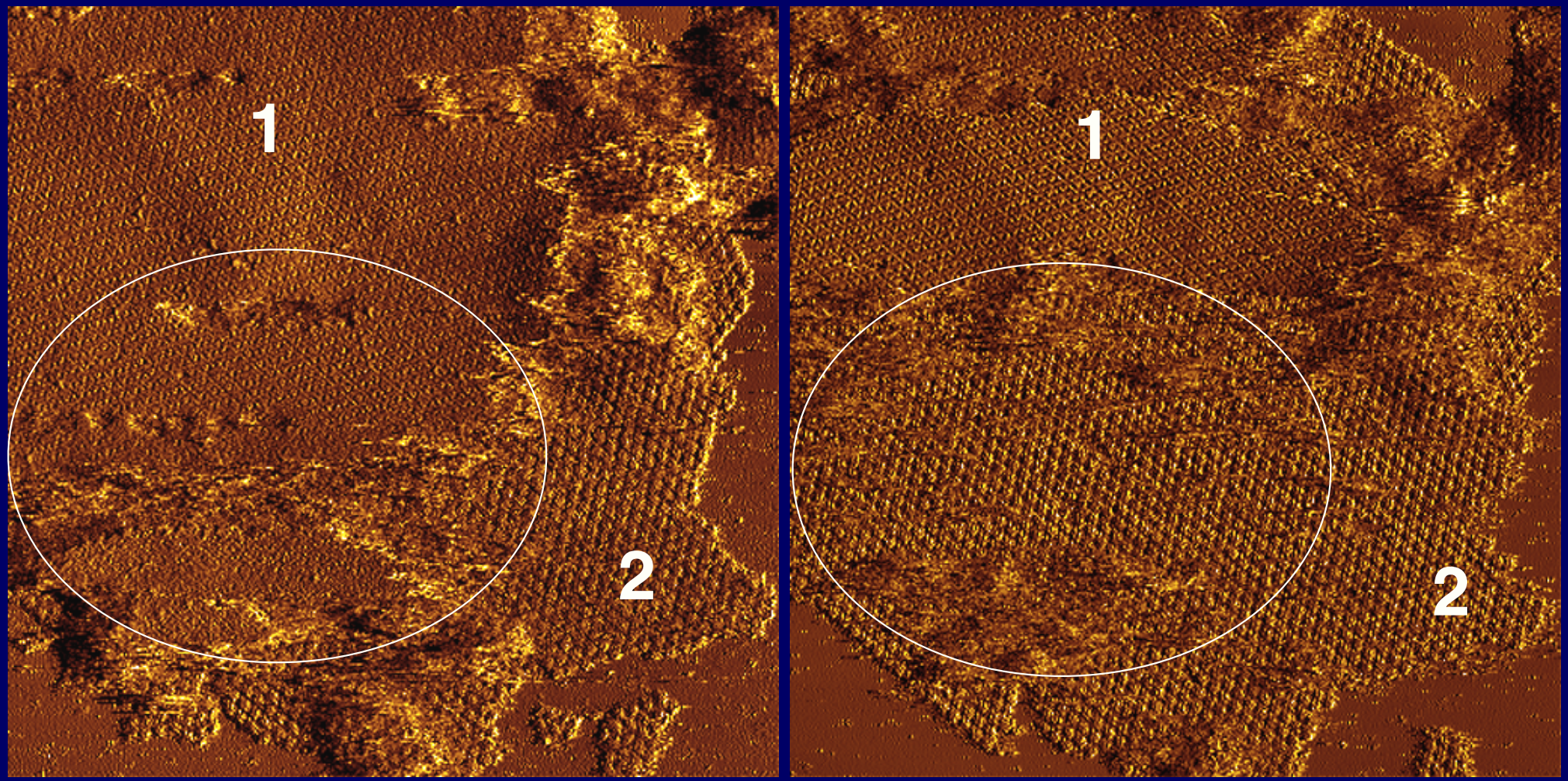

1: triangular surface

2: flower-shaped surface

Native S-layer adsorbs double layered and can be dissected with the AFM tip

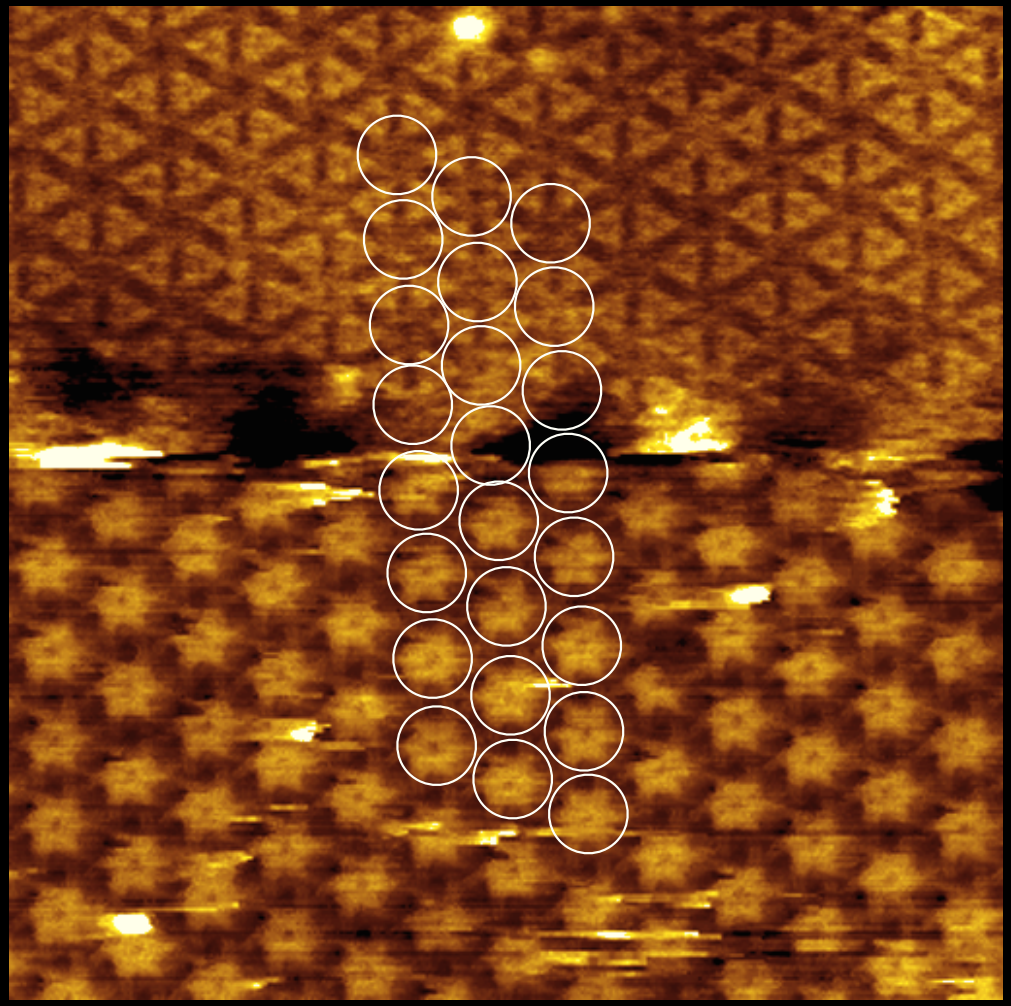

1

2

minimal force (~100pN)

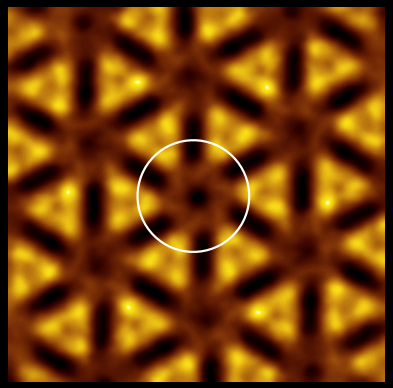

+600pN

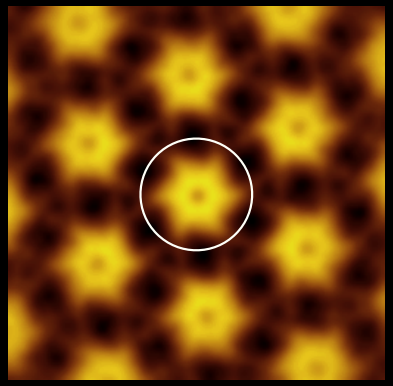

1: triangular surface
2: flower-shaped surface

force applied to the AFM tip

AFM overview topograph of the proteolyzed sample

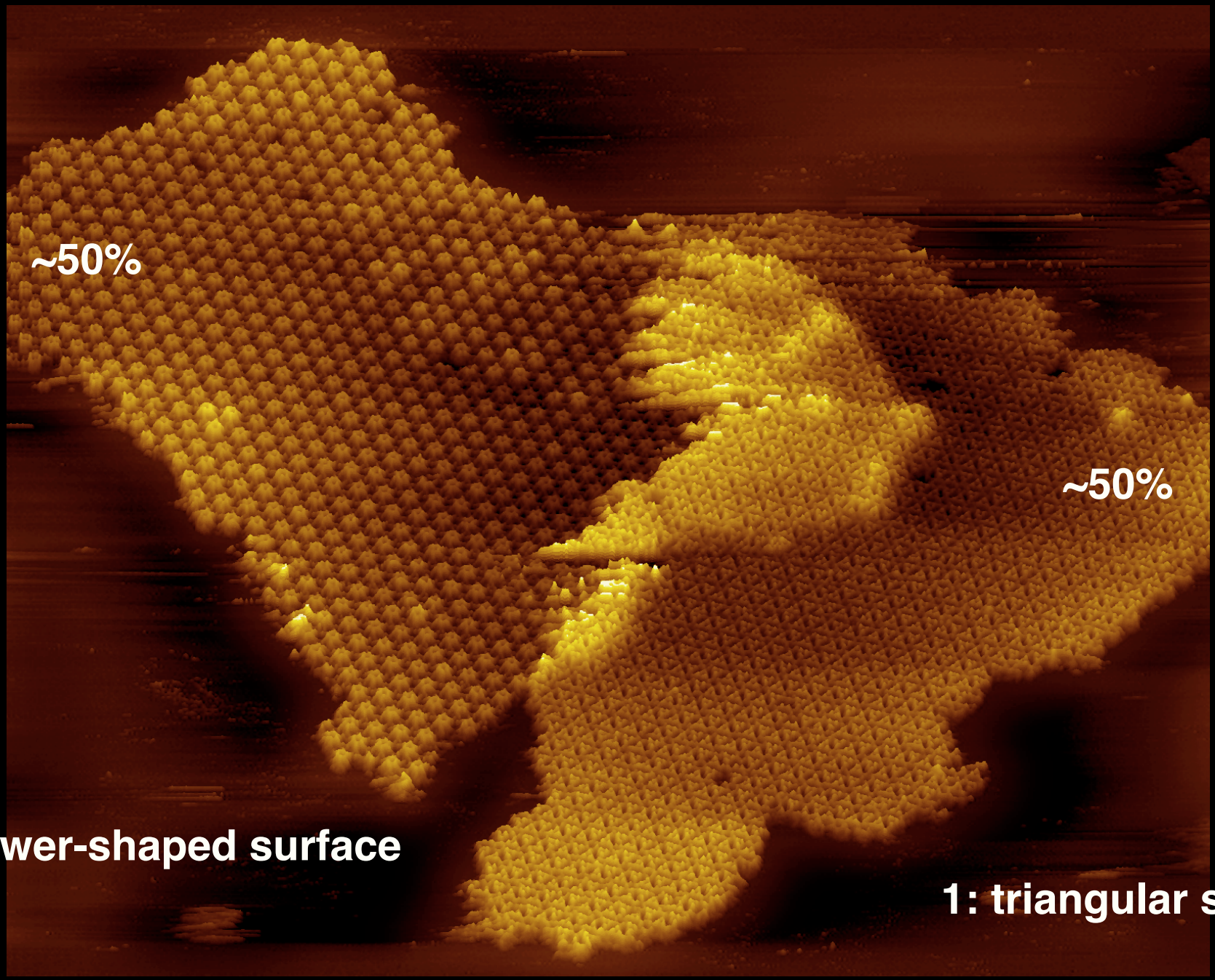

Raw data topographs diffract to 1nm resolutiuon

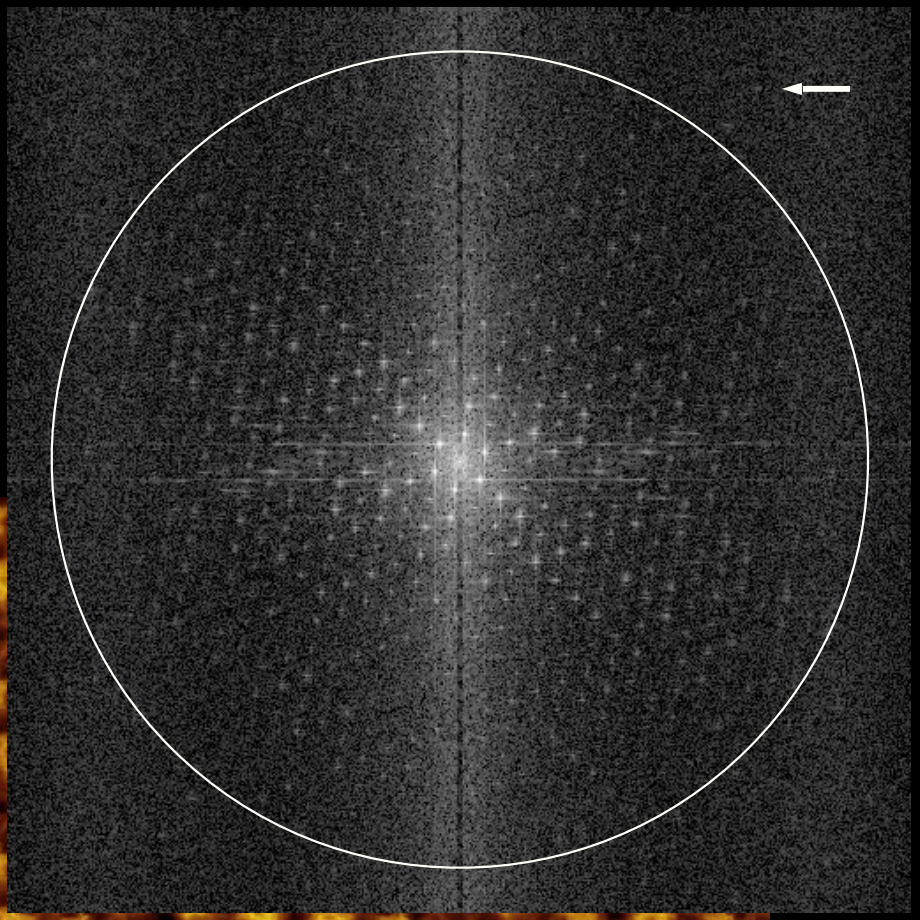

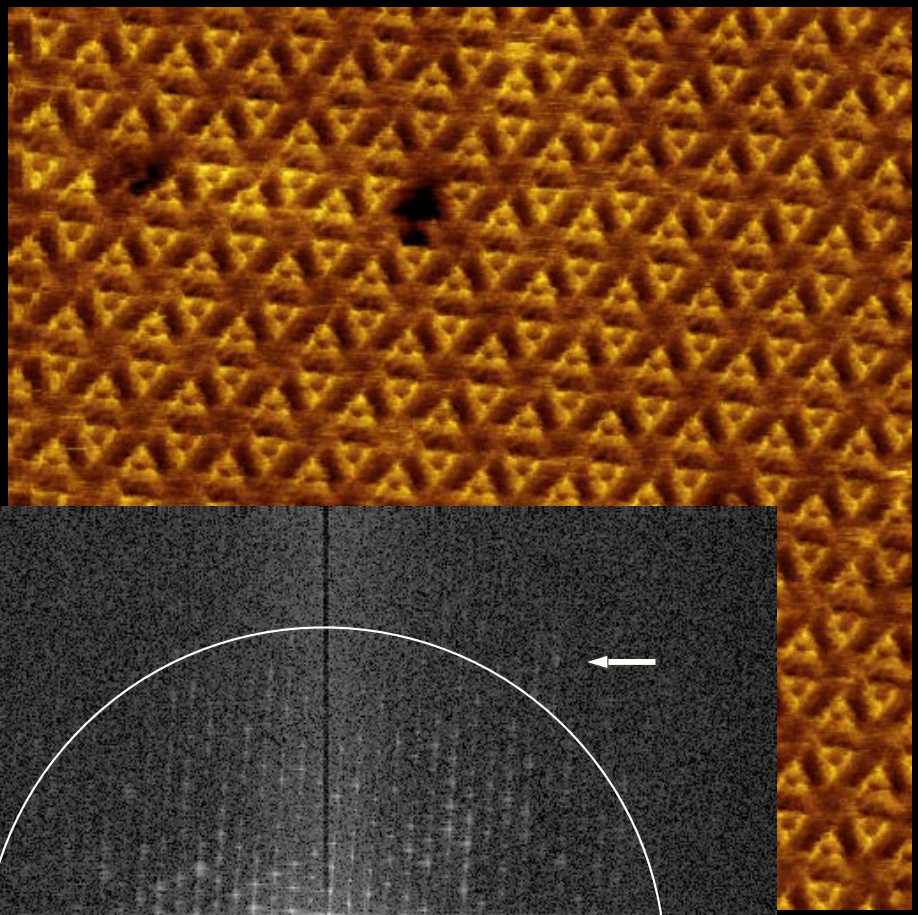

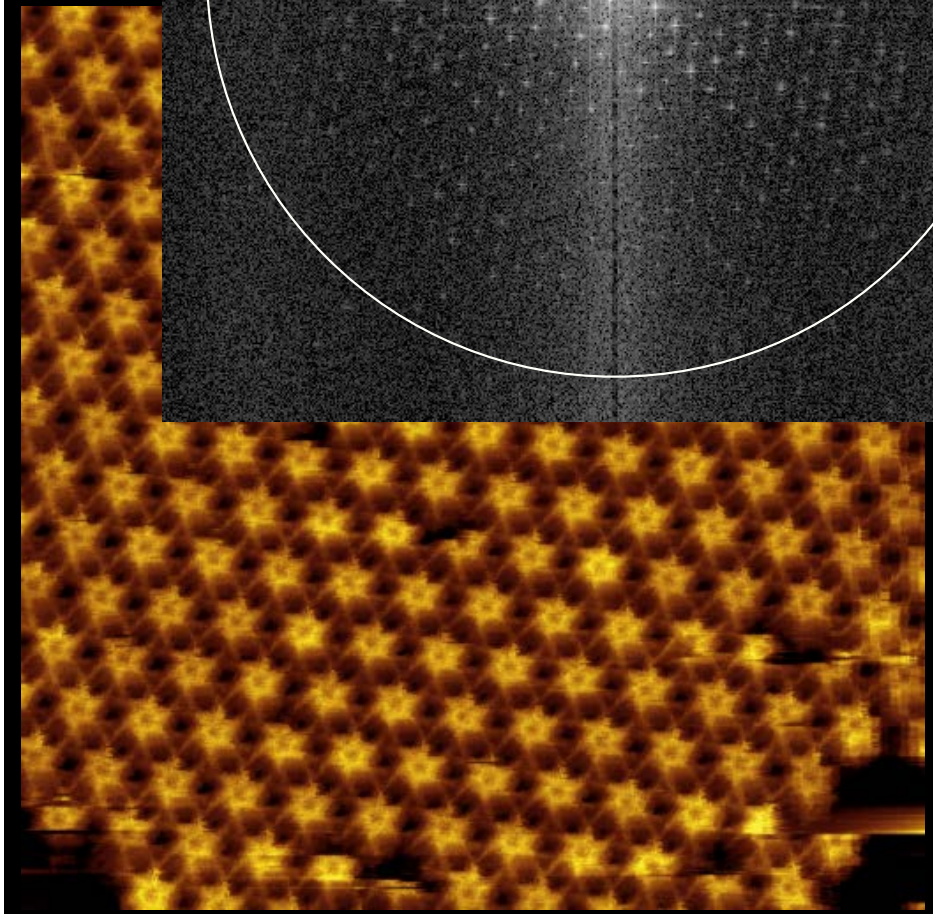

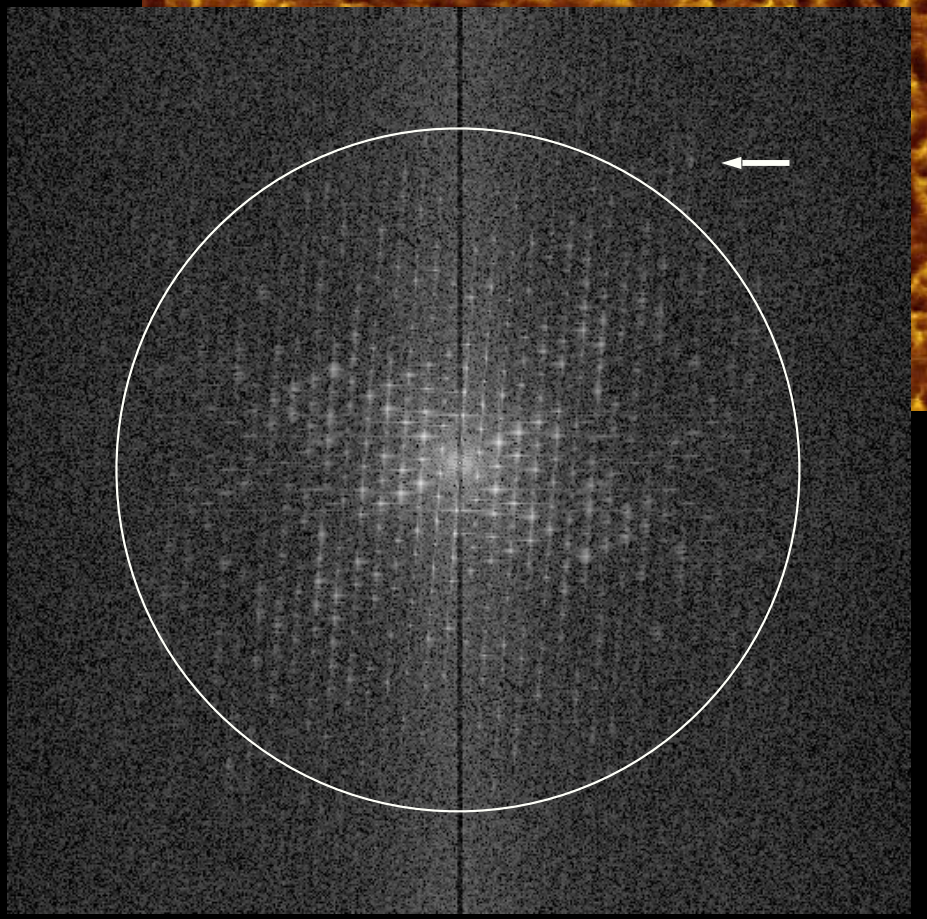

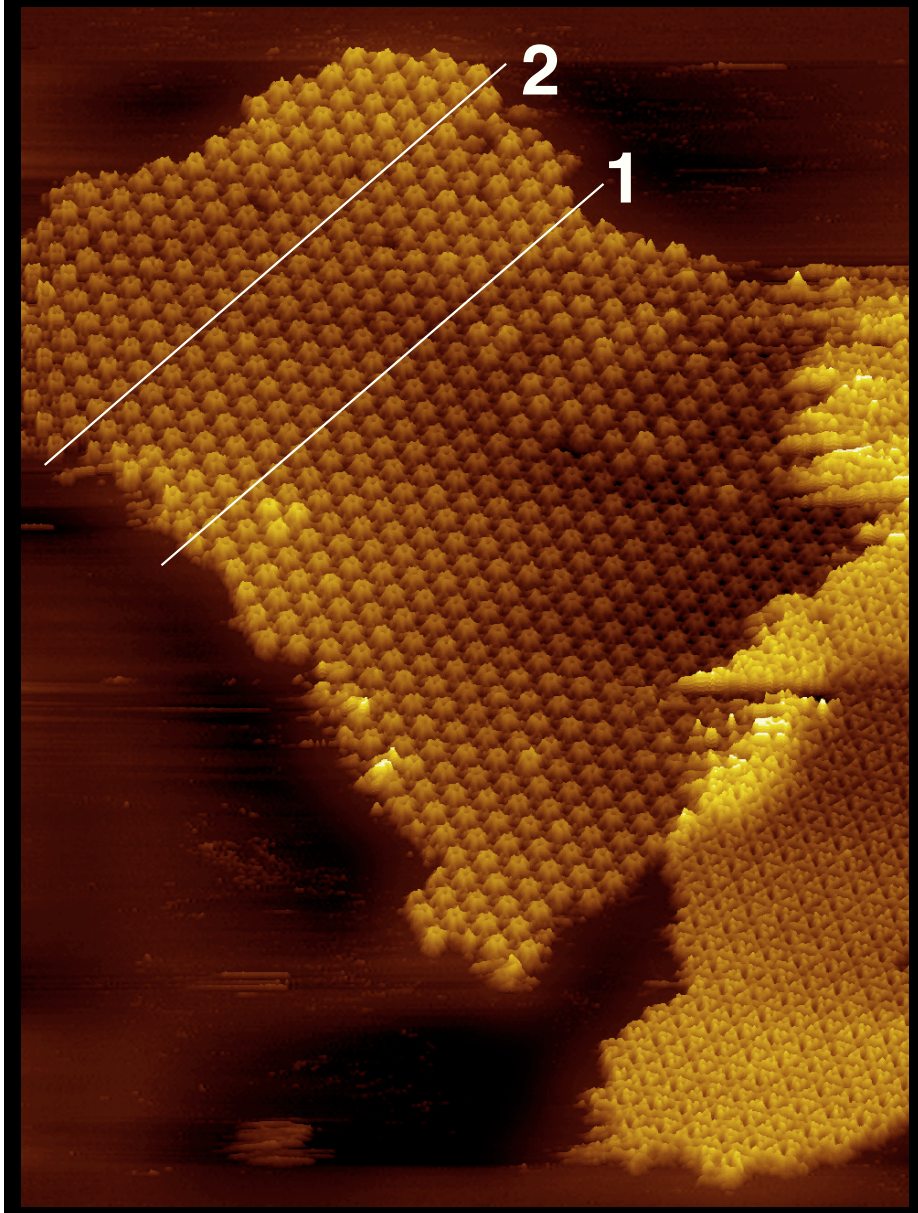

Section analysis

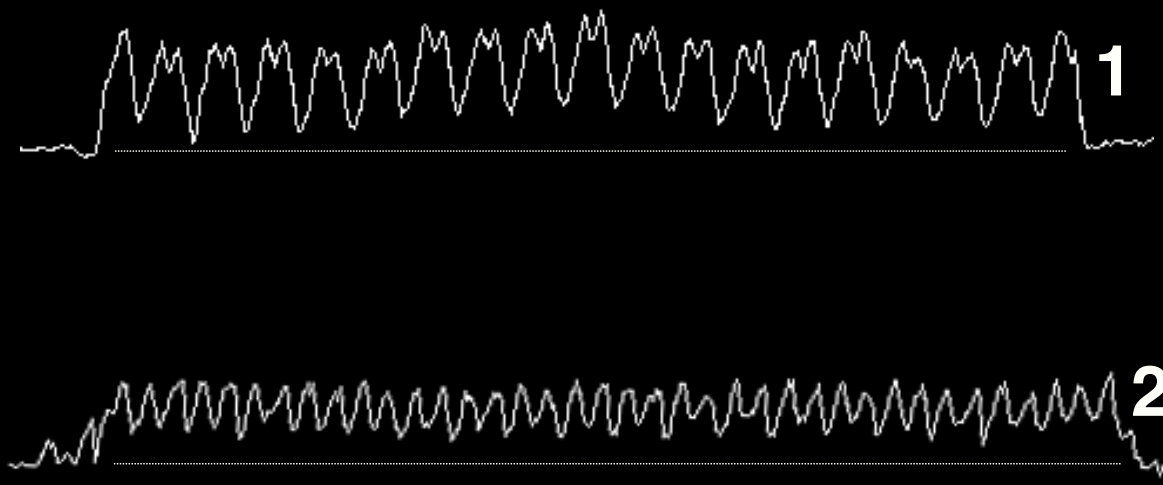

50nm

5nm

Section analysis

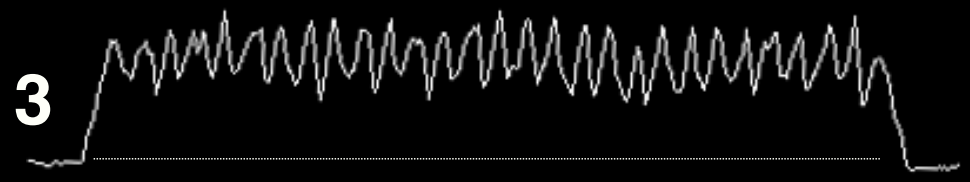

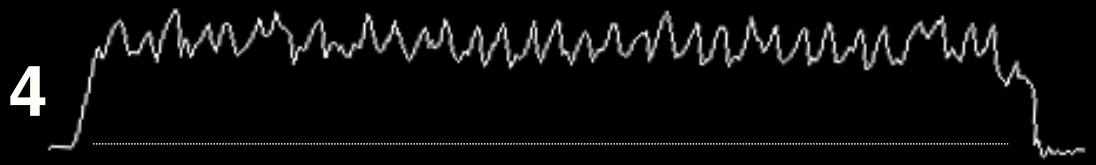

50nm

5nm

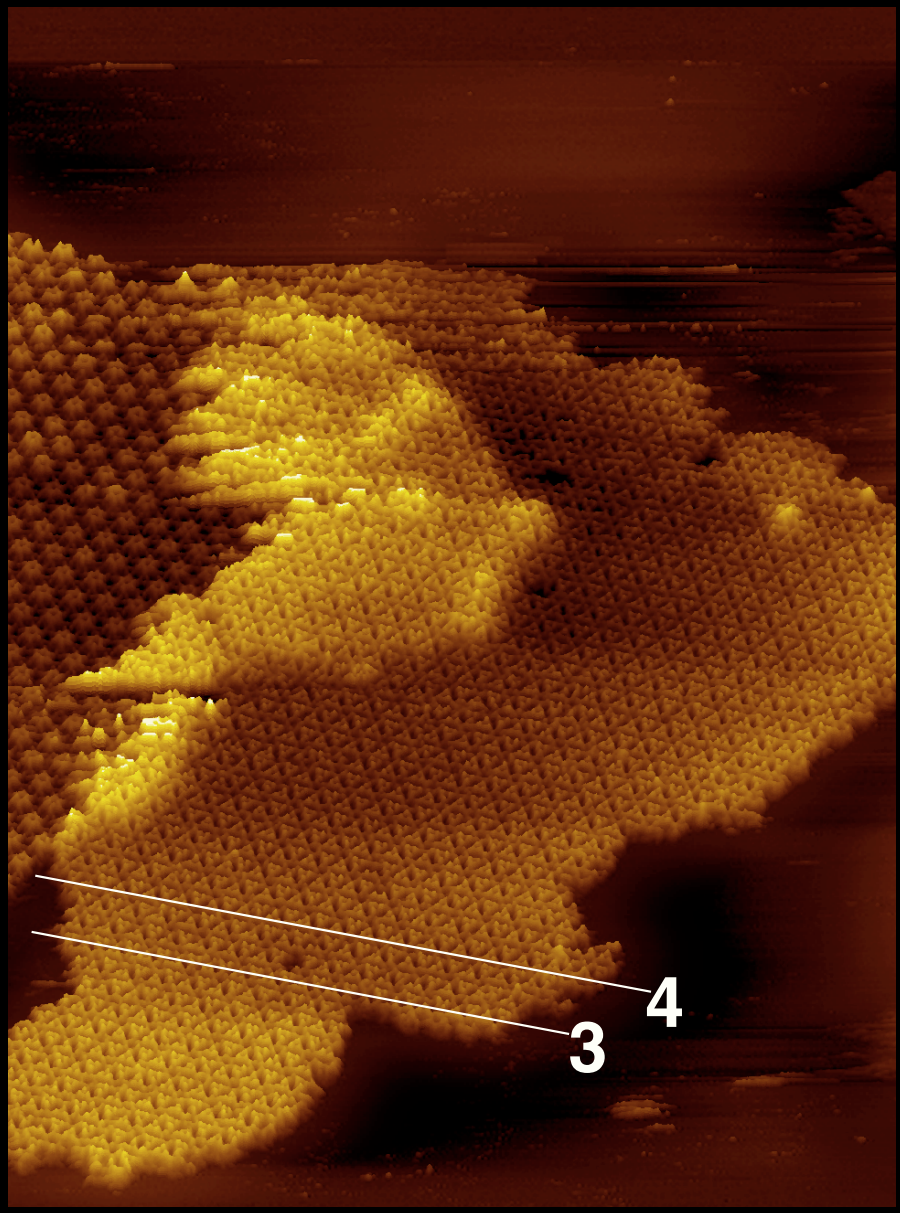

Localization of the C-terminus and sidedness assignment

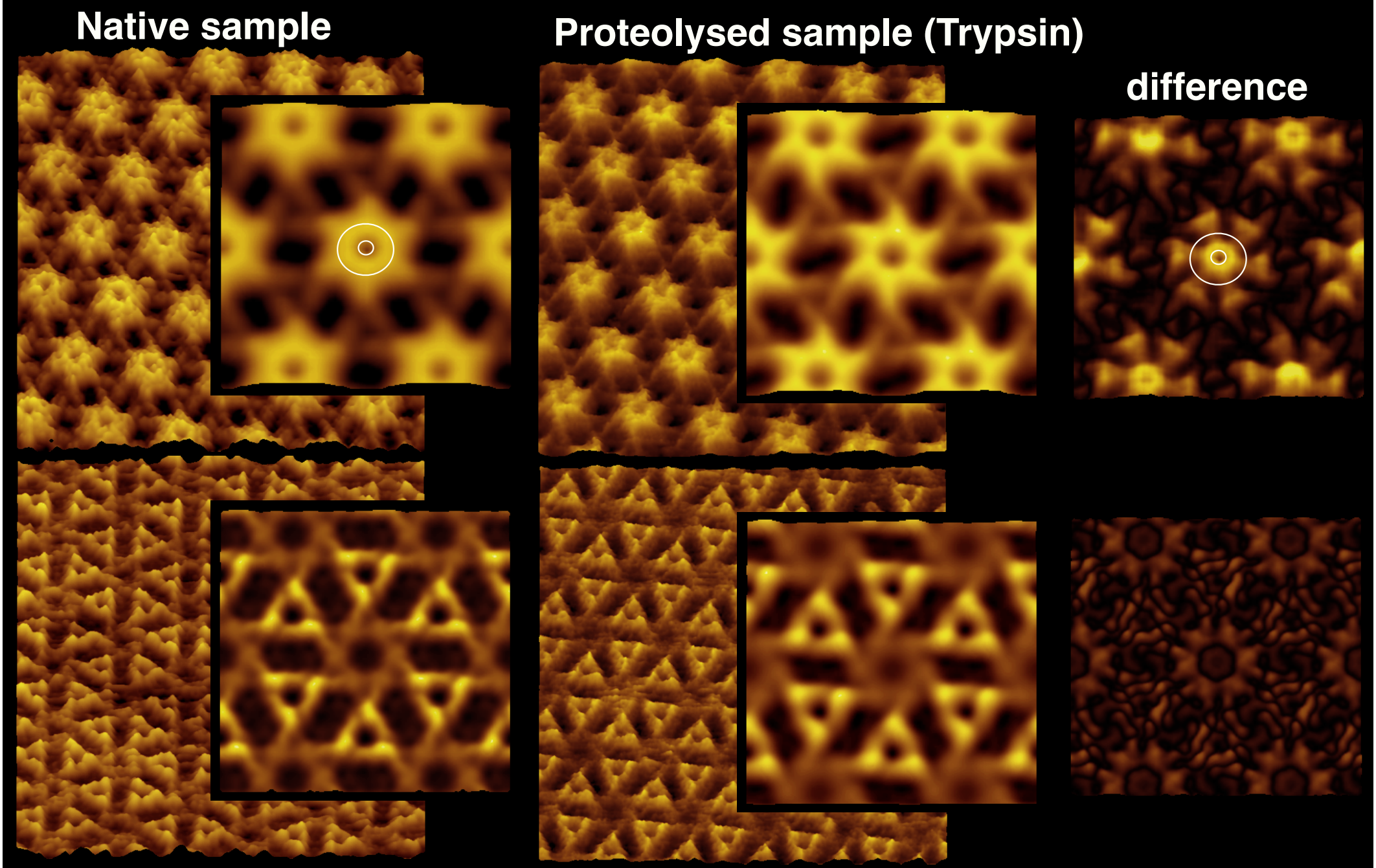

The Conformational Energy Landscape of Aquaporins

The tetrameric aquaporin has four channels through which water can very easily traverse the cellular membrane.
No other molecules or ions can traverse, not even hydrogens!

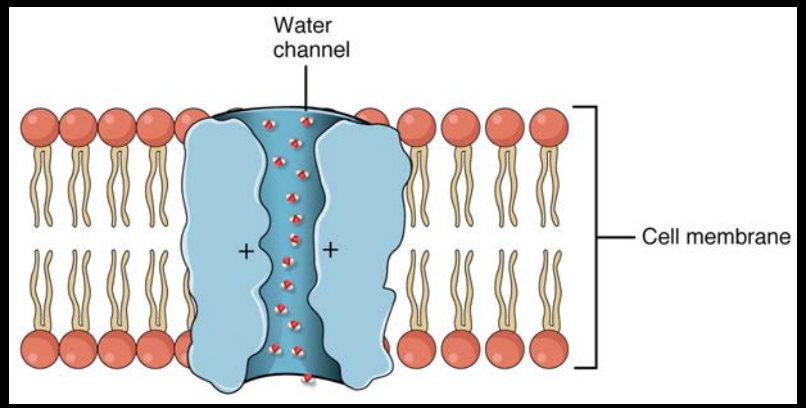

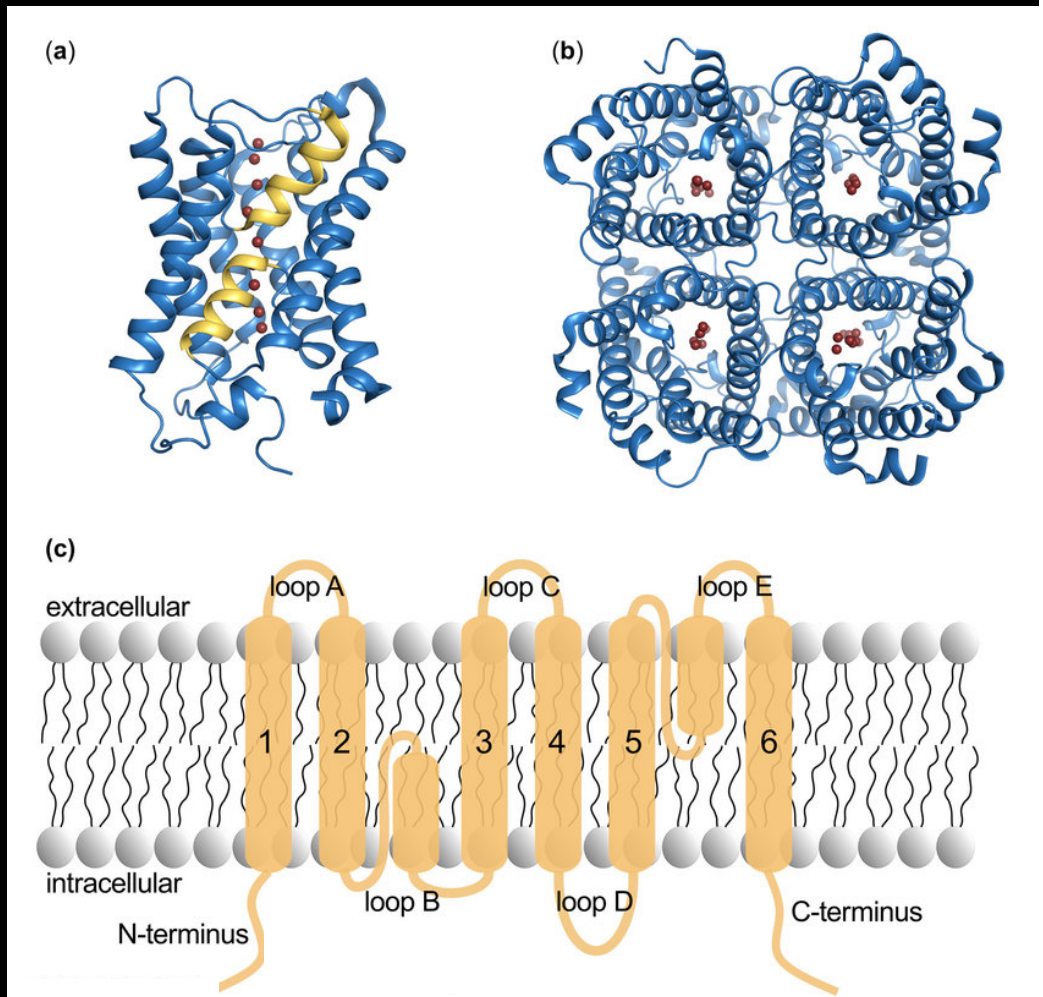

E. Coli Waterchannel AQPZ

Topography and molecular surface

The bacterial aquaporin AQPZ is here in an artificial membrane, where it is arranged in a 2D crystalline formation.

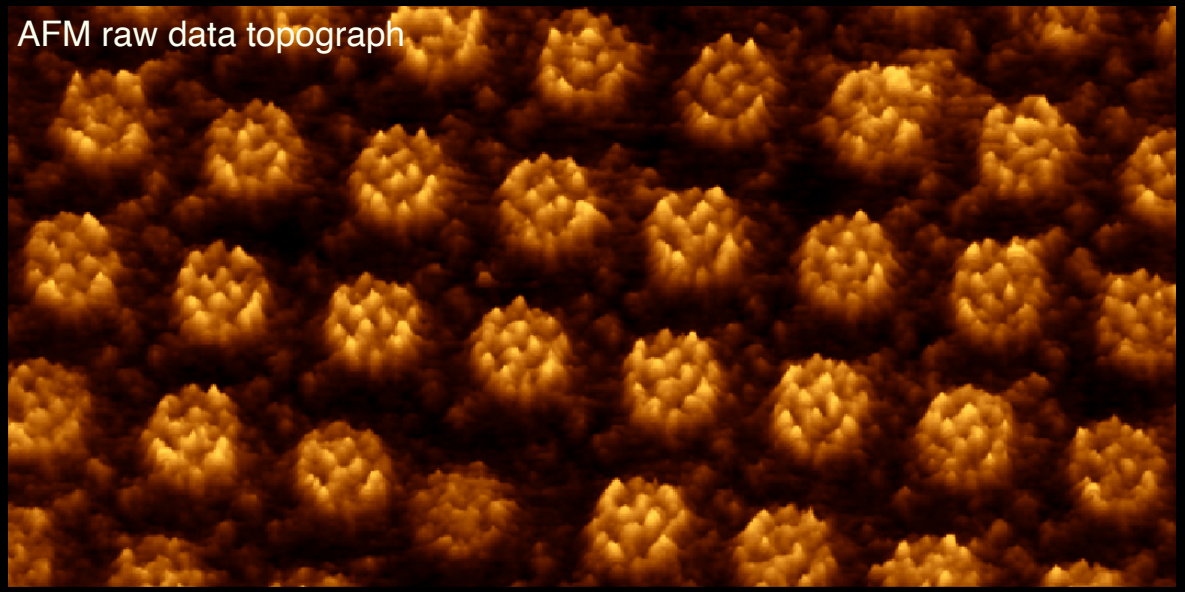

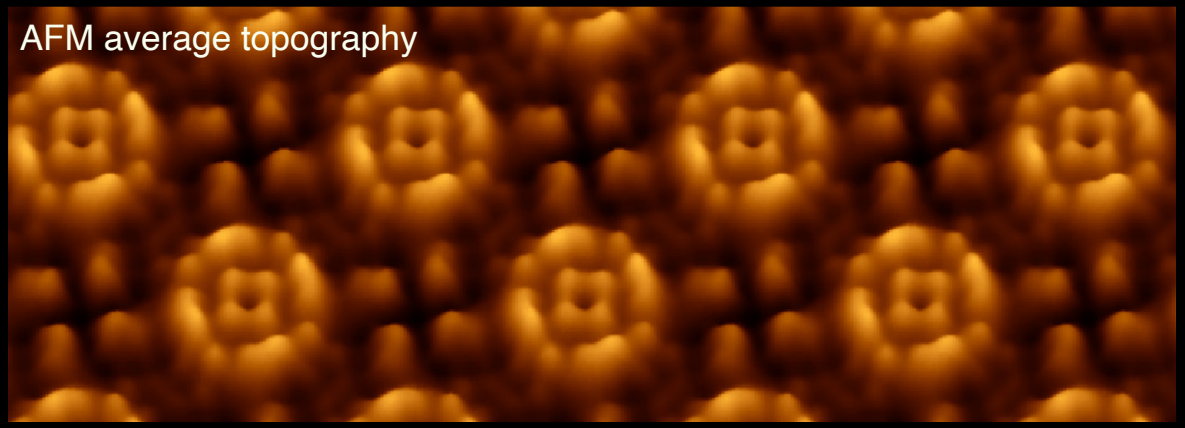

Molecular surface
X-ray structure (2.8Å)

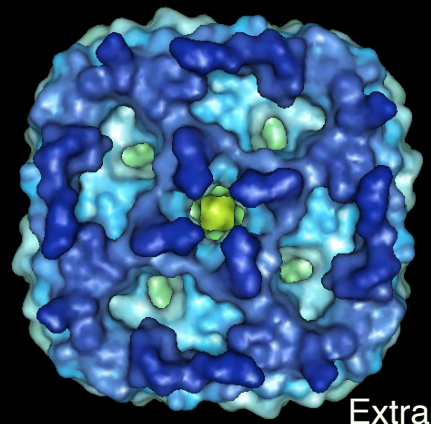

Extracellular surface

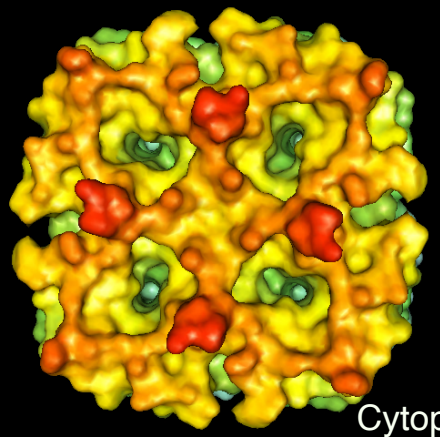

Cytoplasmic surface

Simon Scheuring
simon.scheuring@curie.fr
http://perso.curie.fr/Simon.Scheuring/

Conformational space of the AqpZ surface

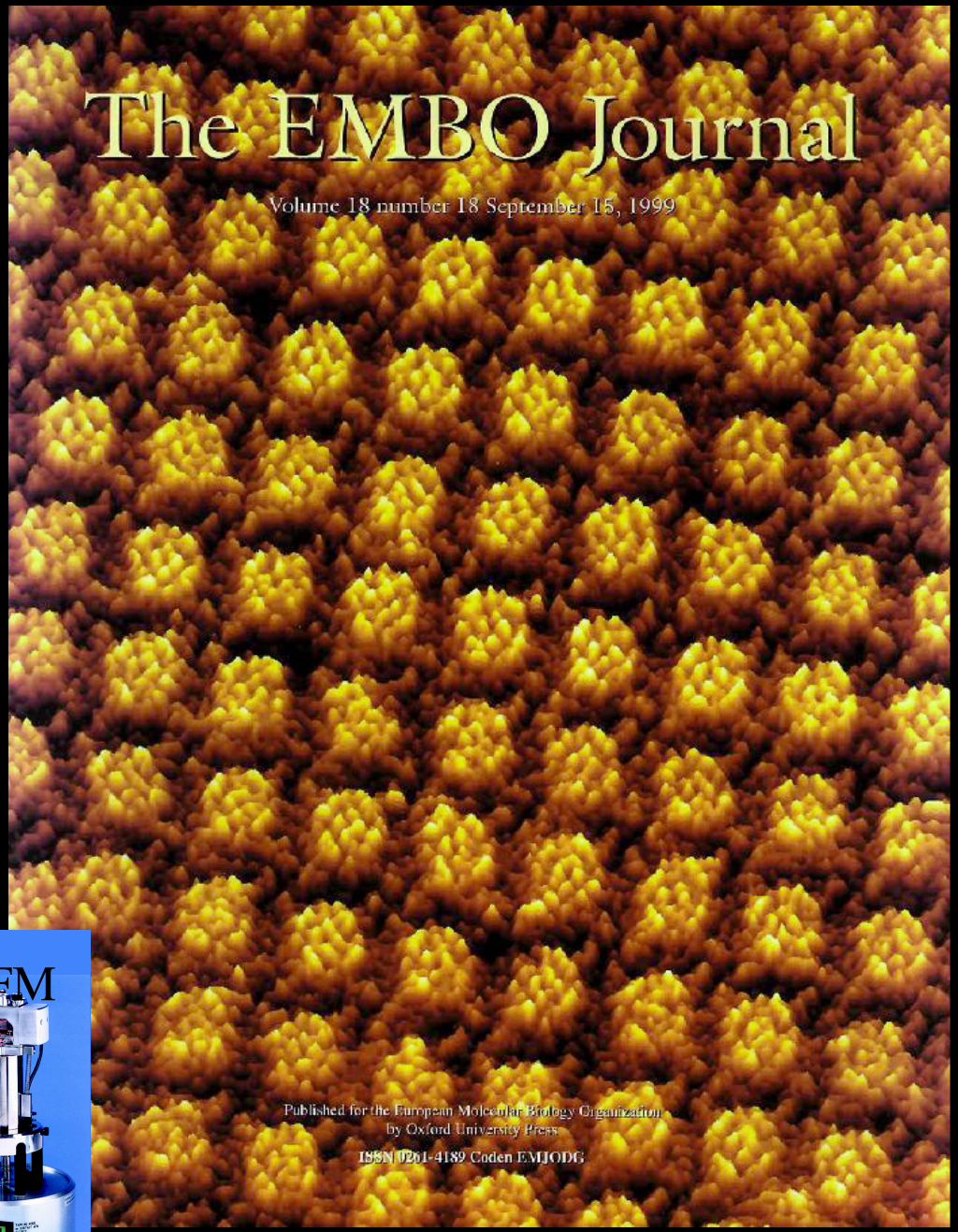

Similarity ranked images
are assembled into a movie

position probability

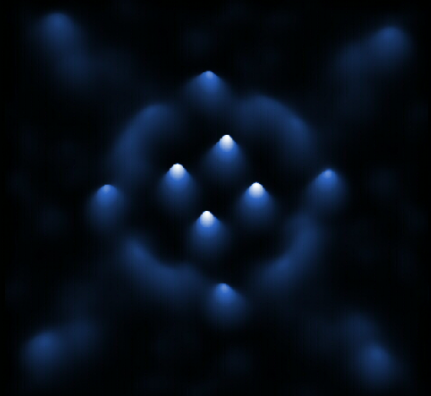

AqpZ: energy landscape

$p_d(r)$
peak position probability
of domain d

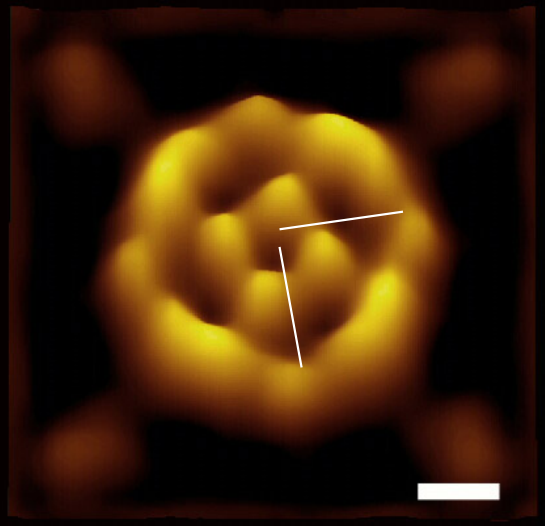

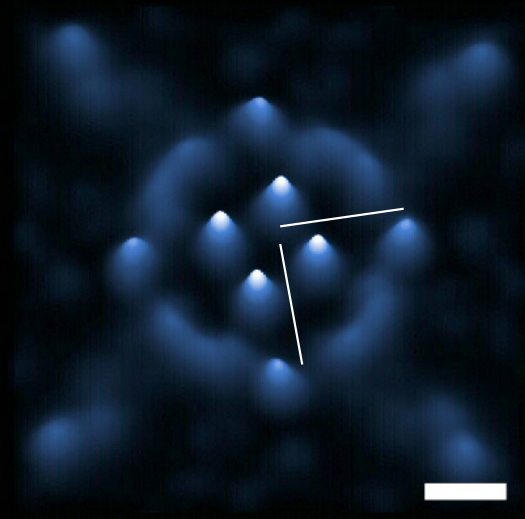

$F_d = -kT \ln p_d(r)$
Relative free energy

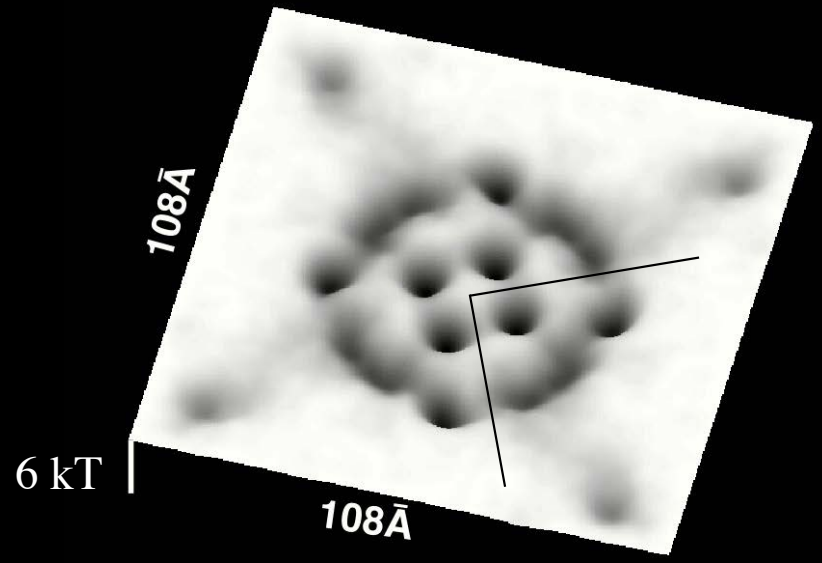

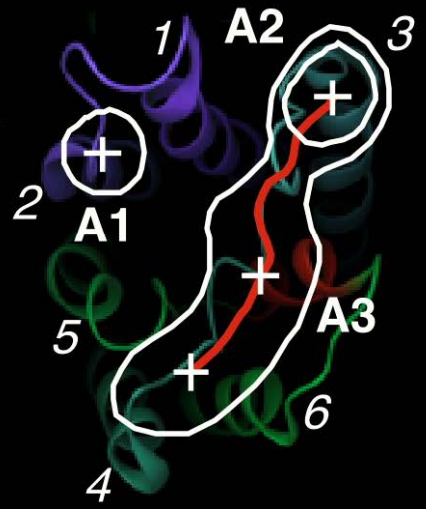

Scheuring *et al*., Europ. Biophys. J., 2003

Imaging
Native Membranes

The Bacterial Photosynthetic Apparatus

The core-complex : reaction center (RC) & light harvesting complex 1 (LH1)

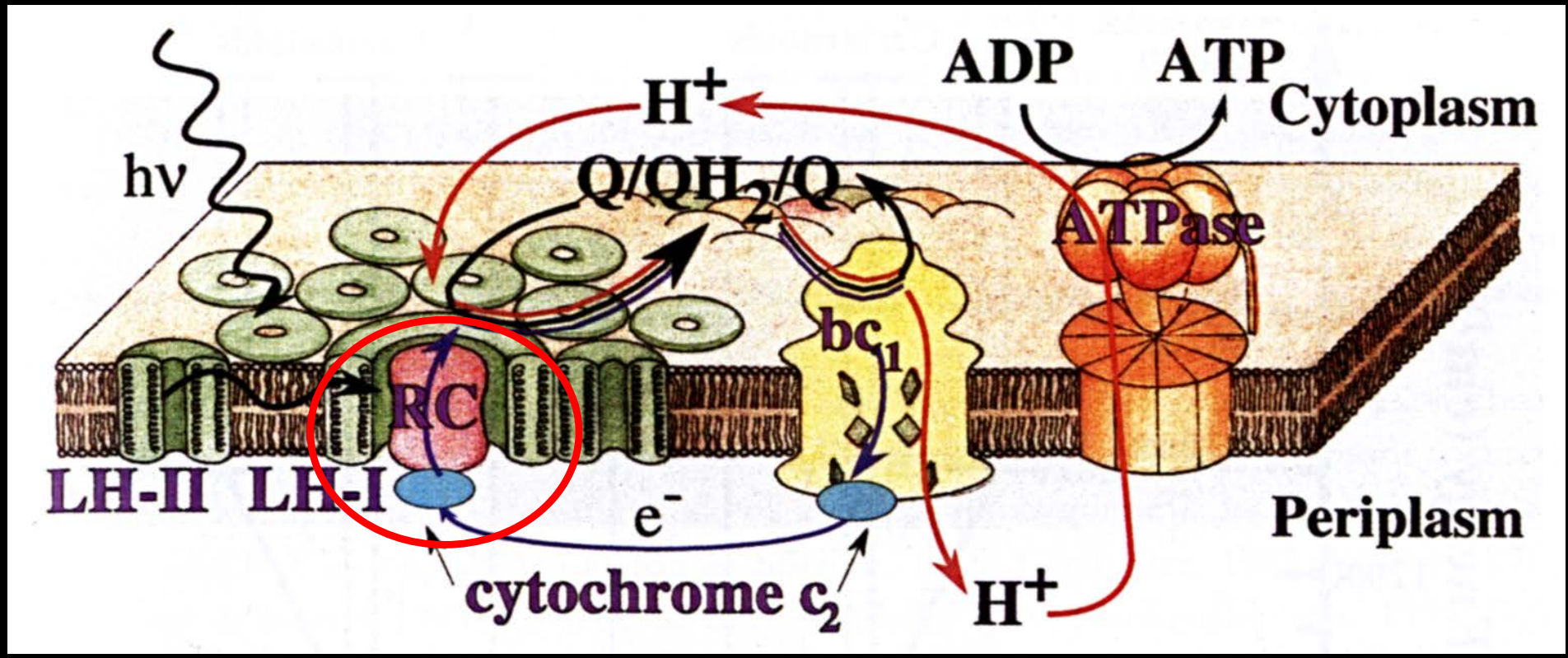

Hu, X., Ritz, T., Damjanovic, A., Autenrieth, F. & Schulten, K. (2002).
Photosynthetic apparatus of purple bacteria. Quart. Rev. Biophys. 35 (1), 1-62.

Blastochloris Viridis Core-Complex

Model

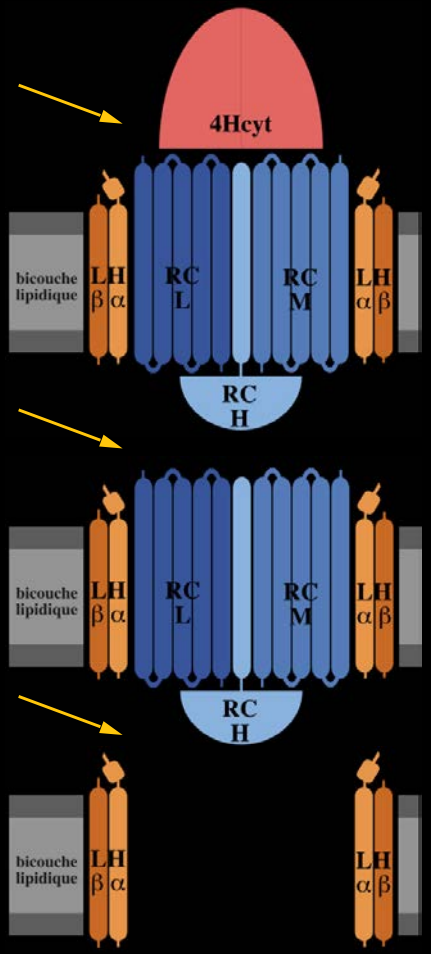

AFM (raw data topograph)

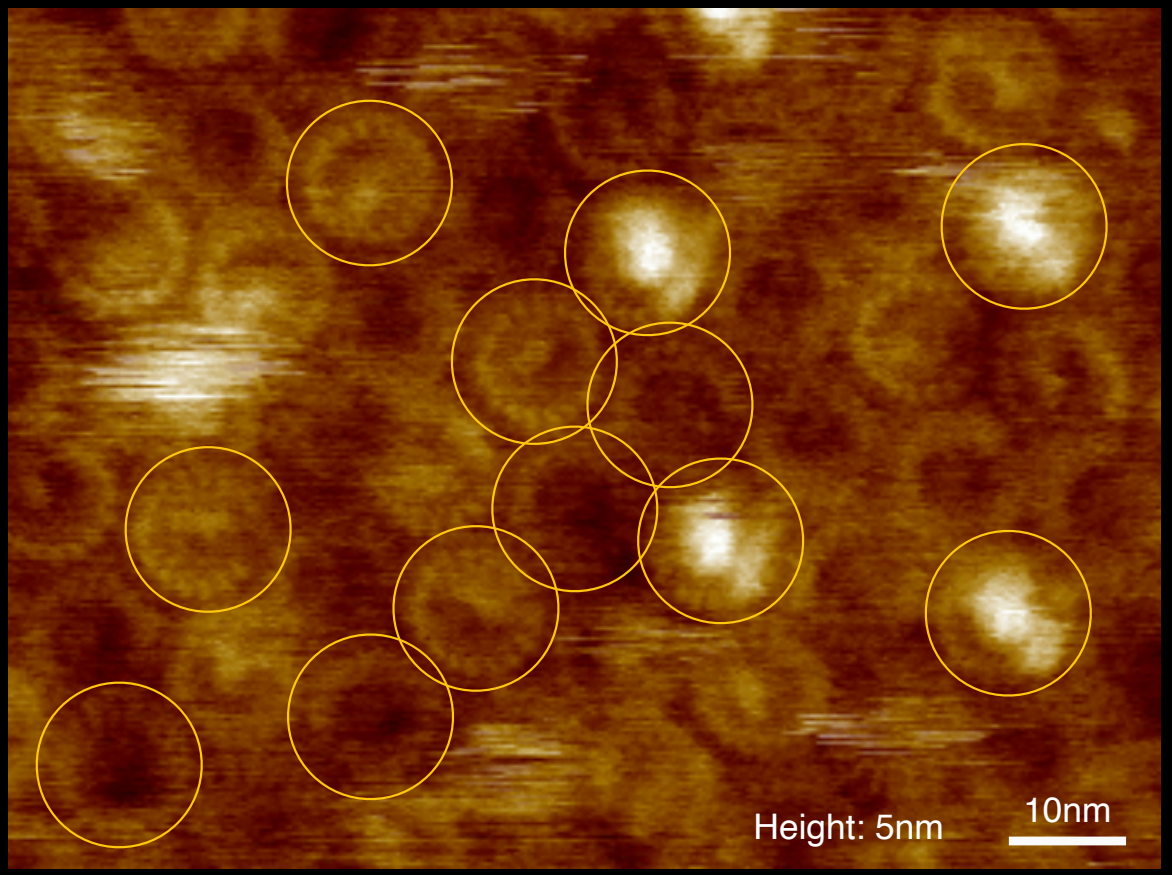

Averages

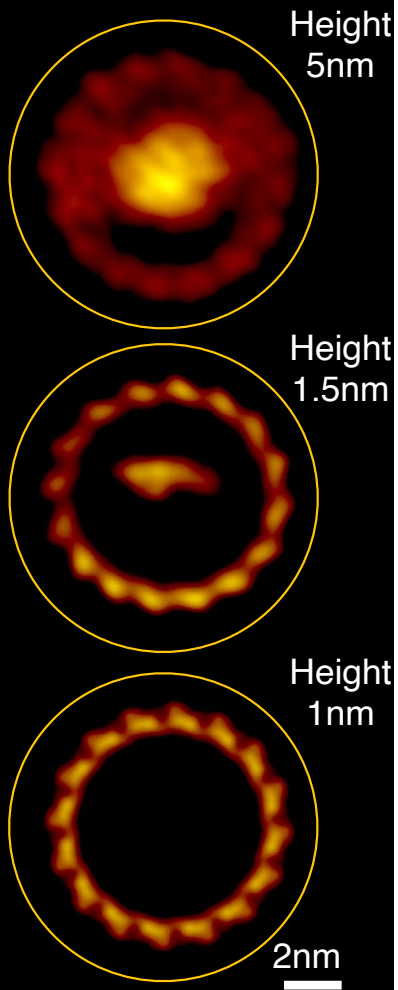

Scheuring, S.*, Seguin, J., Marco, S., Lévy, D., Robert, B. & Rigaud, J.L. (2003)
Nanodissection and high-resolution imaging of the Rhodopseudomonas viridis photosynthetic core-complex in native membranes by AFM.
PNAS, 100, 1690-1693.

Blastochloris Viridis Core-Complex

AFM topograph

AFM topograph

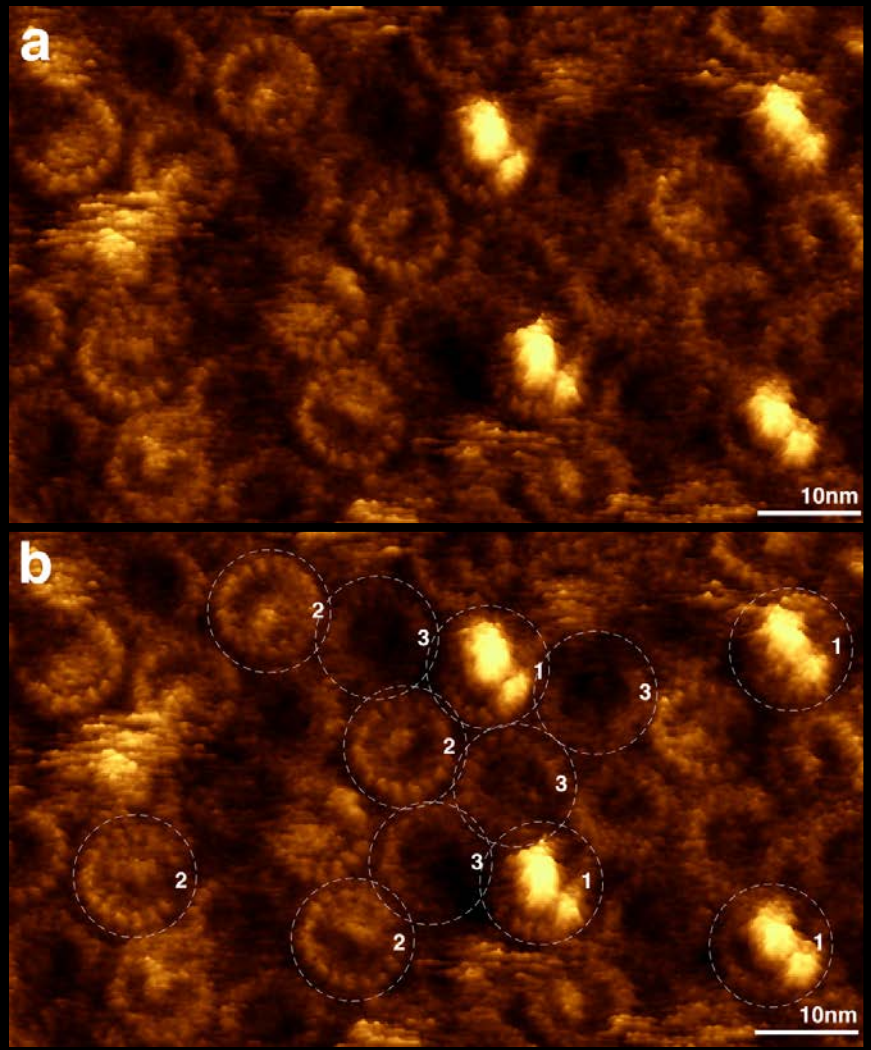

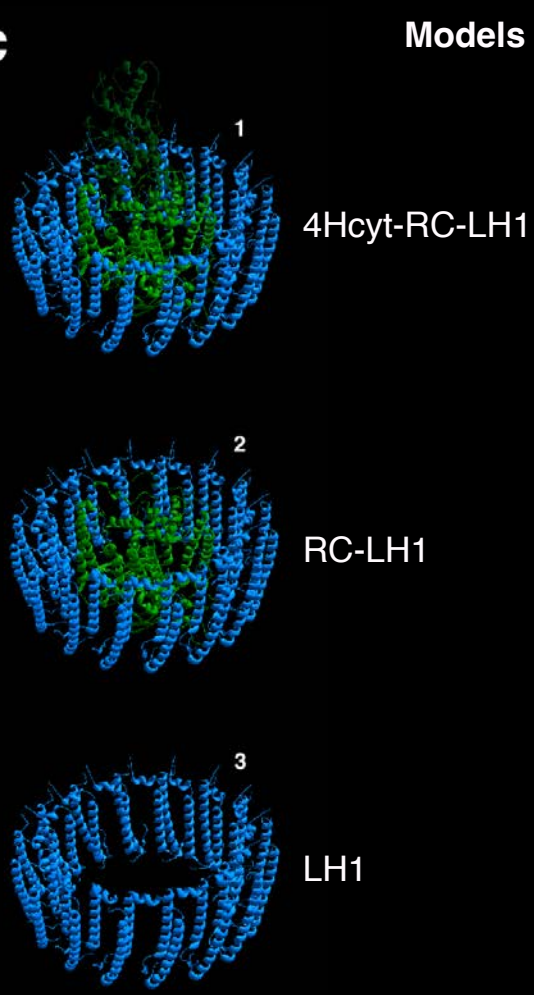

Scheuring, S.*, Seguin, J., Marco, S., Lévy, D., Robert, B. & Rigaud, J.L. (2003)
Nanodissection and high-resolution imaging of the Rhodopseudomonas viridis photosynthetic core-complex in native membranes by AFM.
PNAS, 100, 1690-1693.

Blastochloris Viridis Core-Complex

The LH1 subunits around the RC

Raw data AFM topograph

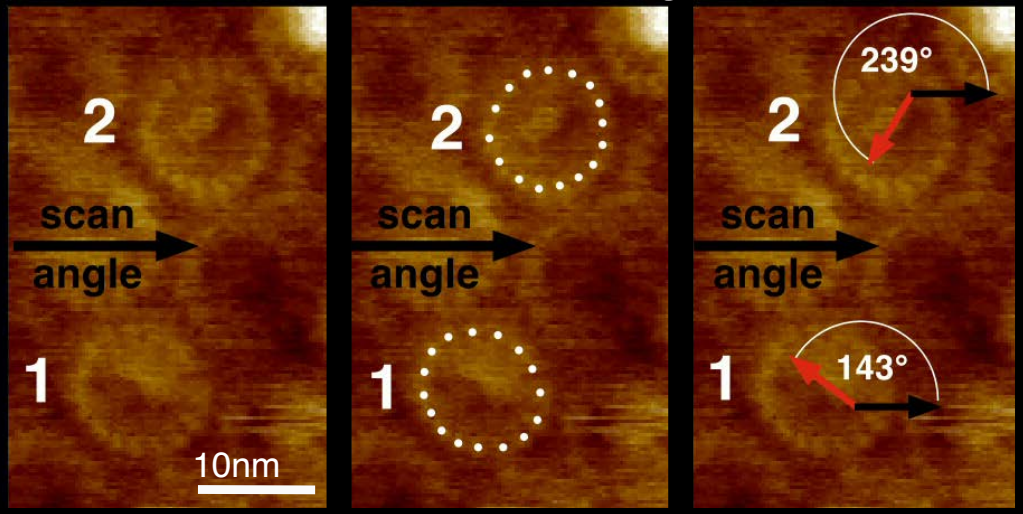

LH1 subunits distribution and RC orientation

Computed models

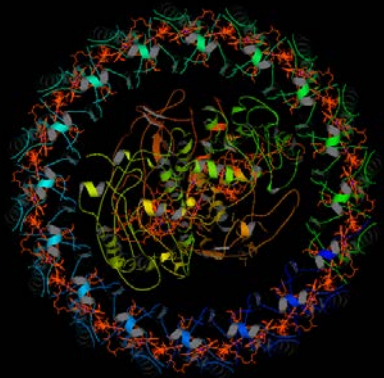

Isaacs group
http://www.chem.gla.ac.uk/protein/LH2/core.html

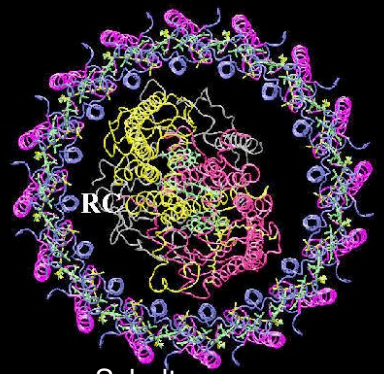

Schulten group
http://www.ks.uiuc.edu/Research/psu/psu_model.html

Scheuring, S.*, Seguin, J., Marco, S., Lévy, D., Robert, B. & Rigaud, J.L. (2003)
Nanodissection and high-resolution imaging of the Rhodopseudomonas viridis photosynthetic core-complex in native membranes by AFM.
PNAS, 100, 1690-1693.

Rhodobacter Blasticus Core-Complex

High-resolutionAFM topograph

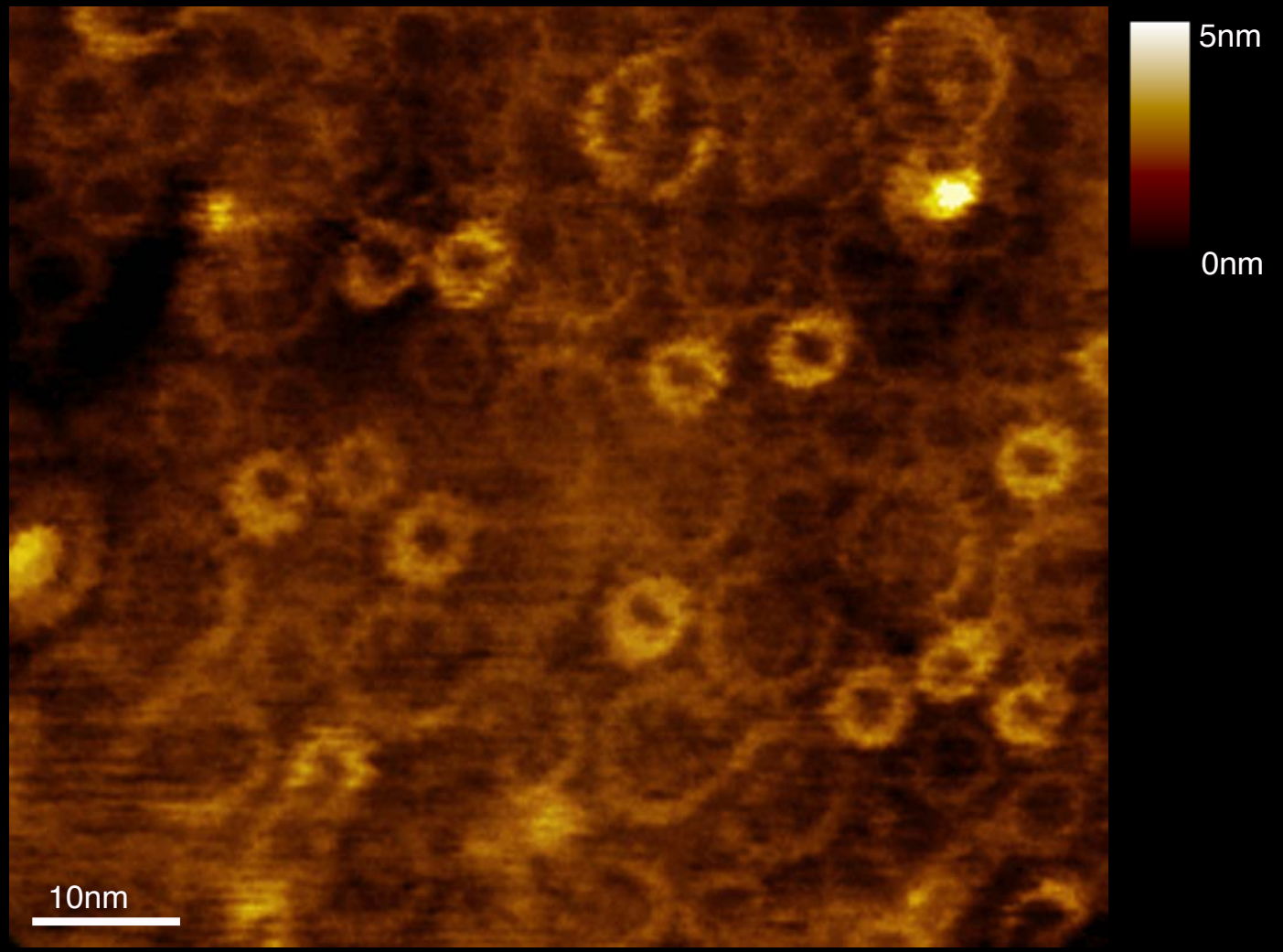

Scheuring, S.*, Busselez, J., & Lévy, D. (2005)
Structure of the dimeric PufX–containing core complex of Rhodobacter blasticus by in situ AFM.
JBC, 2005, 280, 2, 1426-1431.

Rhodobacter Blasticus Core-Complex

S-shaped dimeric core-complexes

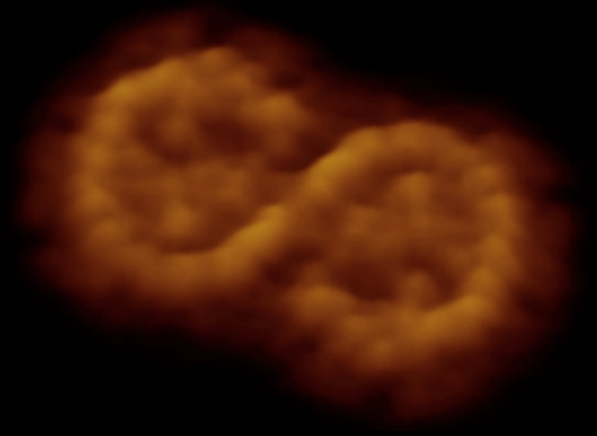

Height: 8Å

10nm

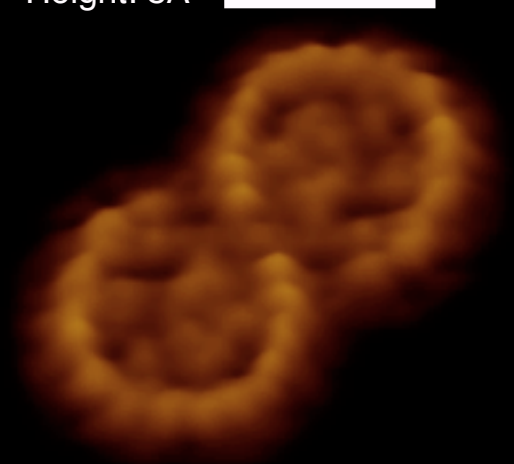

2-fold-symmetrized

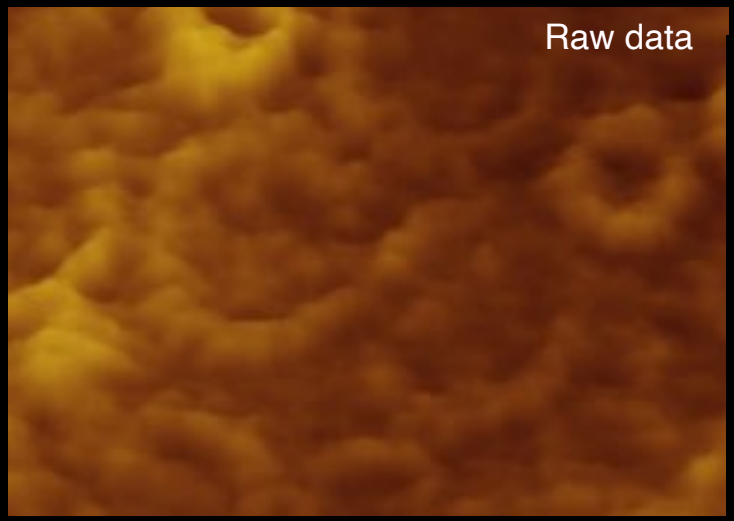

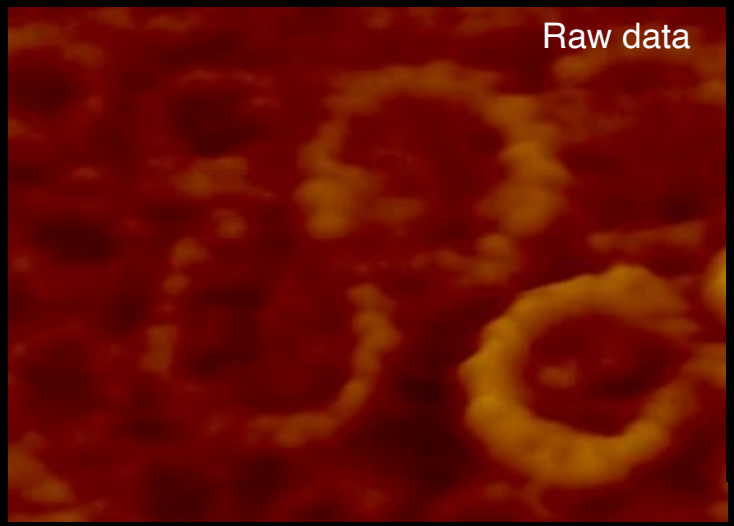

Average

Scheuring, S.*, Busselez, J., & Lévy, D. (2005)
Structure of the dimeric PufX–containing core complex of Rhodobacter blasticus by in situ AFM.
JBC, 2005, 280, 2, 1426-1431.

Rhodobacter Blasticus Core-Complex

Localization of PufX

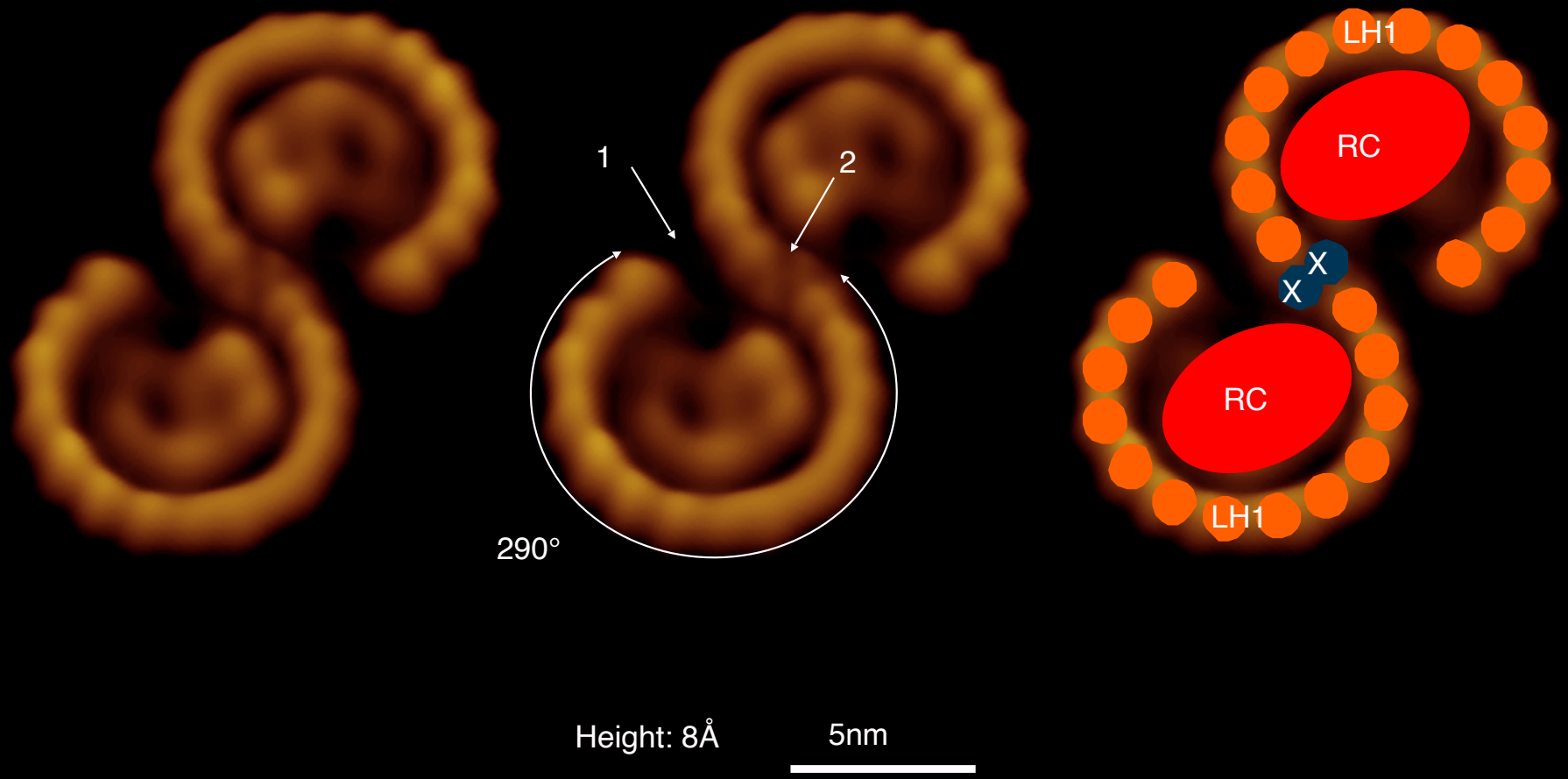

Scheuring, S.*, Busselez, J., & Lévy, D. (2005)
Structure of the dimeric PufX–containing core complex of Rhodobacter blasticus by in situ AFM.
JBC, 2005, 280, 2, 1426-1431.

Rhodobacter Blasticus Core-Complex

Model & Data

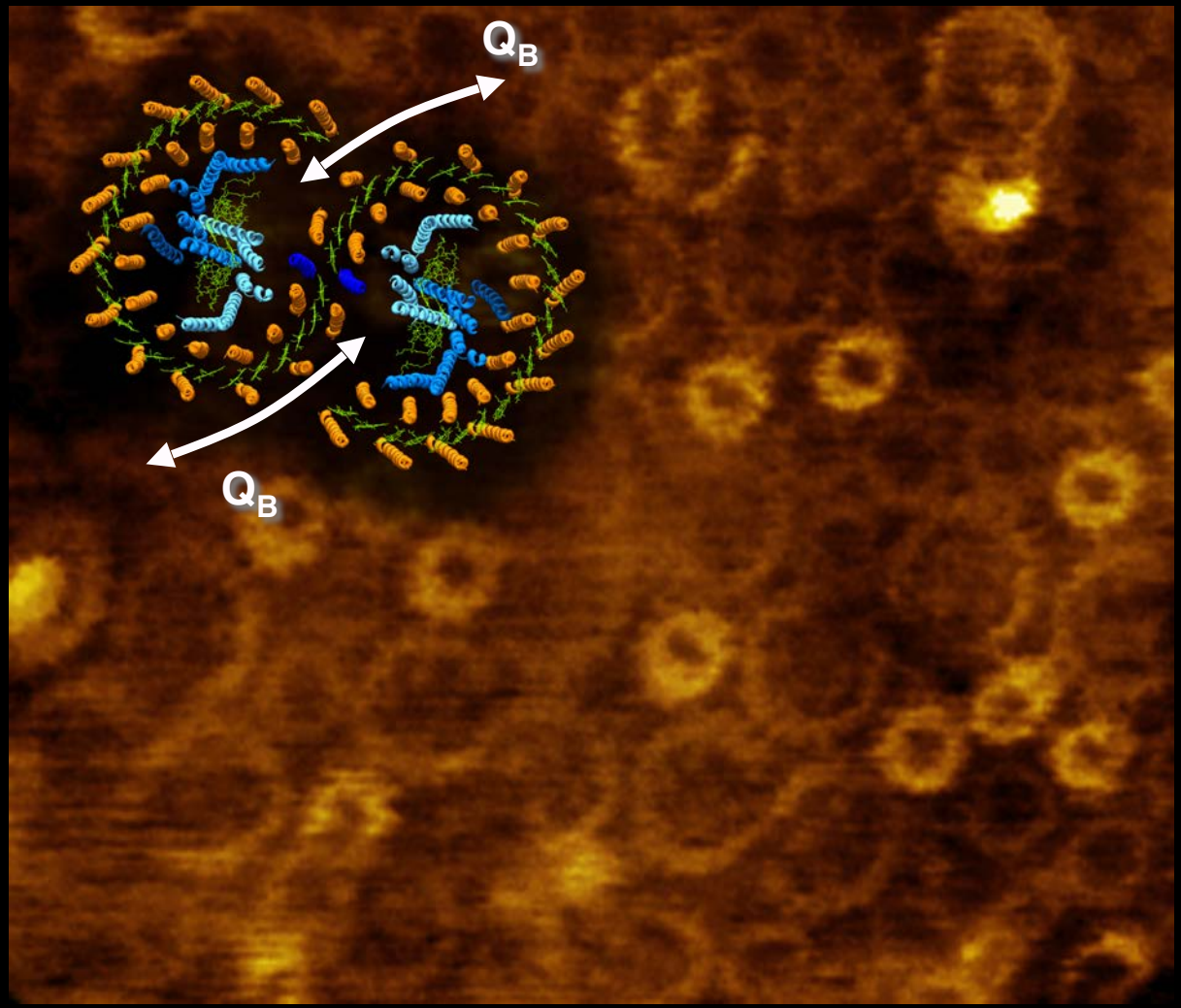

Scheuring, S.*, Busselez, J., & Lévy, D. (2005)
Structure of the dimeric PufX–containing core complex of Rhodobacter blasticus by in situ AFM.
JBC, 2005, 280, 2, 1426-1431.

Imaging of membrane protein supercomplexes

The Bacterial Photosynthetic Apparatus

The apparatus : light harvesting complex 2 (LH2) & light harvesting complex 1 (LH1) & reaction center (RC)

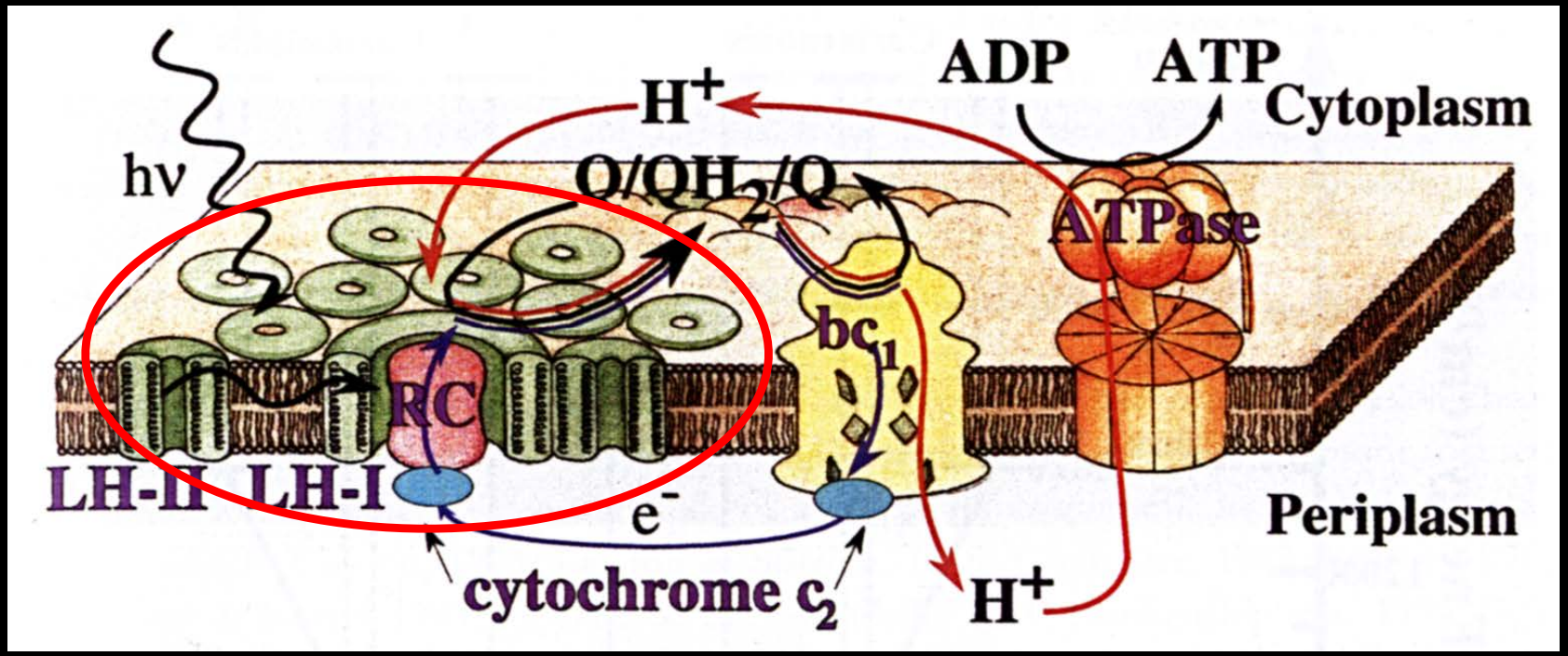

Hu, X., Ritz, T., Damjanovic, A., Autenrieth, F. & Schulten, K. (2002).
Photosynthetic apparatus of purple bacteria. Quart. Rev. Biophys. 35 (1), 1-62.

Rps. Photometricum Photosynthetic Apparatus

***Rhodopseudomonas photometricum* cells contain stacked intracytoplasmic membranes**

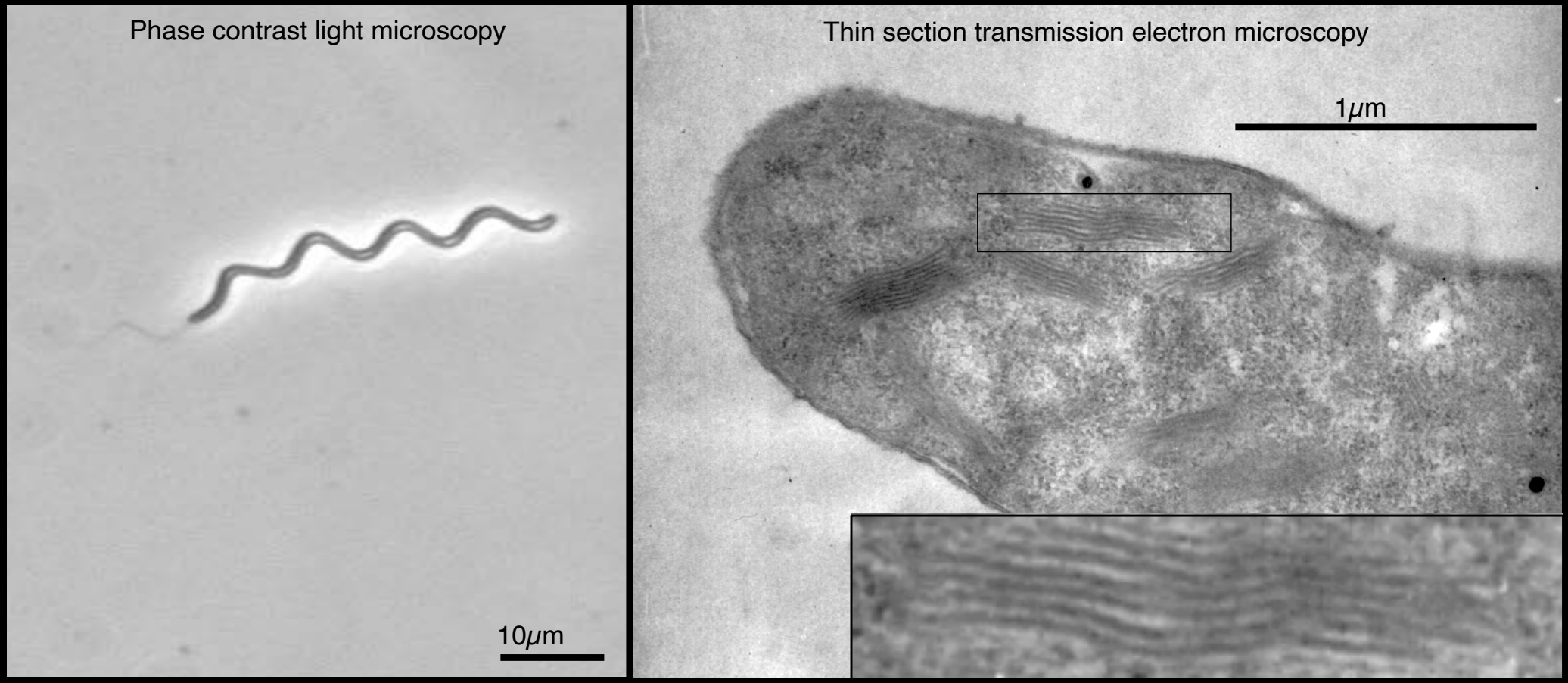

Scheuring, S.*, Sturgis, J., Prima, V., Bernadac, A., Lévy, D. & Rigaud, JL. (2004)
Watching the photosynthetic apparatus in native membranes.
PNAS, 2004, 101, 31, 11293-11297.

Rps. Photometricum Photosynthetic Apparatus

High-resolution topographs

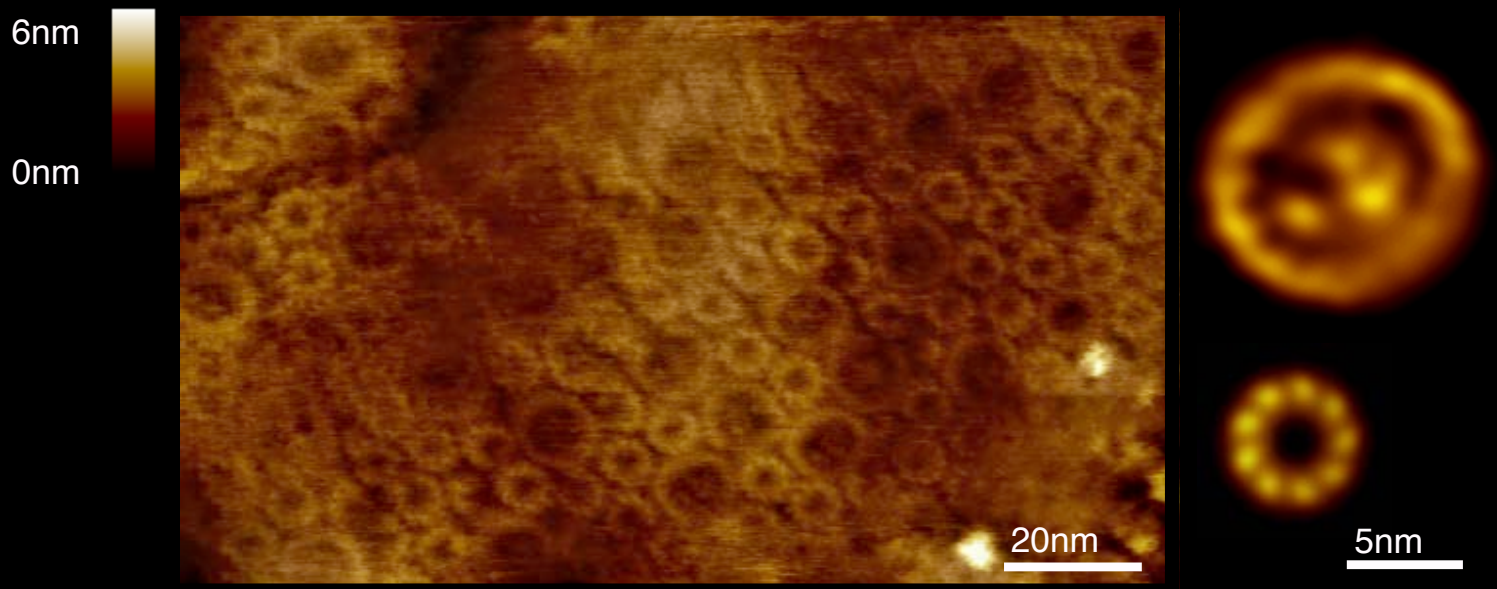

Scheuring, S.*, Rigaud, JL. & Sturgis, J. (2004)
Variable LH2 stoichiometry and core clustering in native membranes of Rhodospirillum photometricum.
EMBO J., 2004, 23, 21, 4127-4133.

Rps. Photometricum Photosynthetic Apparatus

Heterogeneity of LH2 complexes

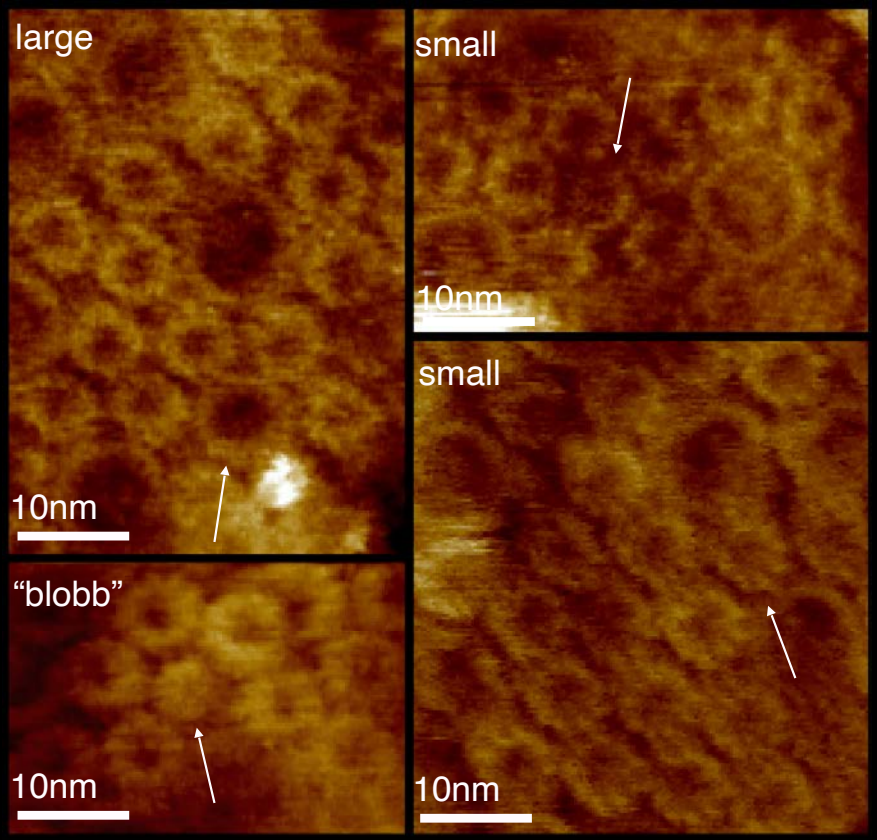

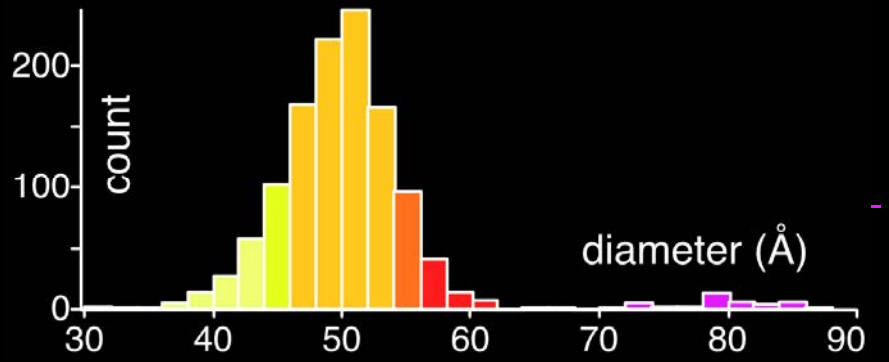

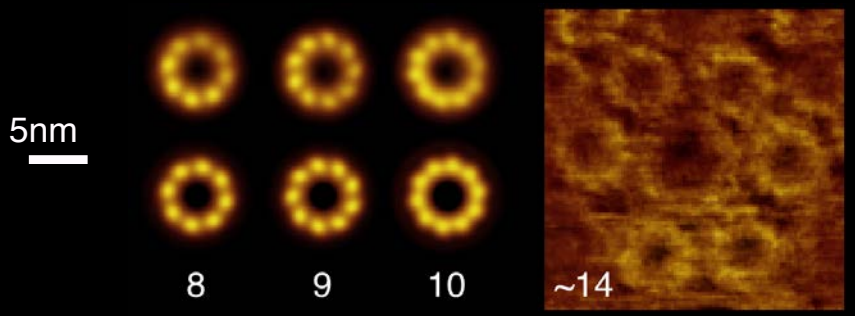

Scheuring, S.*, Rigaud, JL. & Sturgis, J. (2004)
Variable LH2 stoichiometry and core clustering in native membranes of Rhodospirillum photometricum.
EMBO J., 2004, 23, 21, 4127-4133.

Rps. Photometricum Photosynthetic Apparatus

There is no fixed assembly unit

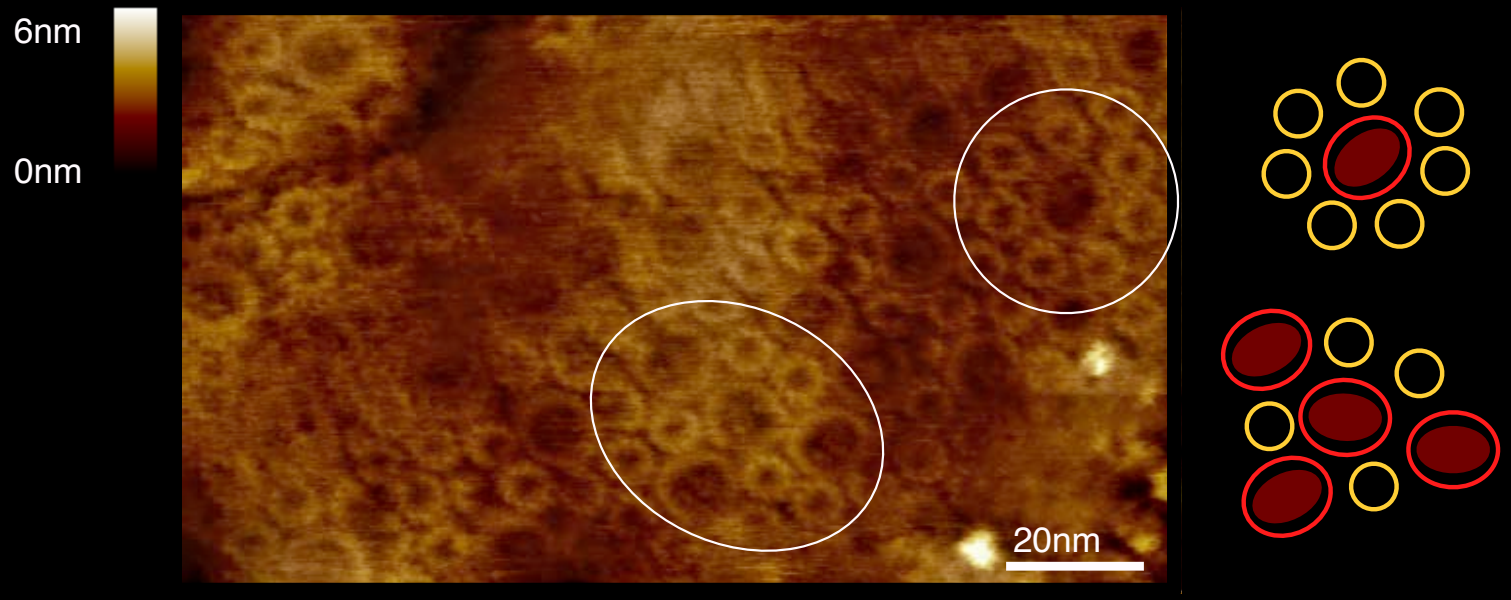

Scheuring, S.*, Rigaud, JL. & Sturgis, J. (2004)
Variable LH2 stoichiometry and core clustering in native membranes of Rhodospirillum photometricum.
EMBO J., 2004, 23, 21, 4127-4133.

Rps. Photometricum Photosynthetic Apparatus

There is no fixed assembly unit

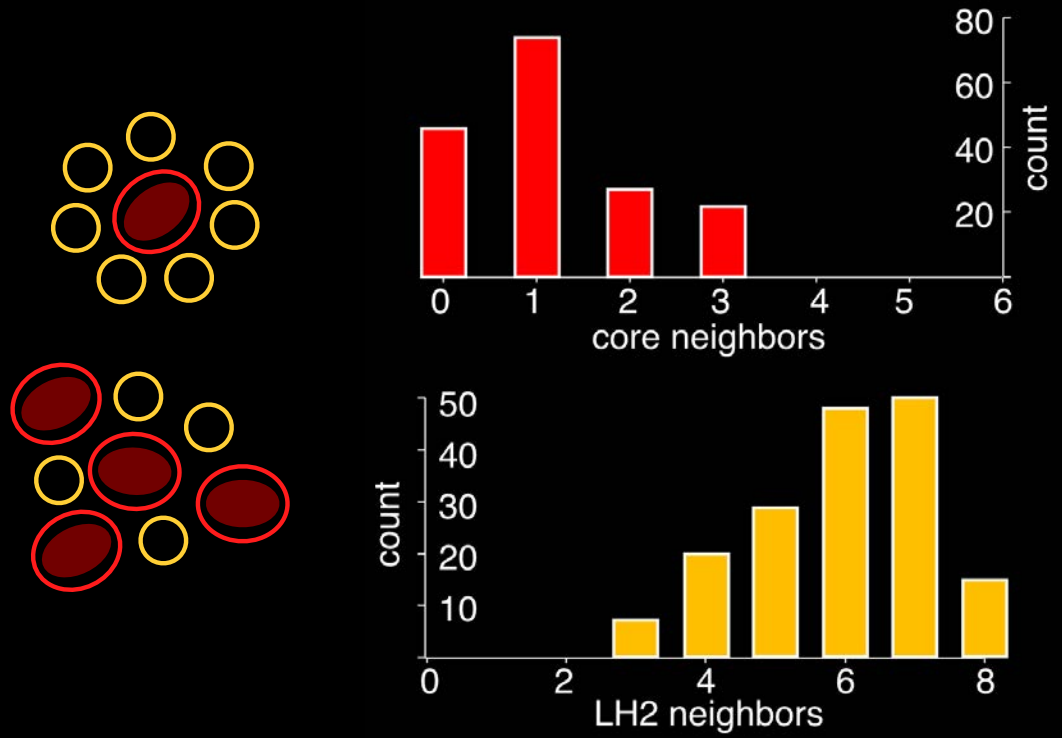

Scheuring, S.*, Rigaud, JL. & Sturgis, J. (2004)
Variable LH2 stoichiometry and core clustering in native membranes of Rhodospirillum photometricum.
EMBO J., 2004, 23, 21, 4127-4133.

Rps. Photometricum Photosynthetic Apparatus

There is no fixed assembly unit

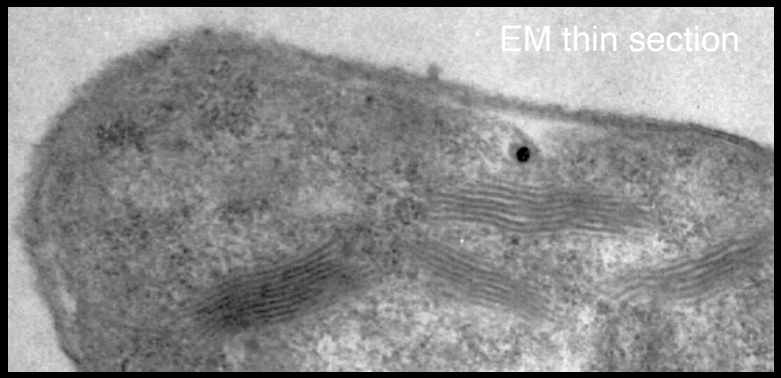

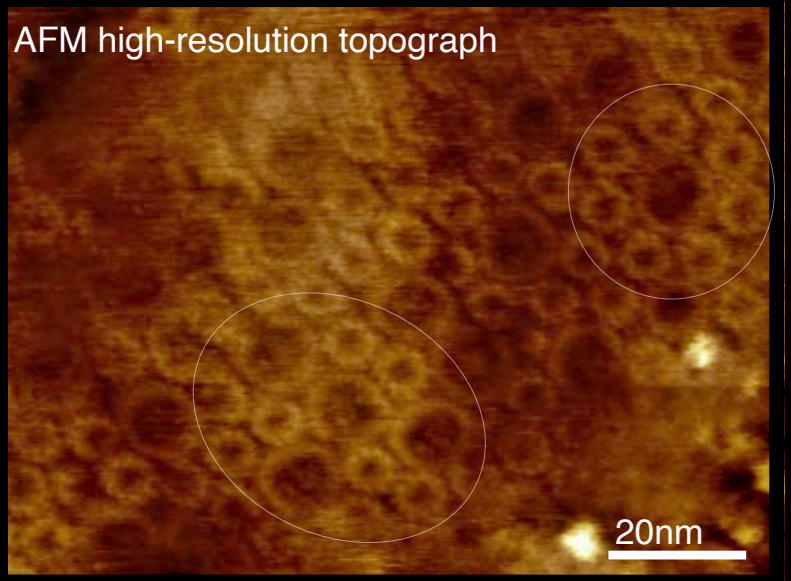

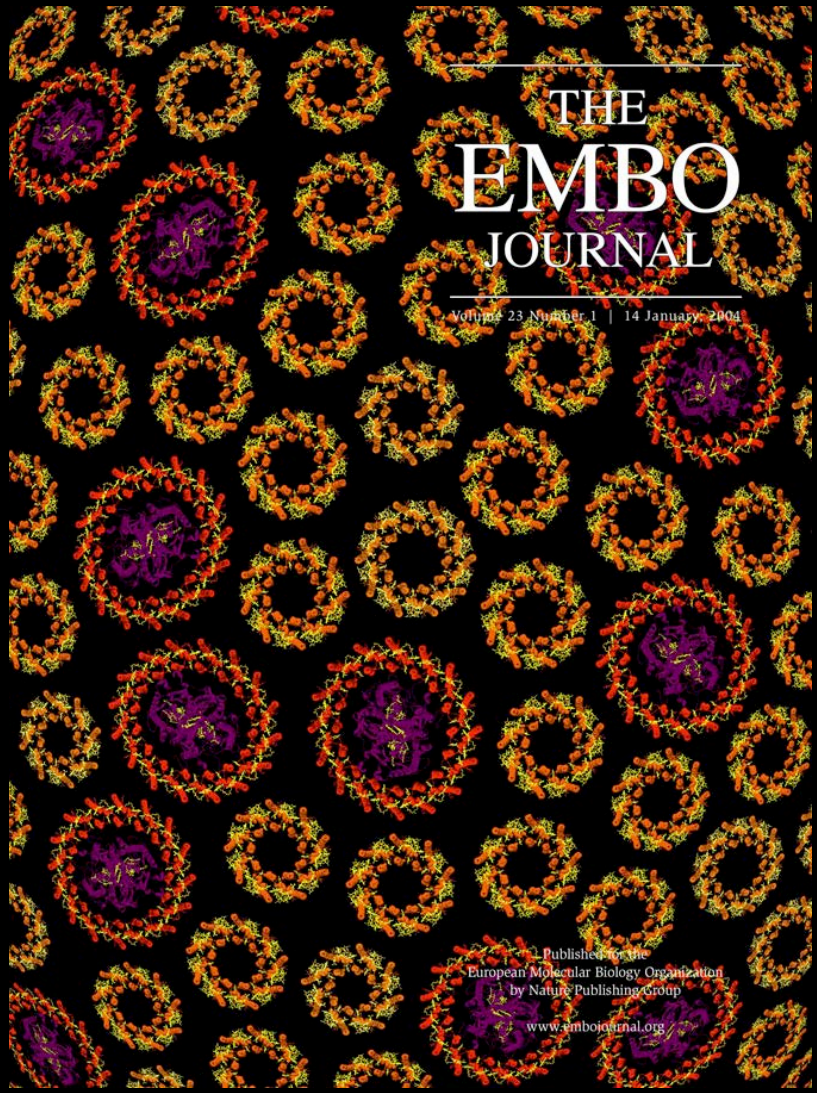

Scheuring, S.*, Rigaud, JL. & Sturgis, J. (2004)
Variable LH2 stoichiometry and core clustering in native membranes of Rhodospirillum photometricum.
EMBO J., 2004, 23, 21, 4127-4133.

Static assembly?

Or rather:

Dynamic Light Adaptation!

Chromatic Adaptation

High-light adapted membranes

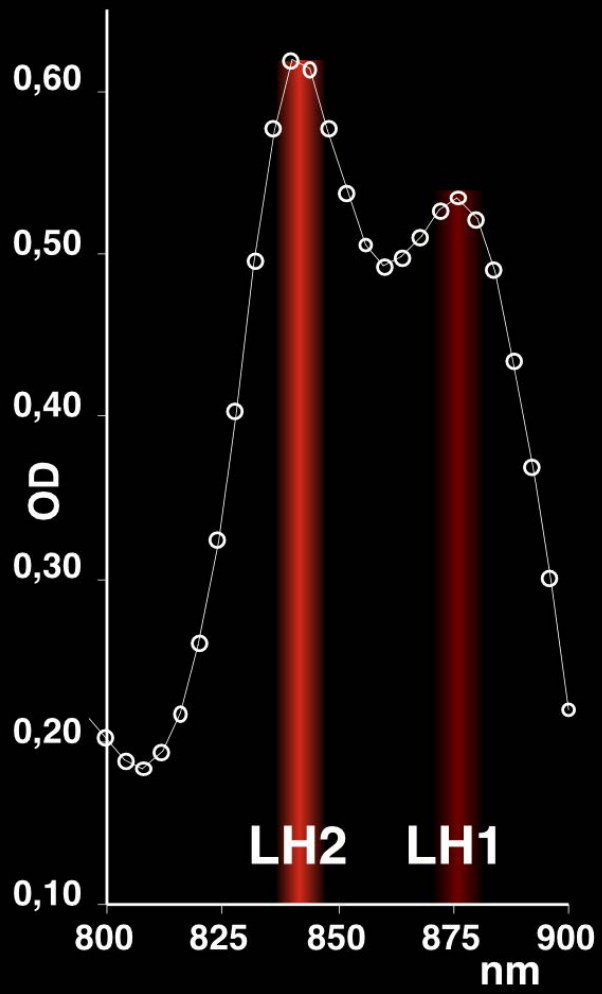

Low-light adapted membranes

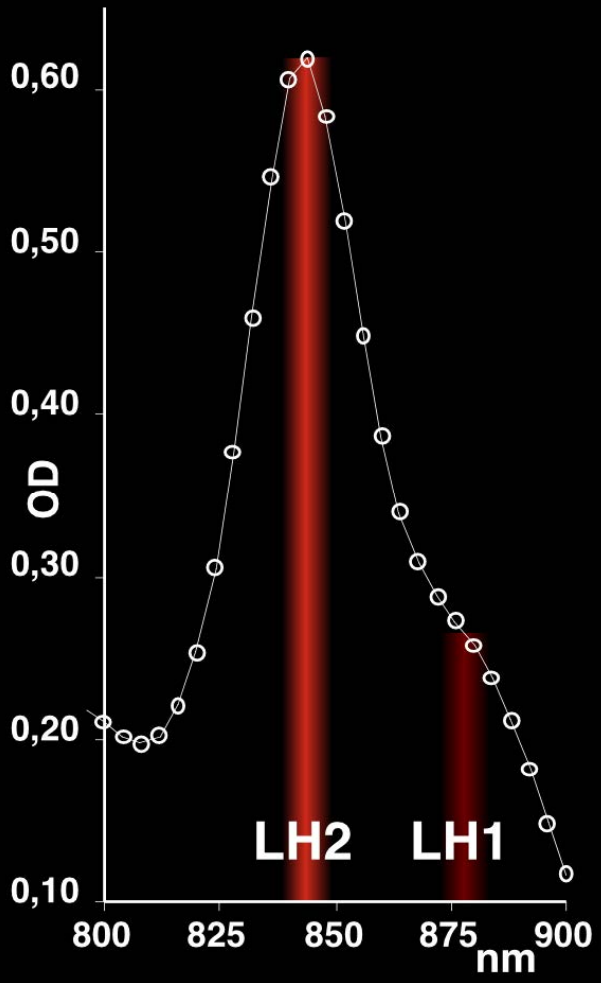

Simon Scheuring*, & James Sturgis (2005).
Chromatic adaptation of photosynthetic membranes.
Science, 2005, 309, 5733, 484-487.

Chromatic Adaptation

The complexes

LH1 - RC
core-complex

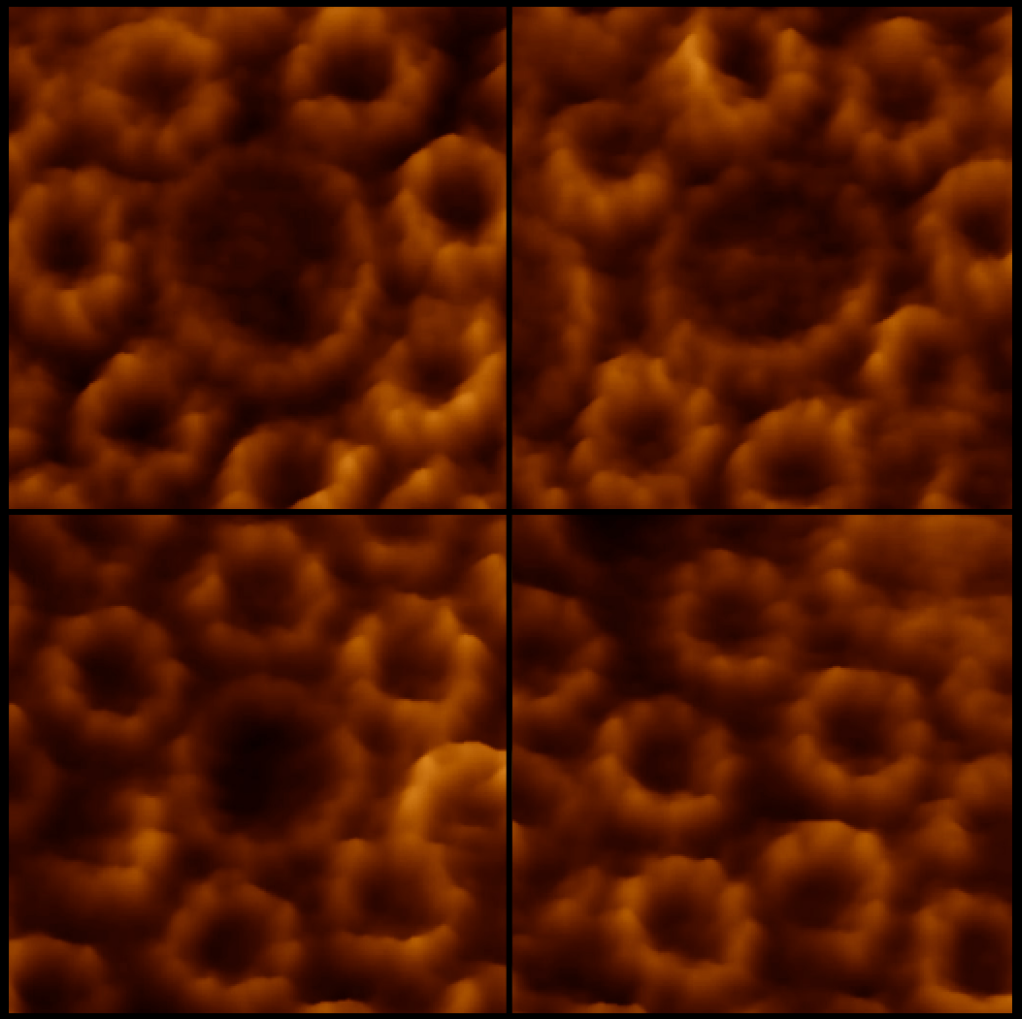

LH1 - RC
core complex

LH?
complex

LH2
complex

Simon Scheuring*, & James Sturgis (2005).
Chromatic adaptation of photosynthetic membranes.
Science, 2005, 309, 5733, 484-487.

Chromatic Adaptation

High-light adapted membranes

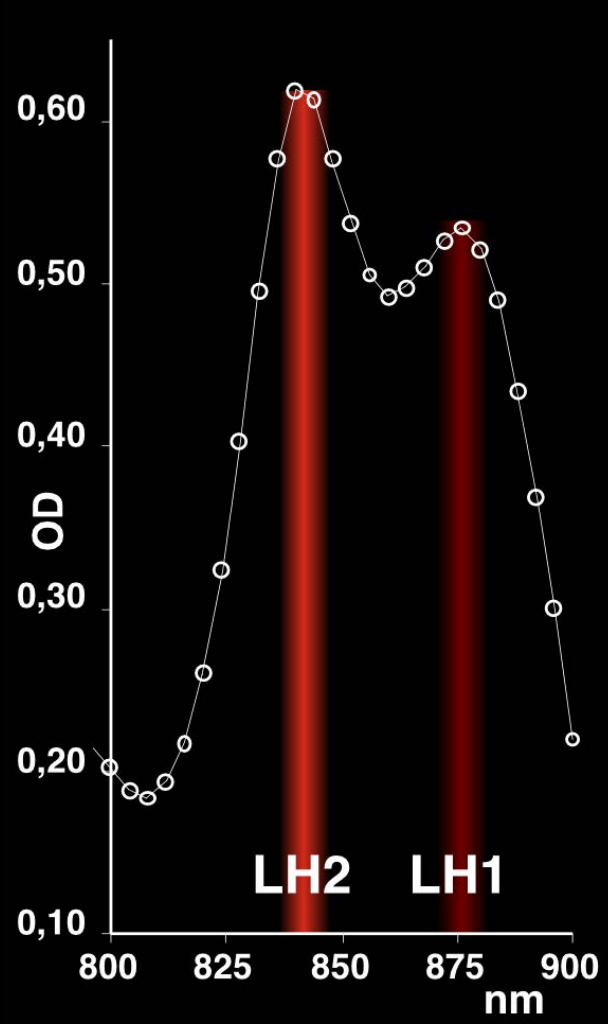

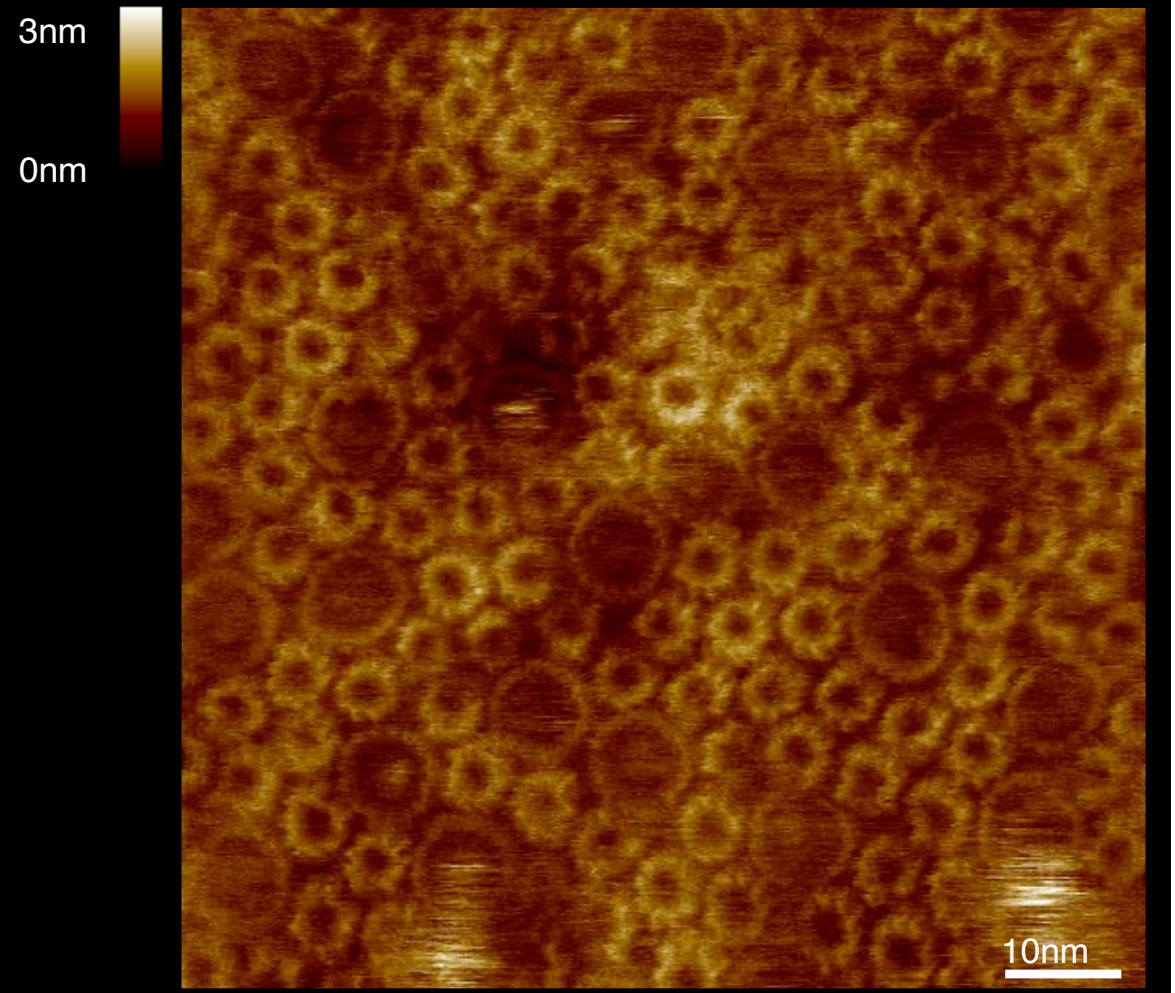

Simon Scheuring*, & James Sturgis (2005).
Chromatic adaptation of photosynthetic membranes.
Science, 2005, 309, 5733, 484-487.

Chromatic Adaptation

Low-light adapted membranes

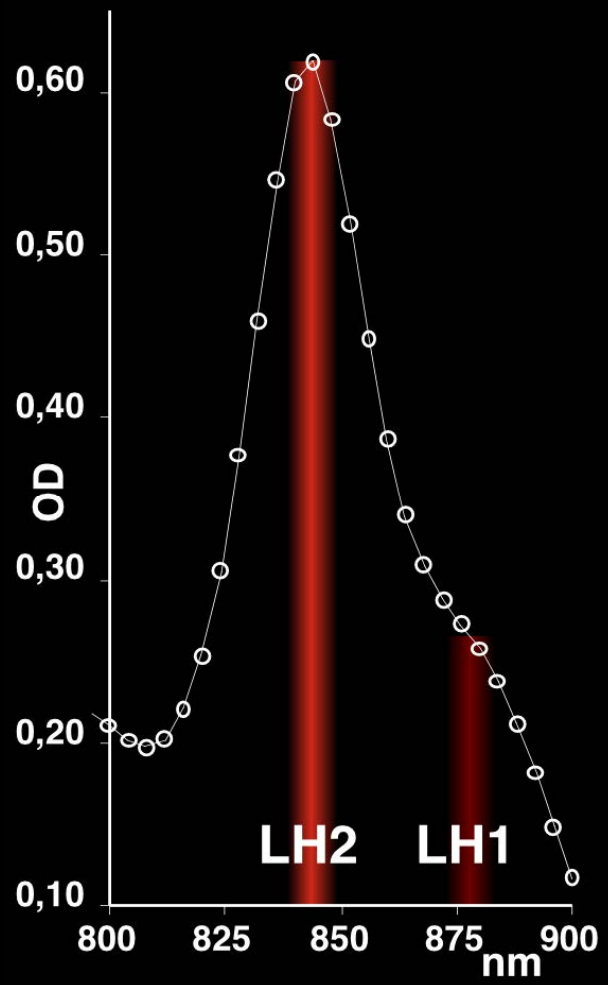

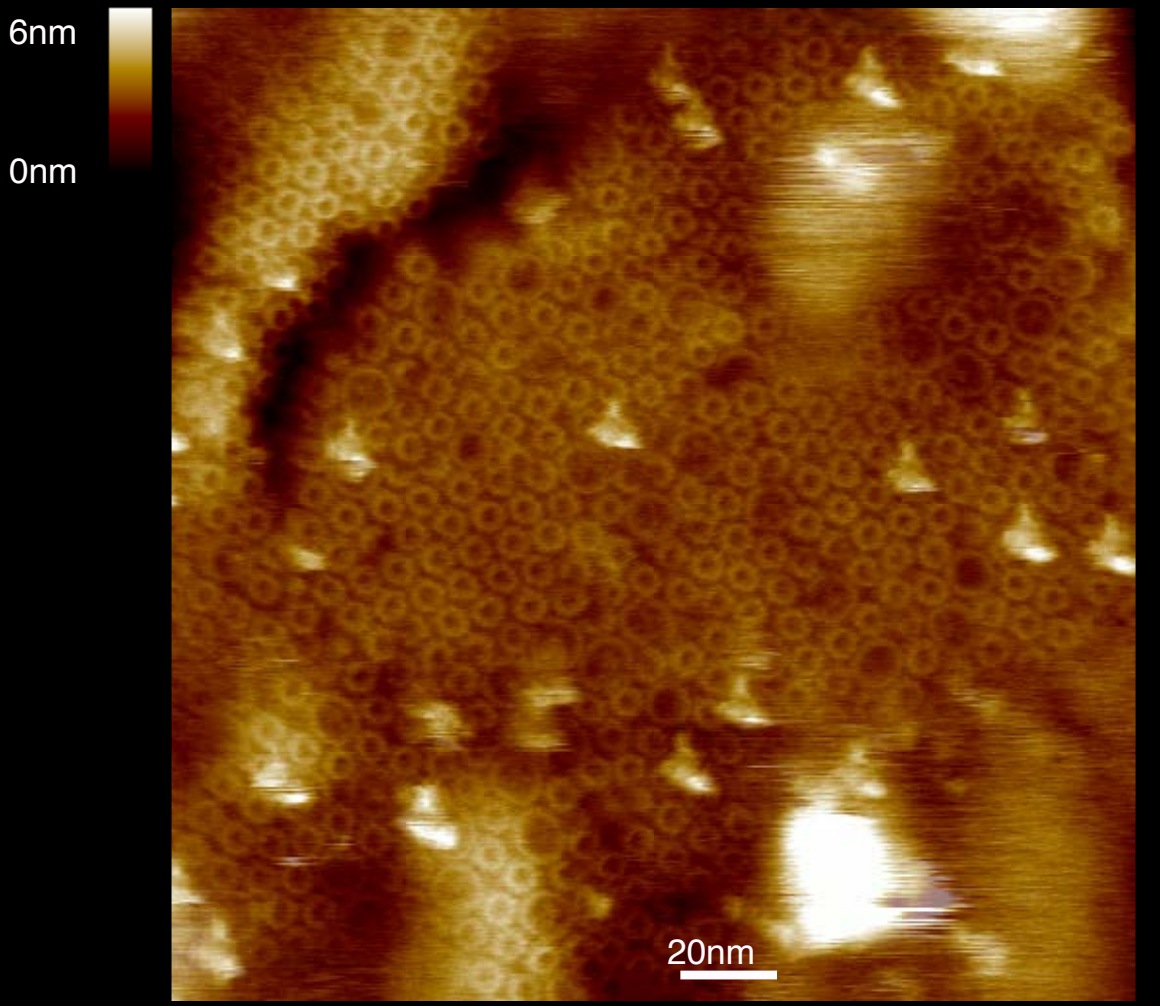

Simon Scheuring*, & James Sturgis (2005).
Chromatic adaptation of photosynthetic membranes.
Science, 2005, 309, 5733, 484-487.

Chromatic Adaptation

Antenna and “photosynthetically active“ domains in low-light adapted membranes

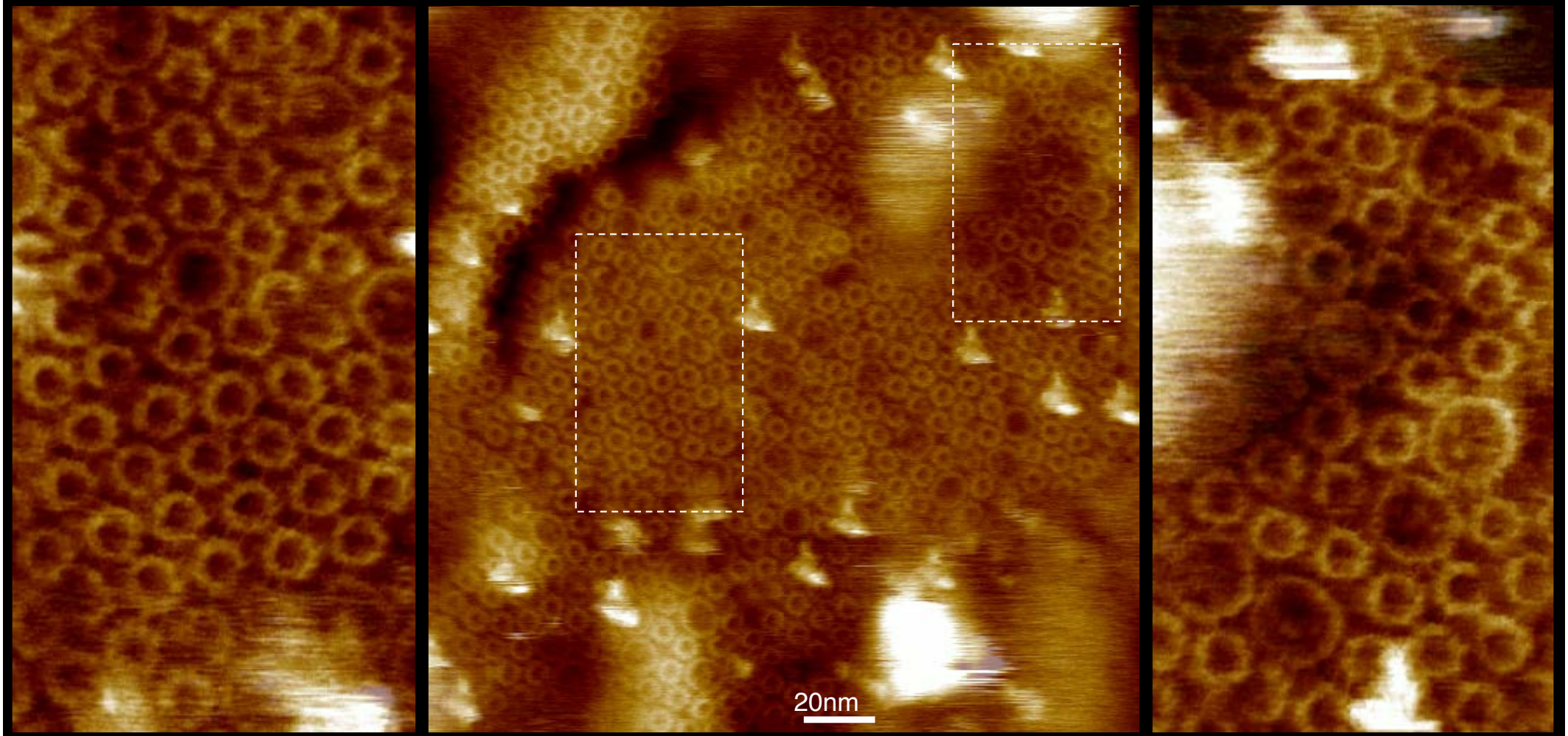

Simon Scheuring*, & James Sturgis (2005).
Chromatic adaptation of photosynthetic membranes.
Science, 2005, 309, 5733, 484-487.

Rsp. Molischianum Photosynthetic Apparatus

Atomic model of the photosynthetic complex assembly, based on AFM topography

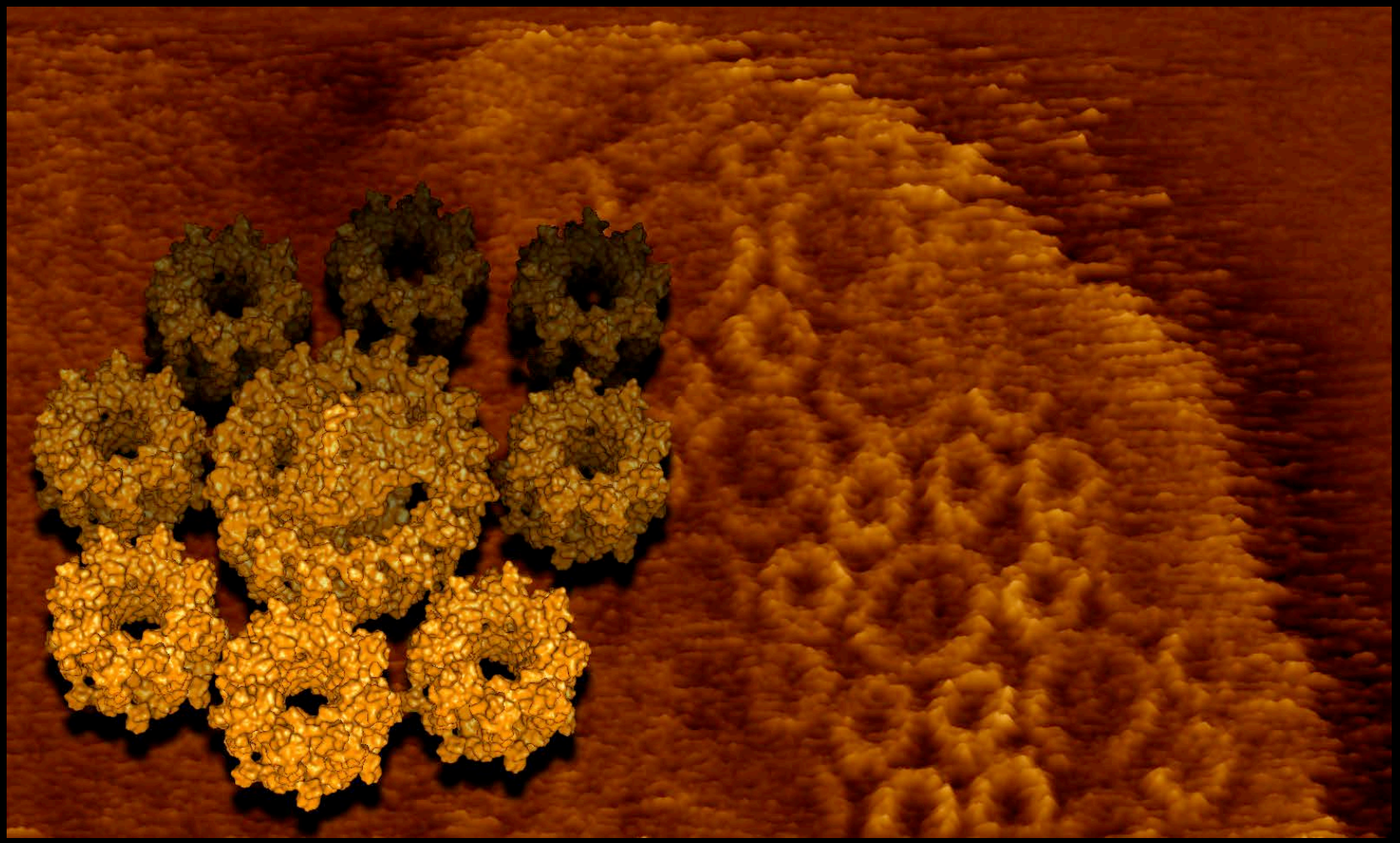

Imaging modes

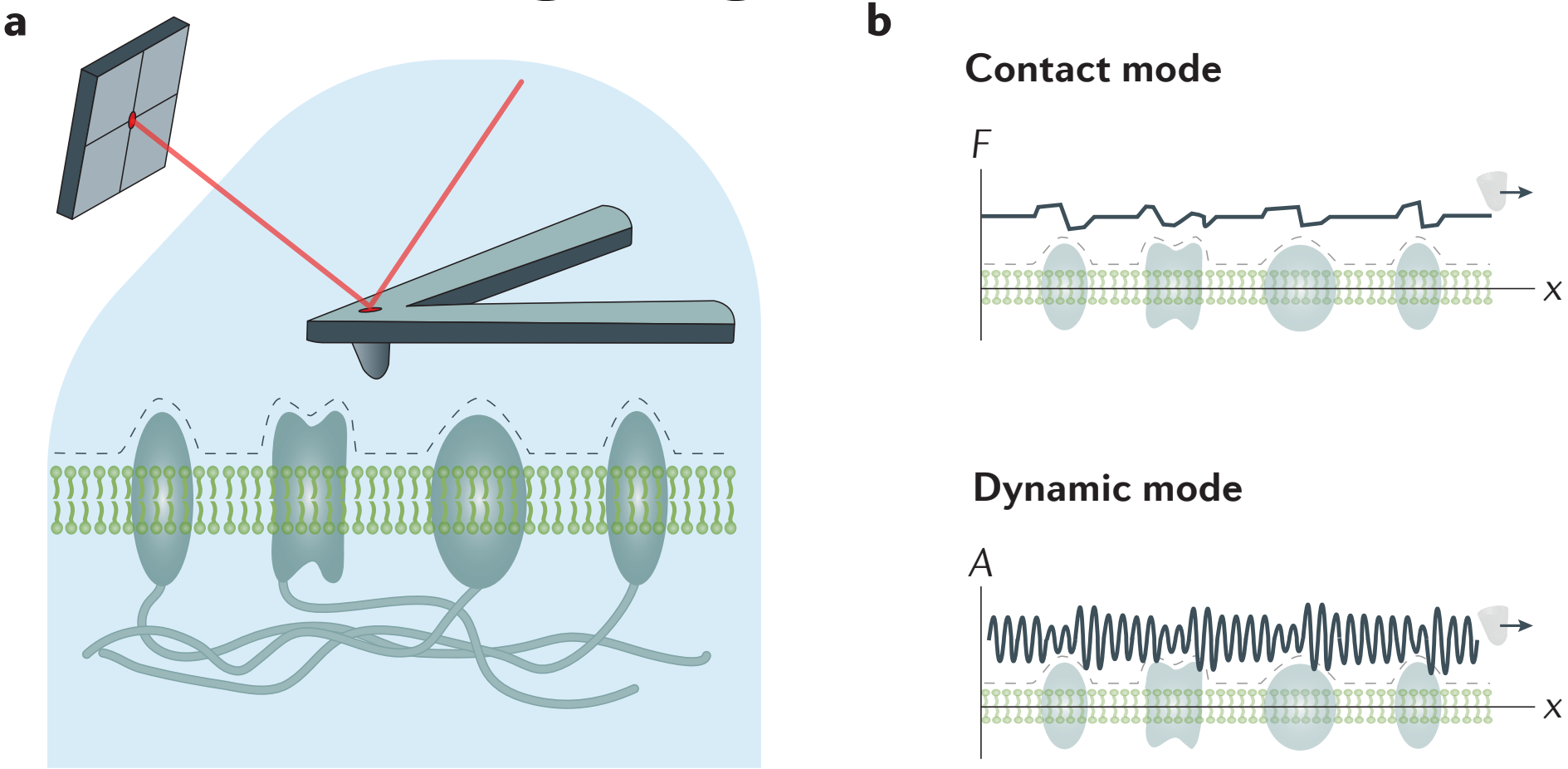

Review:

D. Alsteens, H. E. Gaub, R. Newton, M. Pfreundschuh, C. Gerber, and D. J. Müller, “Atomic force microscopy-based characterization and design of biointerfaces,” Nature Publishing Group, vol. 2, pp. 1–16, Mar. 2017.

High-Speed AFM

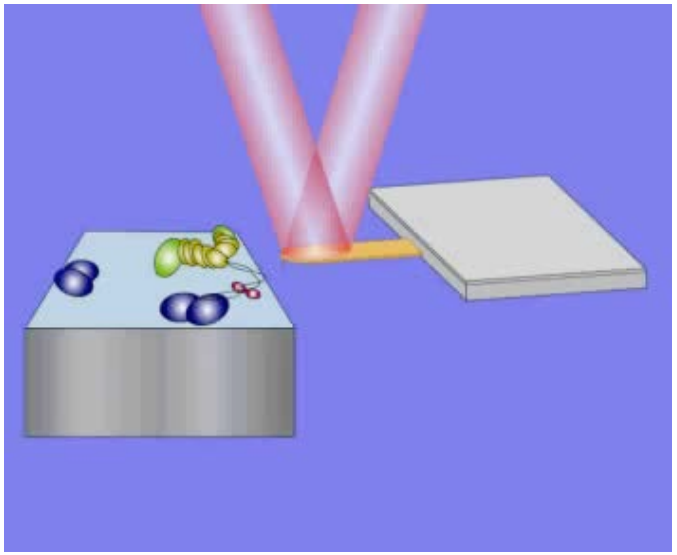

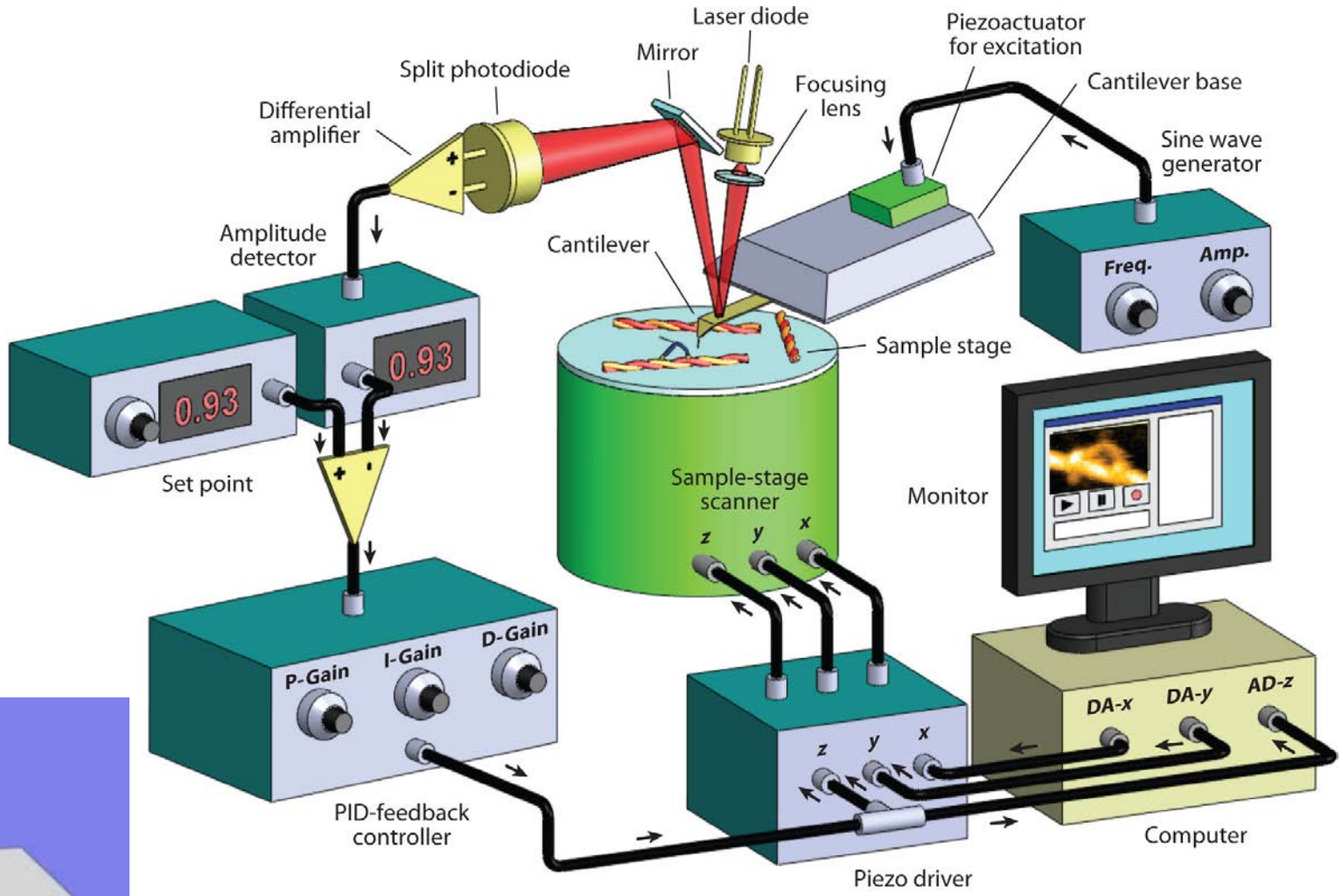

Toshio Ando,Takayuki Uchihashi, Noriyuki Kodera, Annual Review of Biophysics 42, 393-414 (2013)

High-Speed AFM shows myosin walking along actin

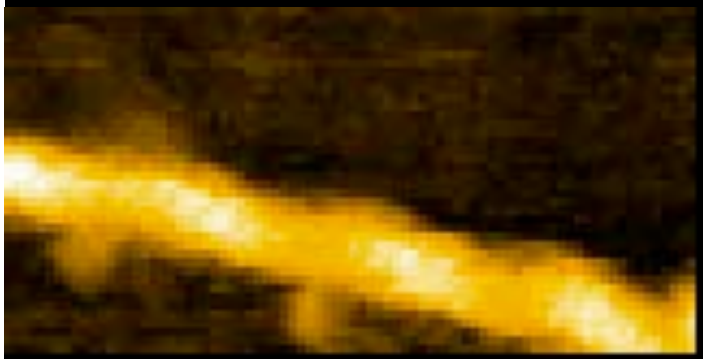

Processive movement of myosin V (M5-HMM). The dynamic process in 1 μM ATP was captured at 7 fps. Scan range, 130 × 65 nm^2 with 80 × 40 pixel.

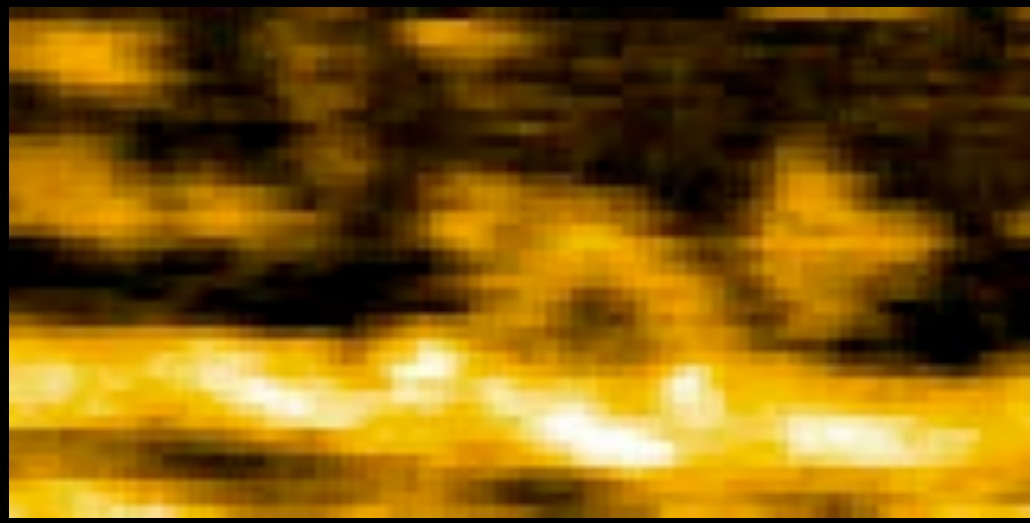

Hand-over-hand movement of myosin V (M5-HMM) including foot stomp of the leading head. The dynamic process in 1 μM ATP was captured at 7 fps. Scan range, 150 × 75 nm^2 with 80 × 40 pixel.

Long tracking of myosin V (M5-HMM) walking along actin filament. This typical movie showing long processive runs in 1 μM ATP was captured at 7 fps. To chase the M5-HMM molecule, the scan area was moved. Scan range, 150 × 75 nm^2 with 80 × 40 pixel; the whole imaging area, 560 × 120 nm^2

Toshio Ando,Takayuki Uchihashi, Noriyuki Kodera, Annual Review of Biophysics 42, 393-414 (2013)

Force spectroscopy AFM

Protein unfolding

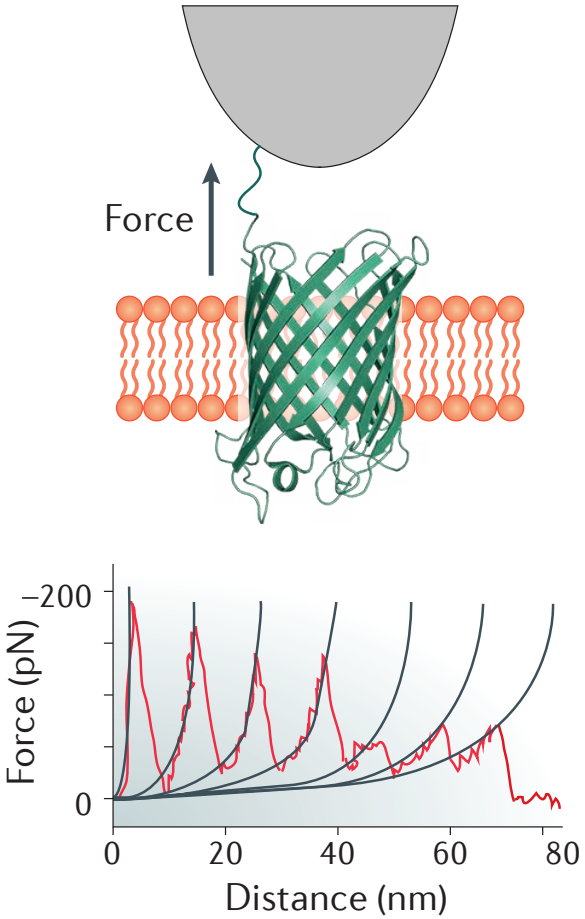

Cellular intention

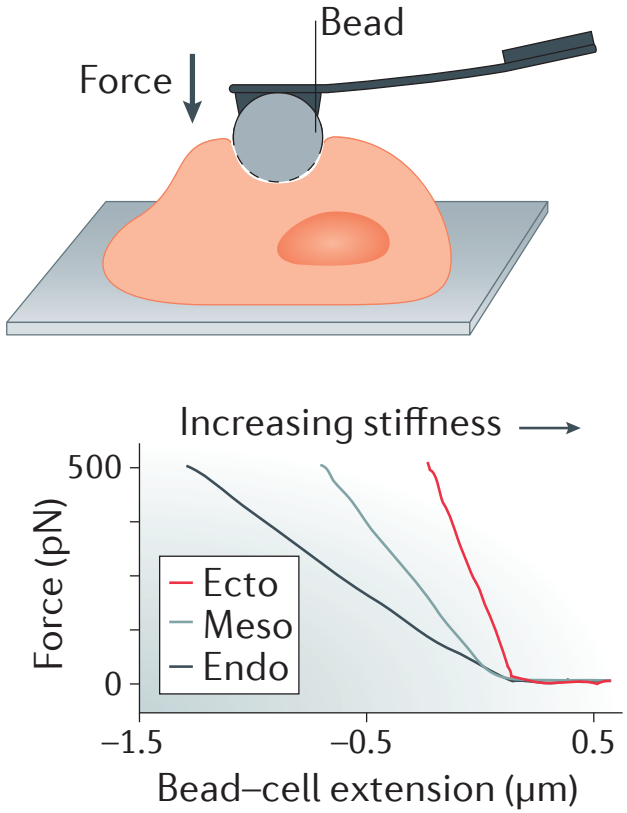

M. Grandbois, W. Dettmann, M. Benoit, and H. E. Gaub, “Affinity imaging of red blood cells using an atomic force microscope,” J. Histochem. Cytochem., vol. 48, no. 5, pp. 719–724, 2000.

Affinity imaging by AFM

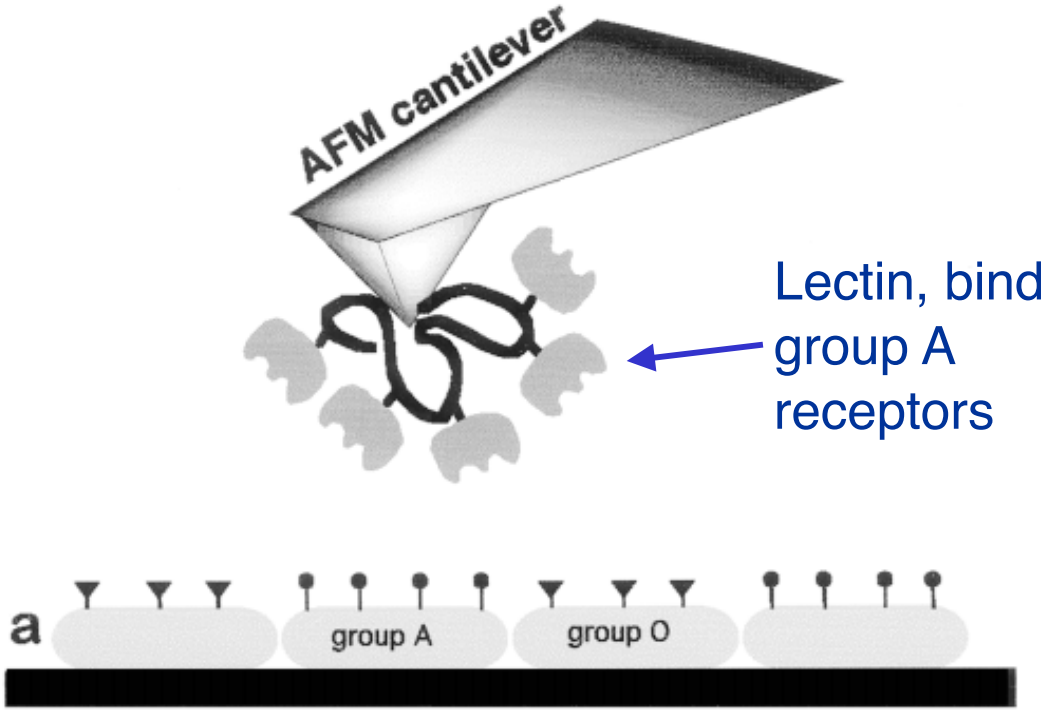

Red blood cells (RB)

Recorded pixel by pixel

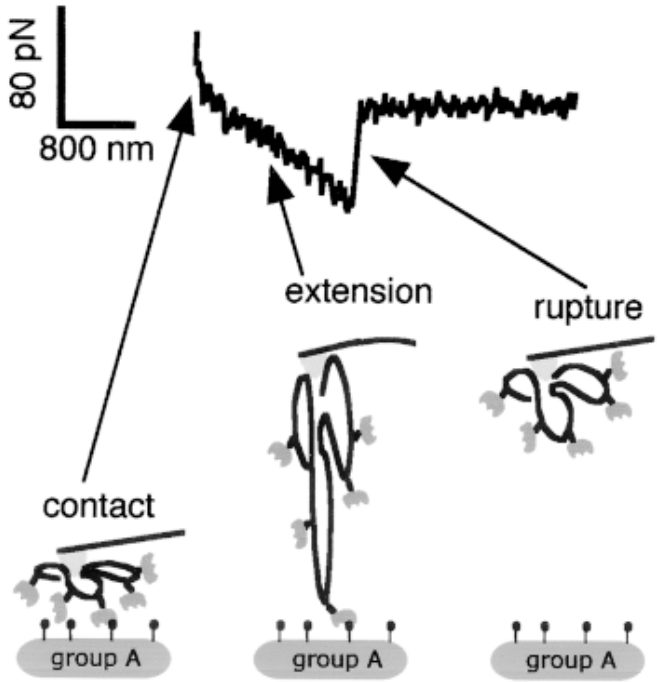

Red blood cells (RB)

M. Grandbois, W. Dettmann, M. Benoit, and H. E. Gaub, “Affinity imaging of red blood cells using an atomic force microscope,” J. Histochem. Cytochem., vol. 48, no. 5, pp. 719–724, 2000.

Affinity imaging by AFM

Adhesion image

Topography

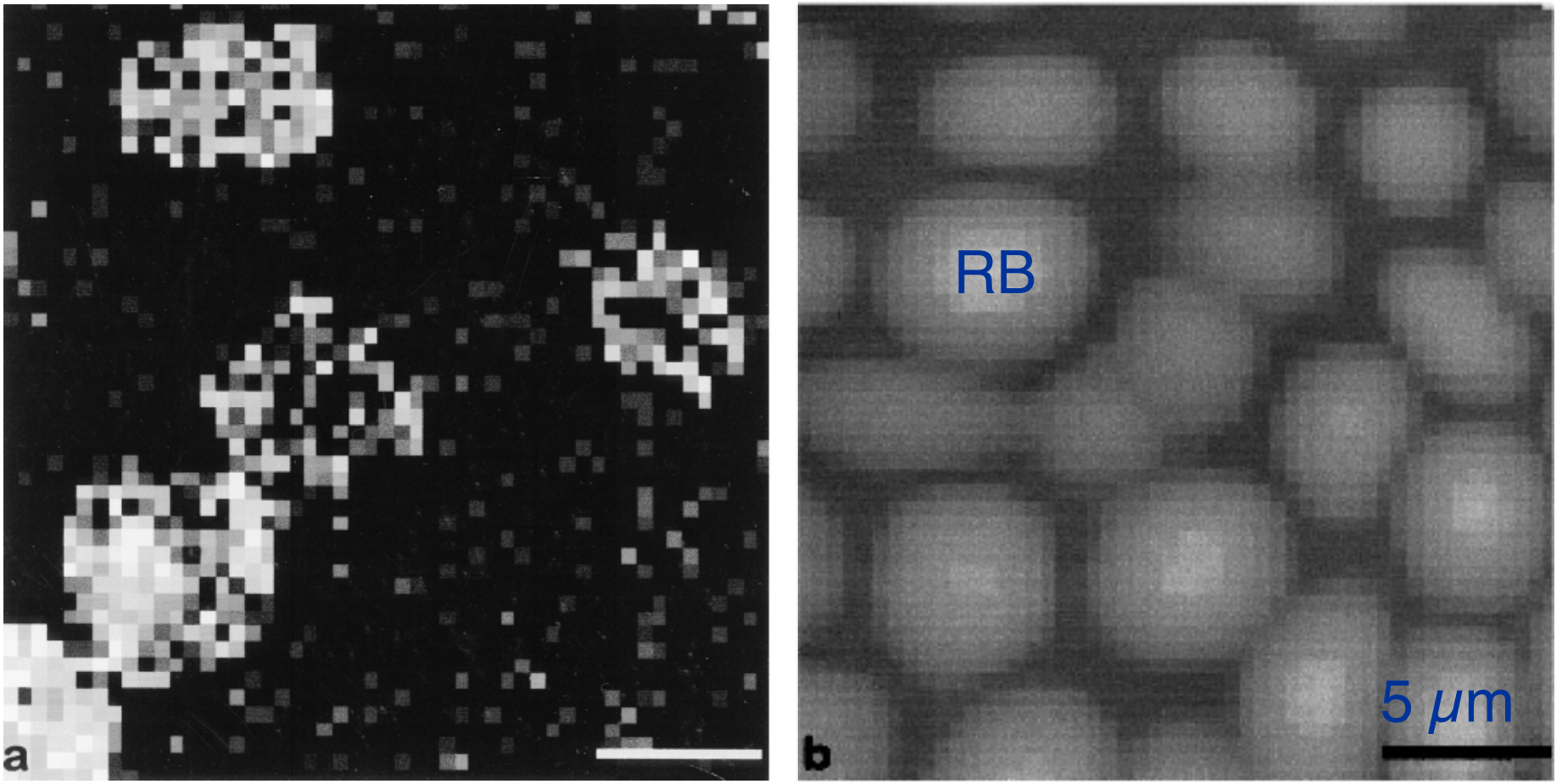

(a) Adhesion image recorded on a layer of mixed group A and O RBCs (1:2) adsorbed on a polylysine-coated glass surface with an AFM tip functionalized with HPL. The bright regions observed in this image correspond to group A RBCs. This image was obtained from the calculation of the rupture force (when observed) for an array of 55 x 55 force curves. Rupture events are responsible for the contrast. (b) Topographic image of the RBC layer scanned in a.

M. Grandbois, W. Dettmann, M. Benoit, and H. E. Gaub, “Affinity imaging of red blood cells using an atomic force microscope,” J. Histochem. Cytochem., vol. 48, no. 5, pp. 719–724, 2000.

Affinity imaging by AFM

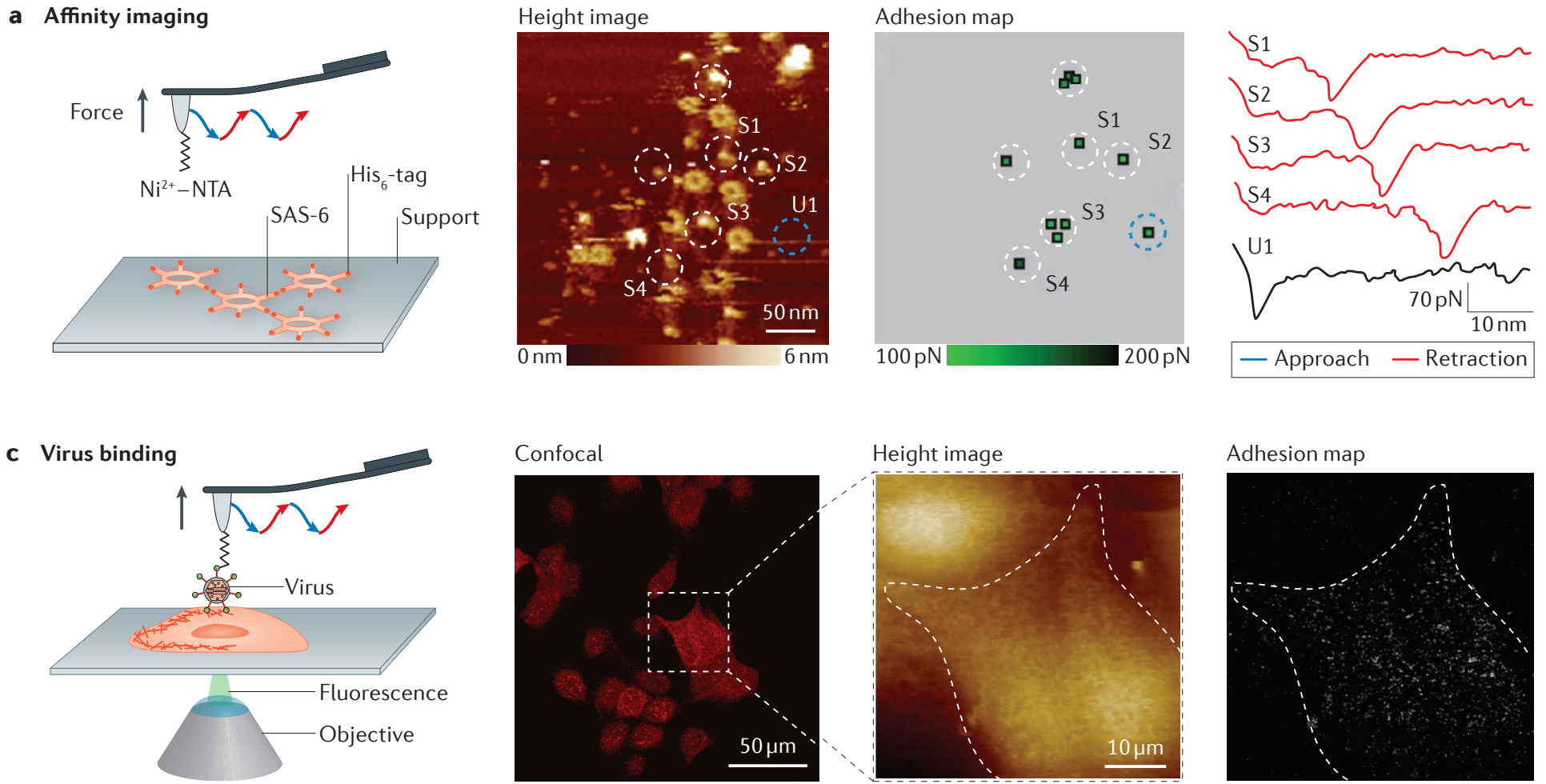

M. Grandbois, W. Dettmann, M. Benoit, and H. E. Gaub, “Affinity imaging of red blood cells using an atomic force microscope,” J. Histochem. Cytochem., vol. 48, no. 5, pp. 719–724, 2000.

Controlled Unzipping of Proteins

Single molecule force spectroscopy (SMFS)

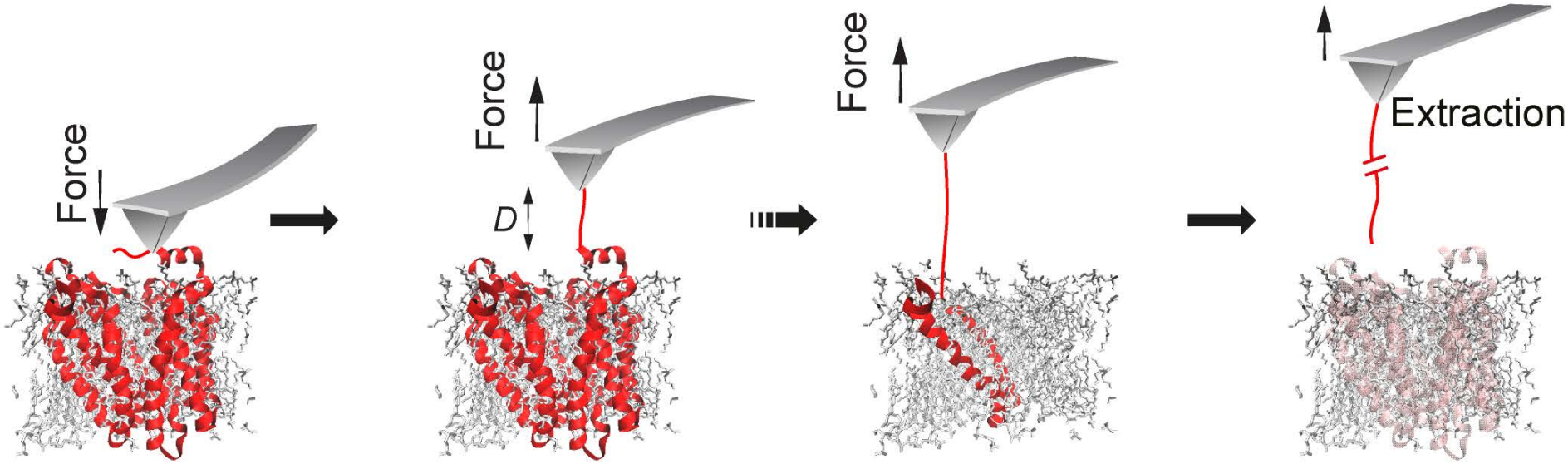

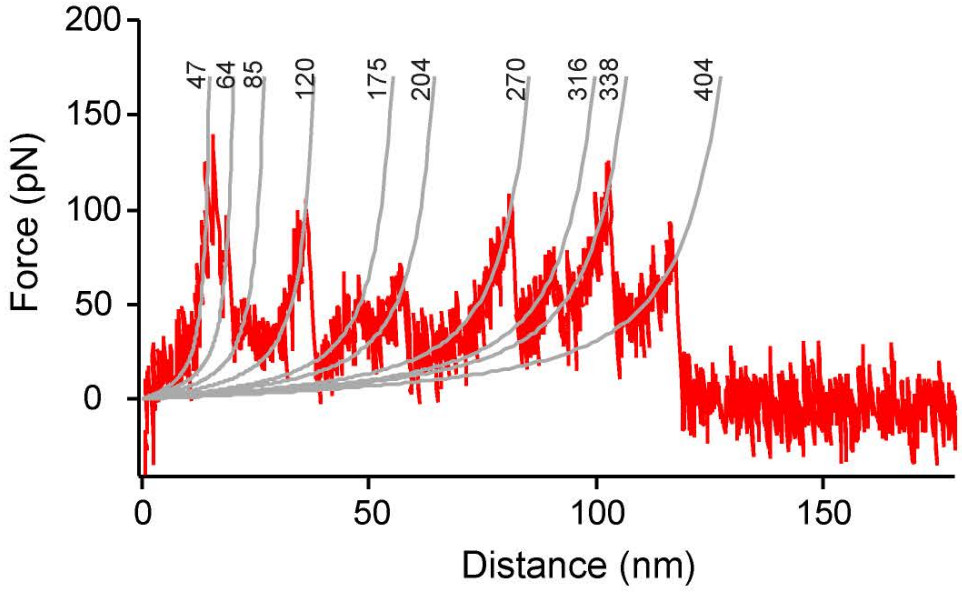

T. Serdiuk, D. Balasubramaniam, J. Sugihara, S. A. Mari, H. R. Kaback, and D. J. Müller, “YidC assists the stepwise and stochastic folding of membrane proteins,” Nat. Chem. Biol., vol. 12, no. 11, pp. 911–917, Sep. 2016.

Force spectroscopy of the native S-layer

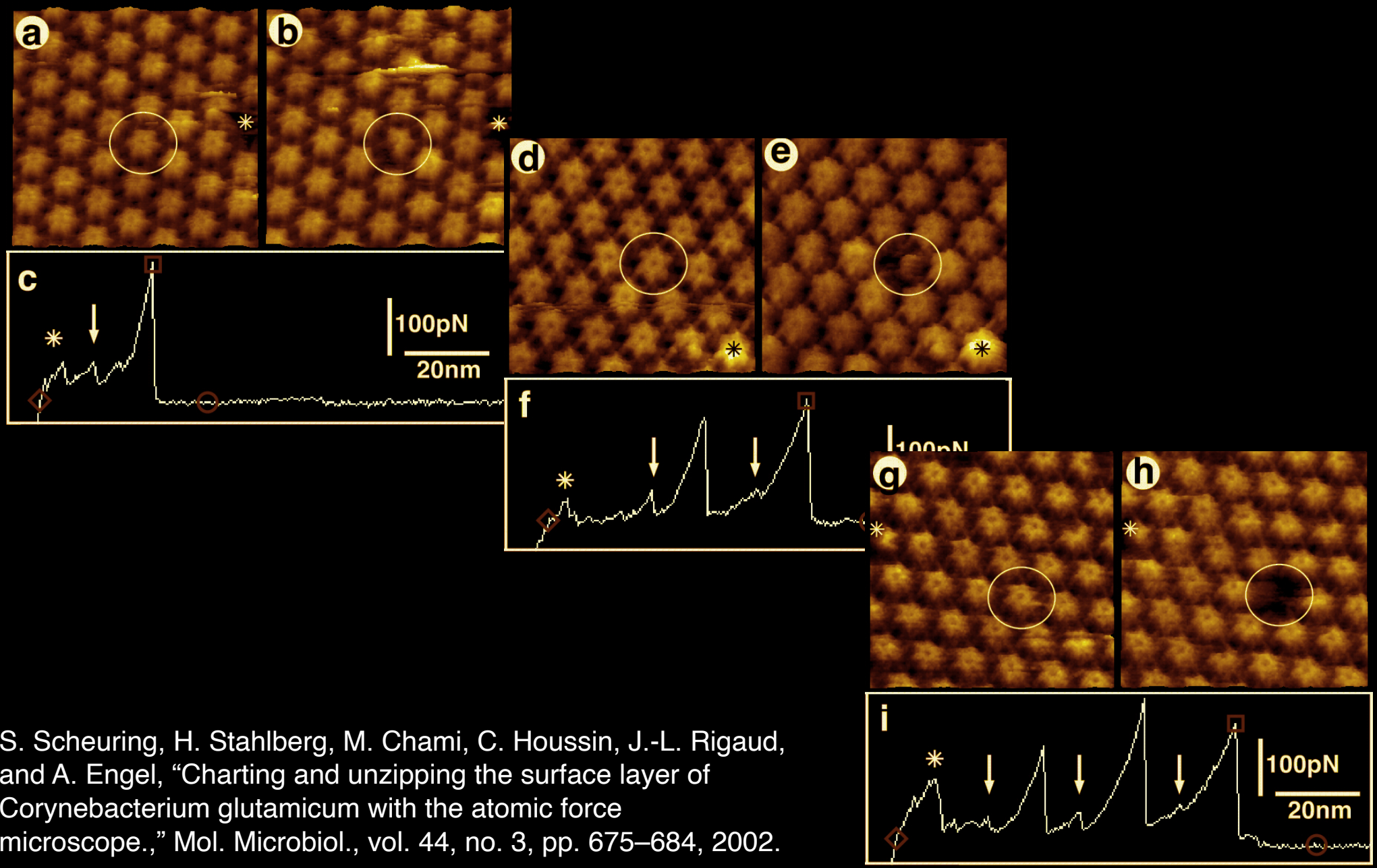

S. Scheuring, H. Stahlberg, M. Chami, C. Houssin, J.-L. Rigaud, and A. Engel, “Charting and unzipping the surface layer of Corynebacterium glutamicum with the atomic force microscope.,” Mol. Microbiol., vol. 44, no. 3, pp. 675–684, 2002.

Force spectroscopy of the native *Corynebacterium glutamicum* S-layer

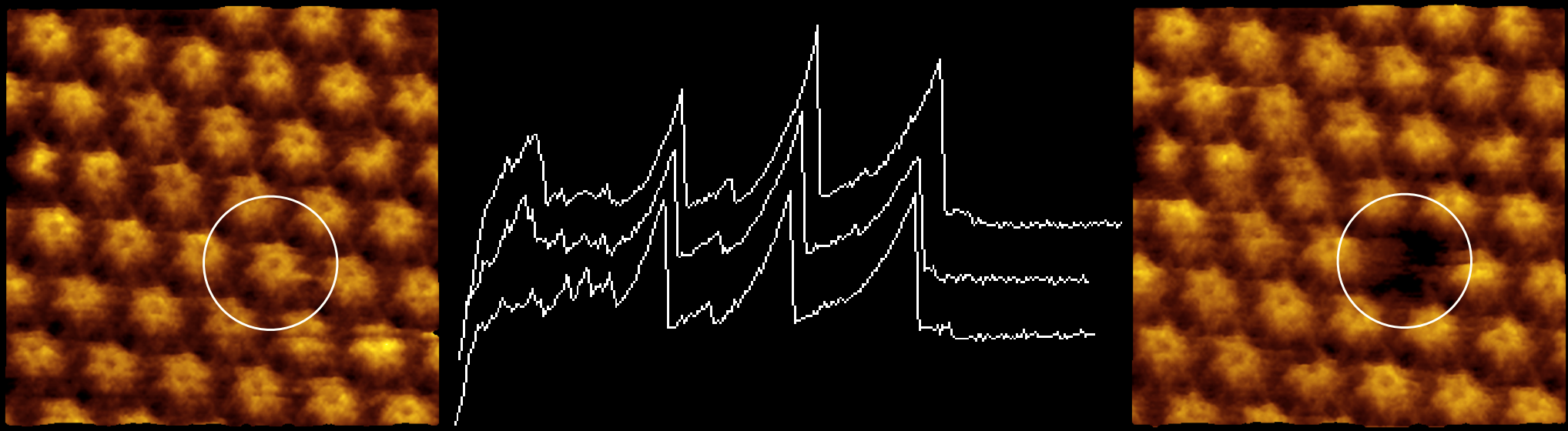

Force spectroscopy of the native *Deinococcus Radiodurans* HPI-layer

Müller *et al.*, 1999

Tissue characterisation (I)

Cancer biopsy and nanmochenical characterisation

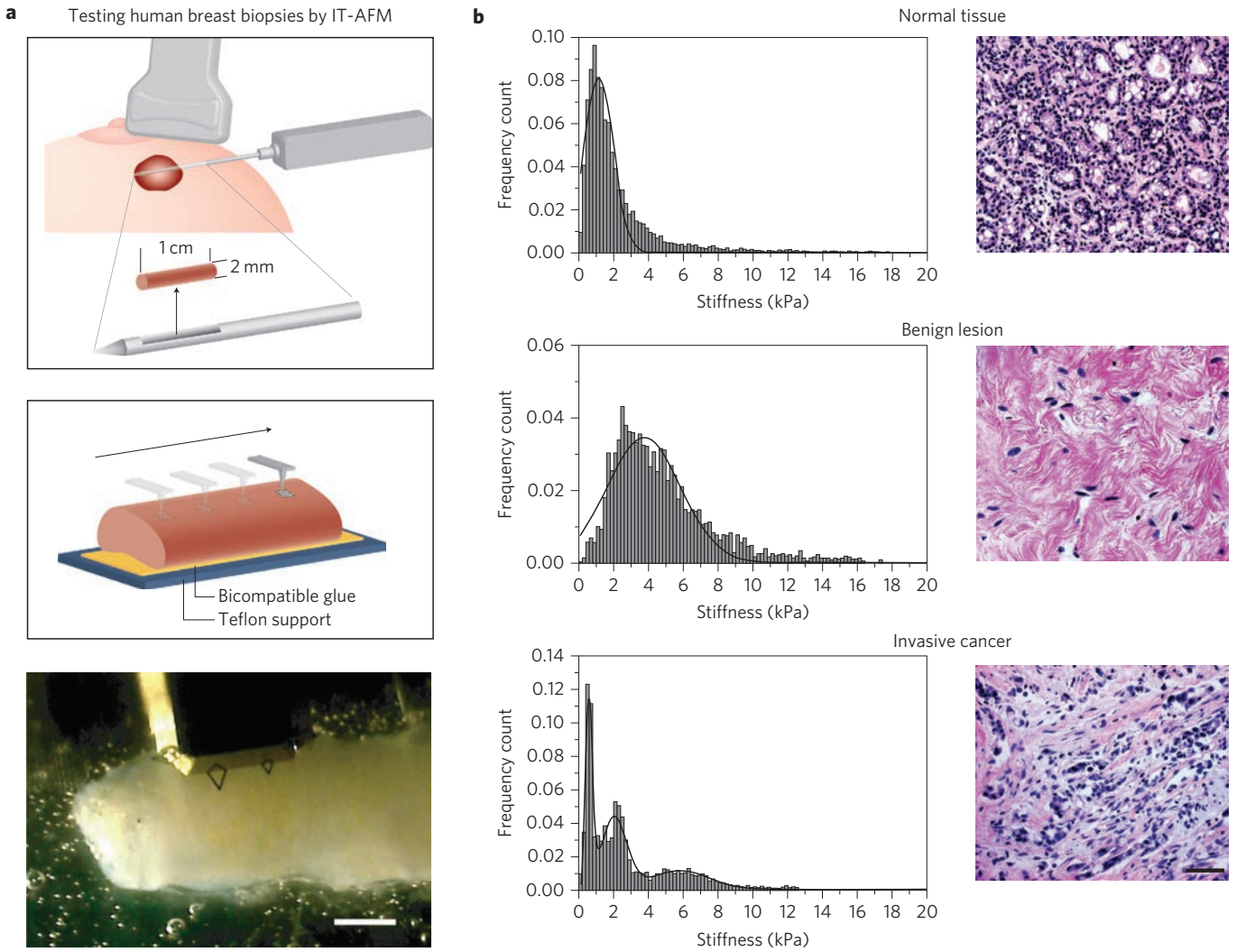

M. Plodinec, M. Loparic, C. A. Monnier, E. C. Obermann, R. Zanetti-Dallenbach, P. Oertle, J. T. Hyotyla, U. Aebi, M. Bentires-Alj, R. Y. H. Lim, and C.-A. Schoenenberger, “The nanomechanical signature of breast cancer,” pp. 1–9, 2012.

Nanomechanical sensors

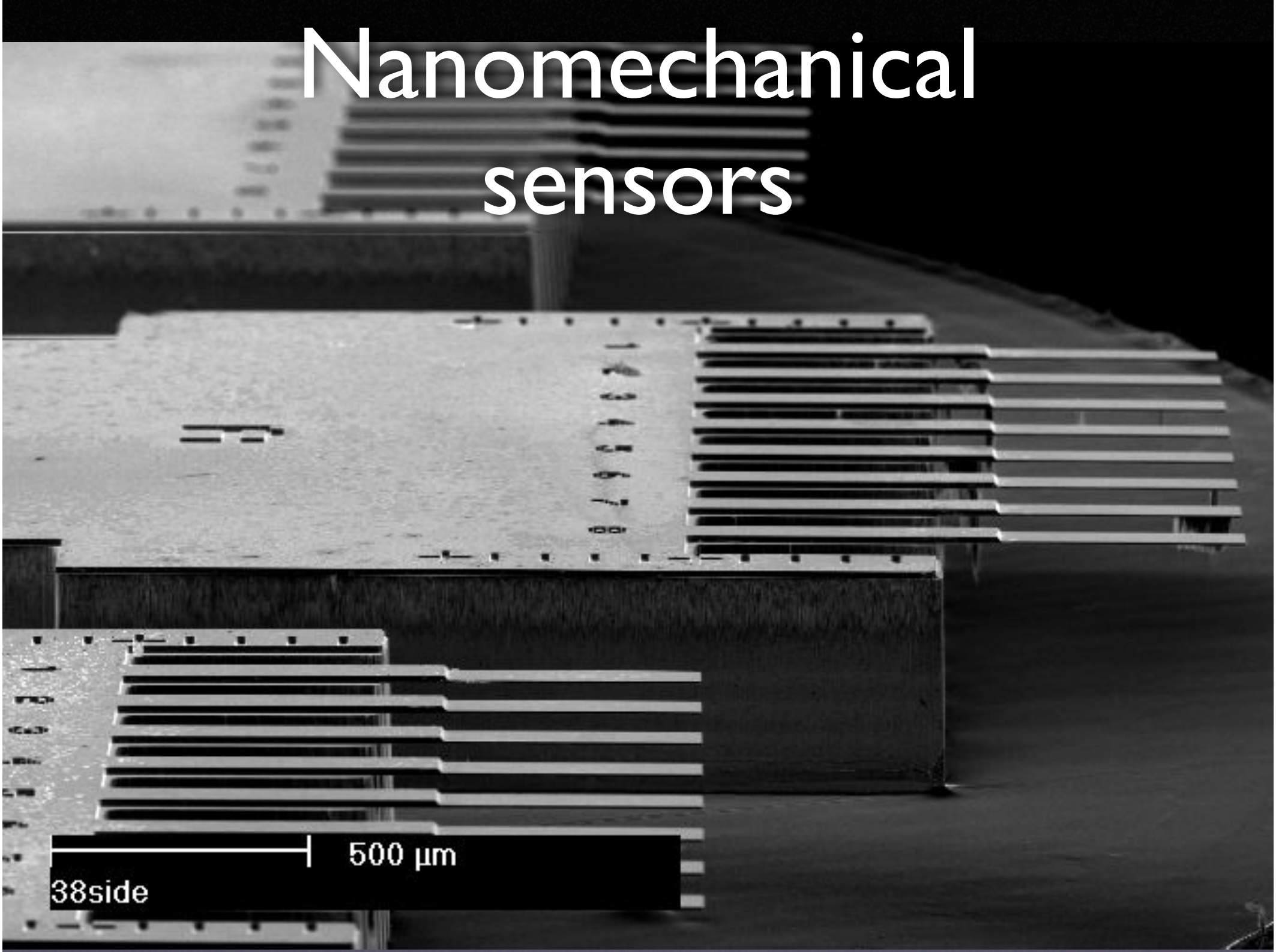

Two modes

Static mode

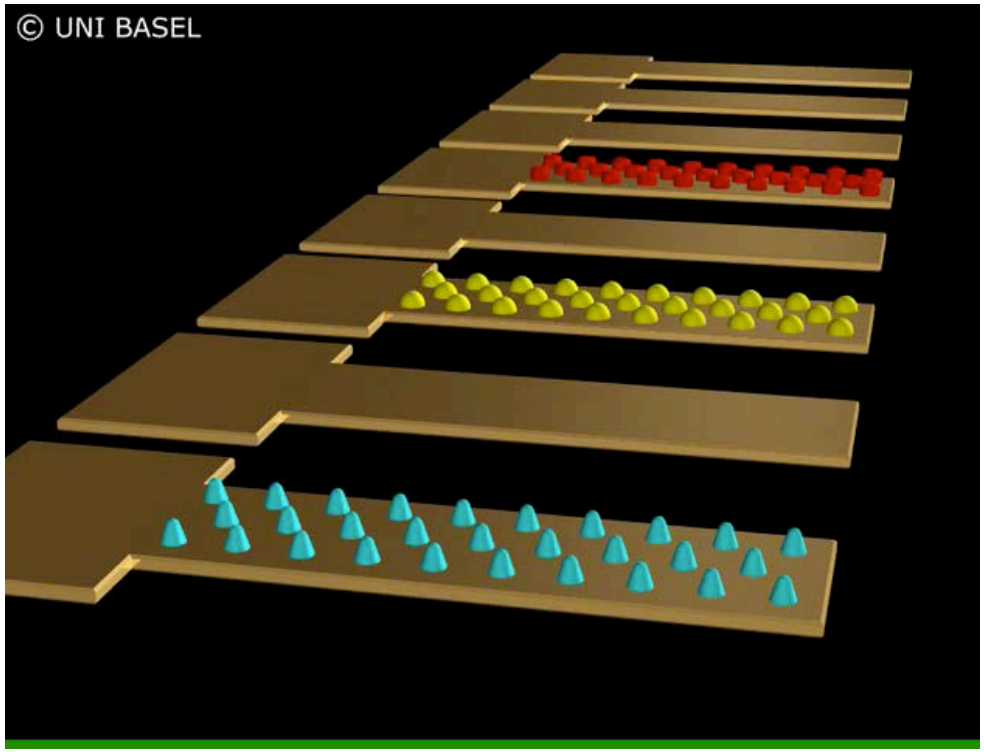

Detects surface stress

Dynamic mode

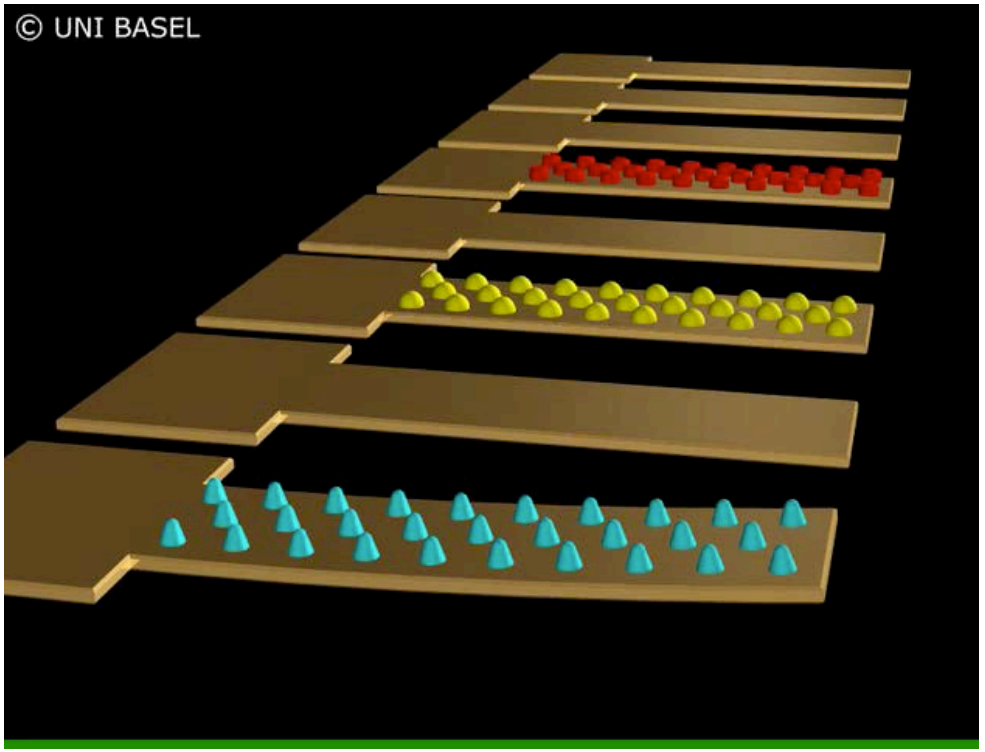

Detects mass increase

Static mode: DNA hybridisation

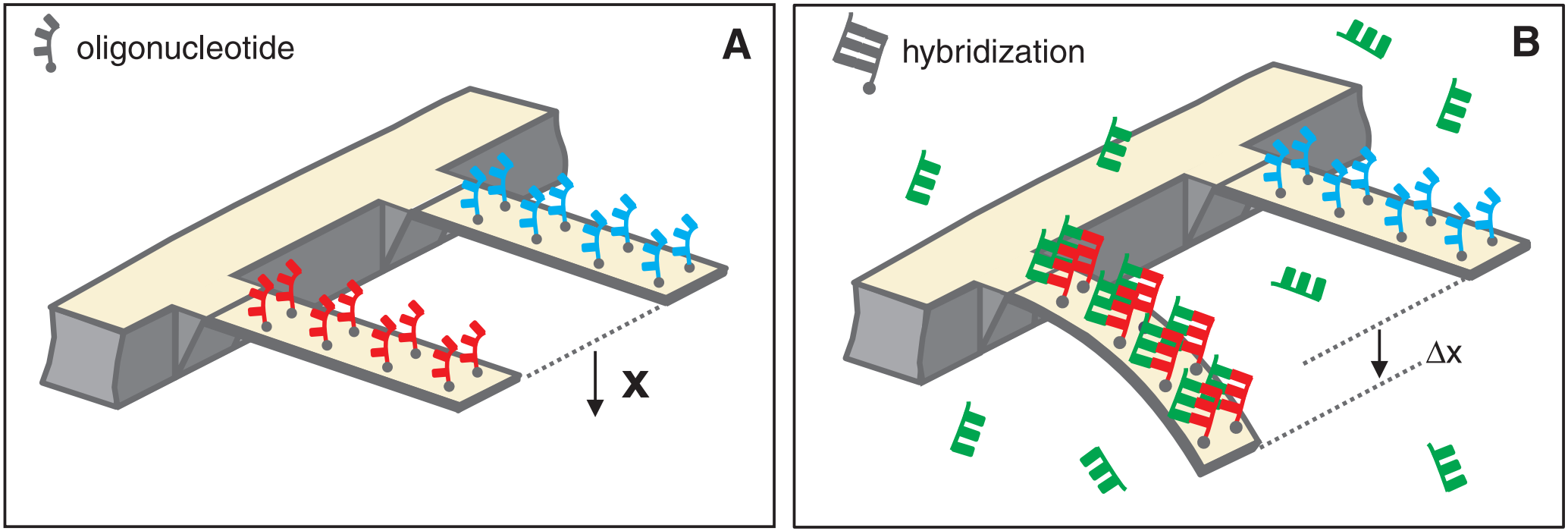

Scheme illustrating the hybridization experiment. Each cantilever is functionalized on one side with a different oligonucleotide base sequence (red or blue). (**A**) The differential signal is set to zero. (**B**) After injection of the first complementary oligonucleotide (green), hybridization occurs on the cantilever that provides the matching sequence (red), increasing the differential signal Δx.

J. Fritz, M. K. Baller, H. P. Lang, H. Rothuizen, P. Vettiger, E. Meyer, H. J. Guntherodt, C. Gerber, and J. K. Gimzewski, “Translating biomolecular recognition into nanomechanics,” Science, vol. 288, no. 5464, pp. 316–318, 2000.

Static mode: DNA hybridisation

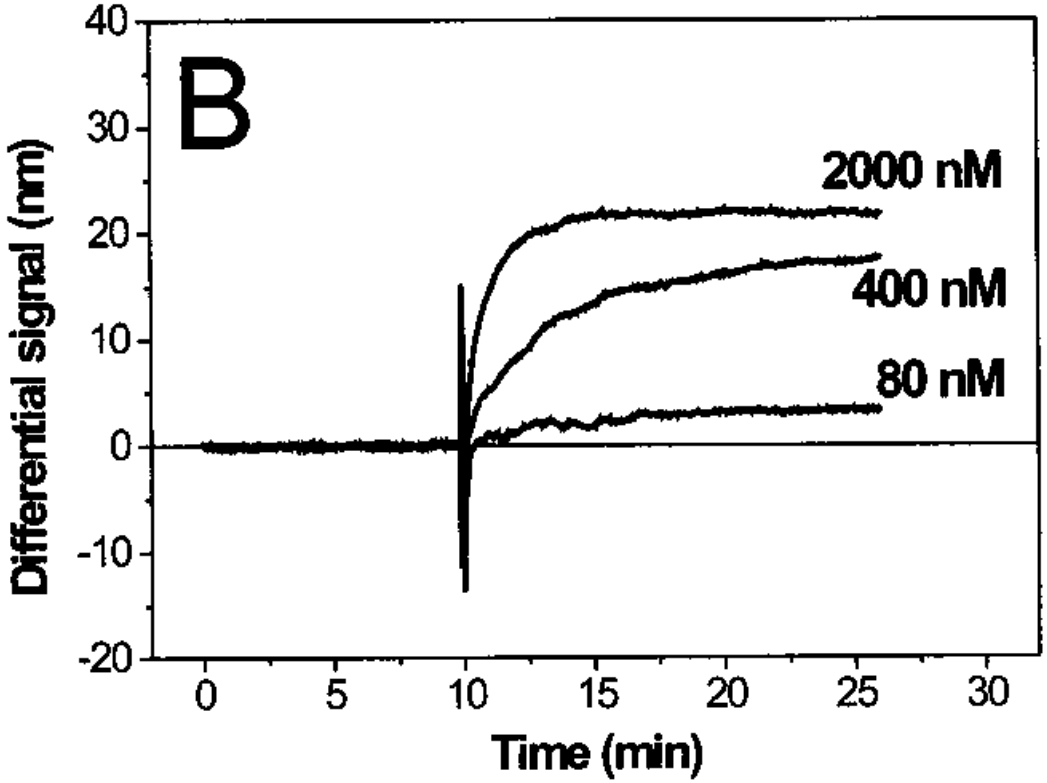

Three successive hybridization experiments with different 12-mer oligonucleotide concentrations using one array.

J. Fritz, M. K. Baller, H. P. Lang, H. Rothuizen, P. Vettiger, E. Meyer, H. J. Guntherodt, C. Gerber, and J. K. Gimzewski, “Translating biomolecular recognition into nanomechanics,” Science, vol. 288, no. 5464, pp. 316–318, 2000.

Dynamic mode

First mode

Second mode

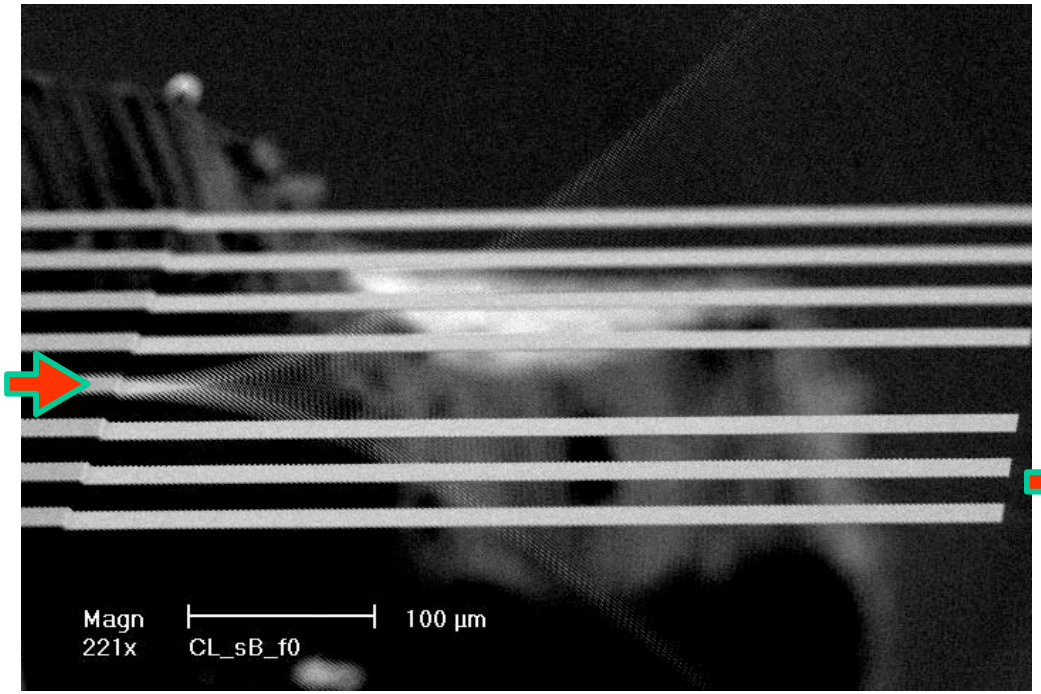

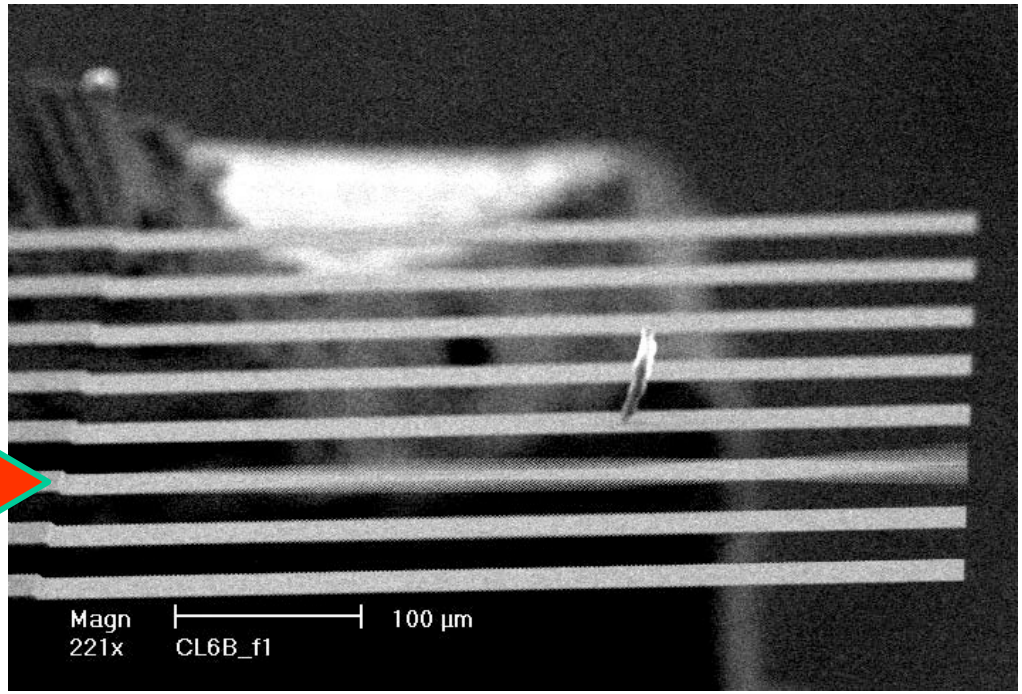

In vacuum

M. K. Ghatkesar, V. Barwich, T. Braun, J.-P. Ramseyer, C. Gerber, M. Hegner, H.-P. Lang, U. Drechsler, and M. Despont, “Higher modes of vibration increase mass sensitivity in nanomechanical microcantilevers,” Nanotechnology, vol. 18, no. 44, pp. 445502–8, 2007.

Dynamic mode

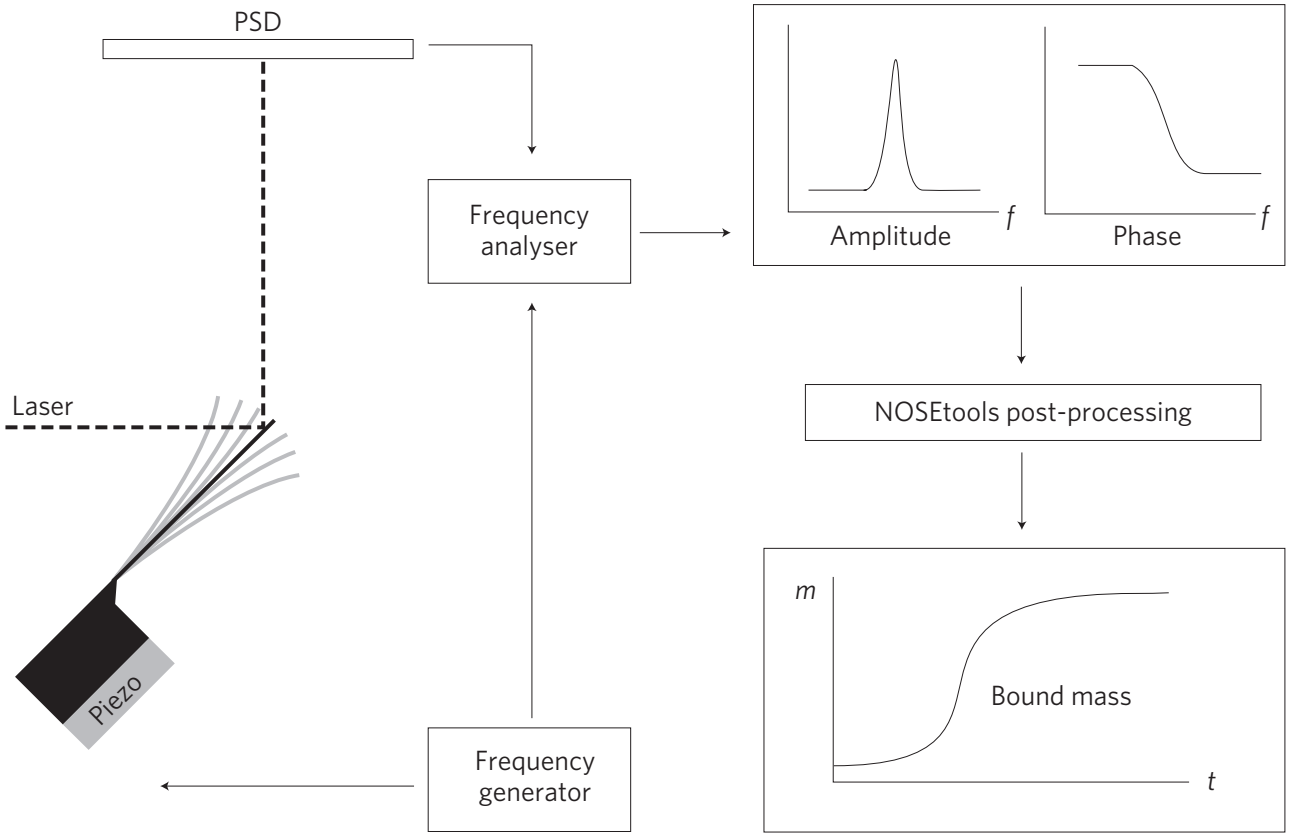

A frequency generator sweeps the frequency by exciting a piezoelectric actuator located beneath the base of the microcantilever array. The response of the cantilever is optically detected with a laser using a position-sensitive detector (PSD). The frequency analyser compares the cantilever response with a reference signal from the frequency generator to determine the phase. The amplitude spectrum is recorded with the corresponding phase values. The raw data are analysed by a post-processing software called NOSEtools, which allows the time evolution of the adsorbed mass to be directly determined from the spectrum.

Virtual mass: also liquid is moved, shifting eigenfrequency. Calibration is needed.
High damping, shifts amplitude peak relative to eigenfrequency.

T. Braun, V. Barwich, M. K. Ghatkesar, A. H. Bredekamp, C. Gerber, M. Hegner, and H. P. Lang, “Micromechanical mass sensors for biomolecular detection in a physiological environment,” Phys. Rev. E,72, 3, 2005.

Dynamic mode

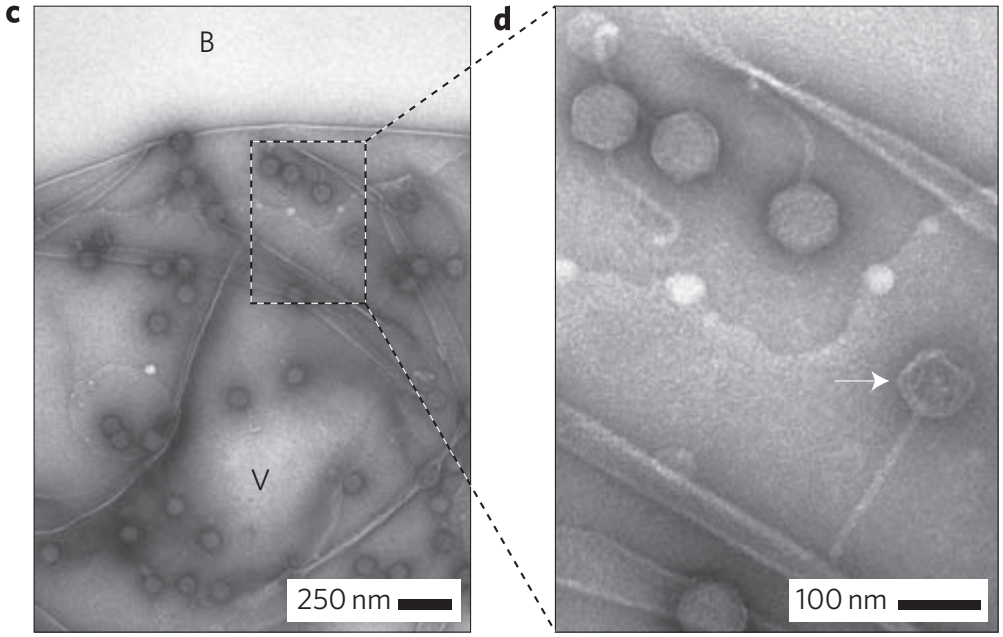

Vesicles with T5 virus receptor FhuA in Transmission electron microscope

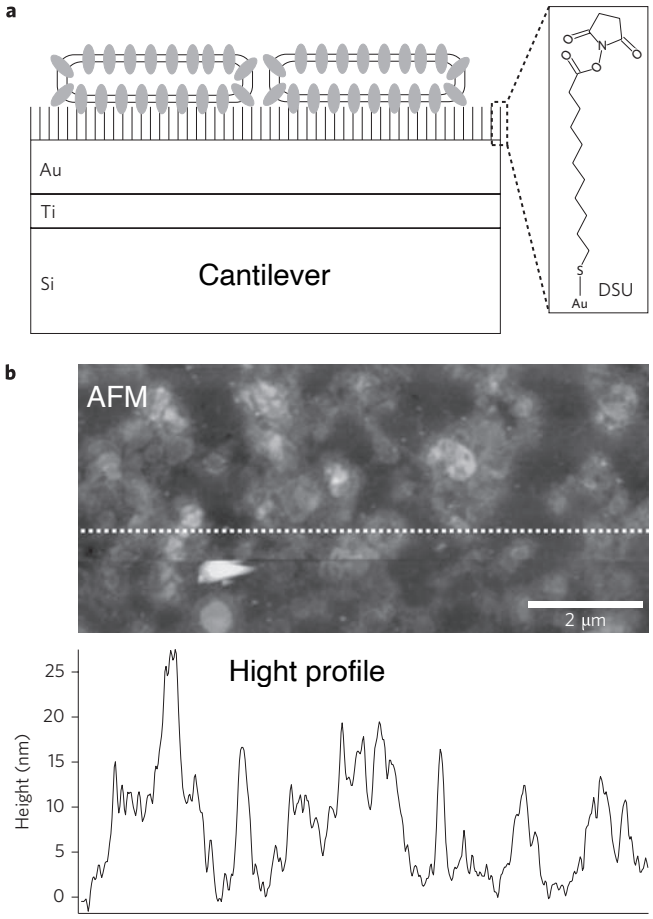

Functionalization of cantilever with FhuA vesicles

a, Schematic of the cantilever functionalization: the gold interface of the cantilever is pre-functionalized with a self-assembling DSU crosslinker, which binds to the gold via a thiol group and reacts by a succimidyl group with primary amines of FhuA–protein reconstituted in lipid vesicles. **b**, Tapping-mode AFM image of the cantilever surface in the middle of the cantilever bar. The line indicates the position of the recorded height profile shown in the lower panel. FhuA-containing proteoliposomes are clearly visible, similar to the one in the image on the left.

T. Braun, M. K. Ghatkesar, N. Backmann, W. Grange, P. Boulanger, L. Letellier, H.-P. Lang, A. Bietsch, C. Gerber, and M. Hegner, “Quantitative time-resolved measurement of membrane protein–ligand interactions using microcantilever array sensors,” *Nature Nanotech*, vol. 4, no. 3, pp. 179–185, 2009.

Dynamic mode

Quantitative realtime virus binding

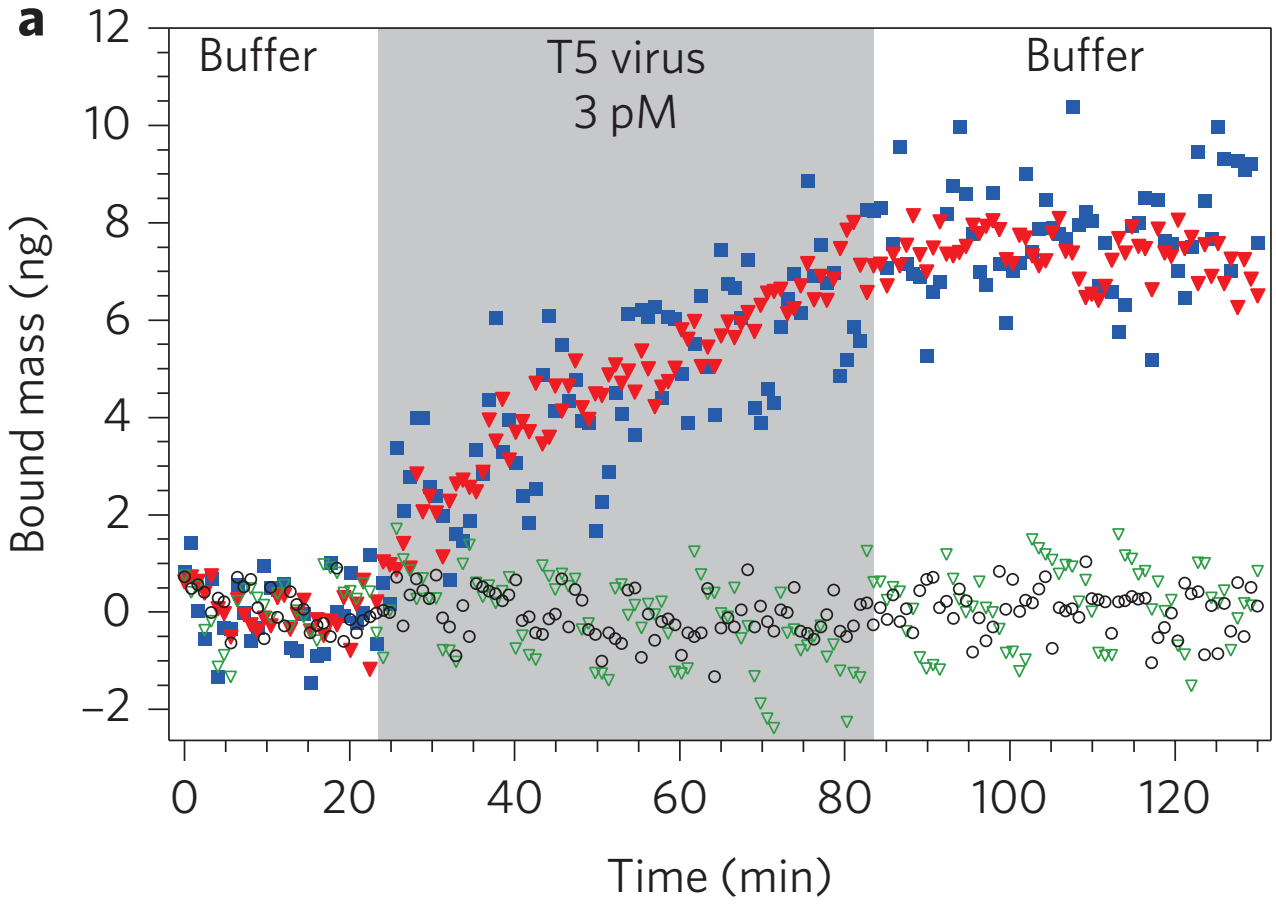

A T5 phage solution (3 pM) was injected for 1 h at a rate of 10 μl min−1. The uptake mass was measured simultaneously on four different cantilevers on one array: two positive controls (FhuA-coated cantilevers, blue squares and red triangles), two negative controls (casein-coated cantilevers, black open circles and green open triangles).

T. Braun, M. K. Ghatkesar, N. Backmann, W. Grange, P. Boulanger, L. Letellier, H.-P. Lang, A. Bietsch, C. Gerber, and M. Hegner, "Quantitative time-resolved measurement of membrane protein–ligand interactions using microcantilever array sensors," *Nature Nanotech*, vol. 4, no. 3, pp. 179–185, 2009.